THE THERMOELASTIC MARTENSITE TRANSFORMATION IN COPPER-ALUMINIUM-NICKEL ALLOYS

A thesis submitted for the degree of

DOCTOR OF PHILOSOPHY

in the University of London

by

MARTIN P. HOLLINS

August 1971

Department of Metallurgy,
Royal School of Mines,
Imperial College of
Science and Technology,
London, S.W.7.

ABSTRACT

The martensitic transformation in aluminium bronzes containing between 13 and 15 weight percent aluminium and upto 4 weight percent nickel has been studied by light and electron microscopy. The course of the ordering and precipitation reactions in these alloys has also been studied by metallography and thermal analysis. Observations of the influence of thermal history, stress, surface to volume ratio and thermal cycling through the transformation, on the course and nature of the transformation have been considered in relation to the existing theories of the kinetics, crystallography and nucleation mechanisms of the transformation.

The course of the transformation has been found to show thermoelastic characteristics with temperature range and temperature hysteresis of between 30 °C and 50 °C. Increasing aluminium and nickel contents were found to result in a proportionate depression of transformation temperatures: -175 °C ± 15 °C per unit w/o Al and -60 °C ± 10 °C per unit w/o Ni. Alloys were selected to permit "in situ" study of the transformation close to room temperature, and it was found possible to control the movement of martensite interfaces within the field of view of the electron microscope by careful temperature control.

The initial martensite plates were always observed at regions of highest surface to volume ratio, and the transformation proceeded into the bulk of the specimen by growth of new plates at existing interfaces. The earliest stages of growth recorded were narrow filaments usually on $\{121\}_{\gamma'}$ (martensite)// $\{110\}_{\beta}$ (matrix) planes, which is the twin plane within fully grown γ' plates. In the thinnest regions of the foils a number of planes of this type, and others, operated to produce a martensitic region which commonly did not promote transformation of the bulk of the specimen. Repeated transformation produced an increased dislocation density in the β-phase but the networks generated did not in general act as nucleation sites for subsequent transformations. Stacking faults were not observed in the β - phase and are therefore not believed to be a significant part of the nucleation mechanism.

A two stage ordering reaction to B2 and then DO_3 ordered structures was recorded by electron metallography and thermal analysis, in alloys containing greater than 13.8 w/o Al. The ordering reaction was not suppressible.

The course of the γ_2 precipitation reaction was determined and the increased transformation temperatures in heavily aged specimens has been accounted for in terms of composition changes in the matrix. Anomalous transformation temperatures in lightly aged specimens were associated with changes in the $a/4\ \langle 111\rangle$ (B2 type) antiphase domain boundary morphology.

Stress induced martensite was observed to catalyse the thermally induced transformation only at stress levels within the elastic limit of the phases. The "shape-memory" was shown by all alloys, deformed elastically both in the β - phase and γ' - phase condition.

ACKNOWLEDGEMENTS

I would like to express my gratitude to Dr. P.R. Swann for his interest, guidance and advice throughout the course of this project. I also wish to thank friends and colleagues of the Physical Metallurgy Department for their stimulating discussions and helpful suggestions. Thanks are due to Mr. W. Bishop for processing the electron microscope photographic plates, and to Miss P. Martins for printing the photographs in this thesis.

I am indebted to Professor J.G. Ball for the provision of laboratory facilities, and to the Science Research Council for financial support for the project.

I would also like to express my appreciation of the encouragement and forbearance of my wife during the course of this work, and my thanks for her assistance in preparing this thesis.

C O N T E N T S

PAGE

Abstract

Acknowledgements

CHAPTER 1 : THE THEORY OF MARTENSITIC TRANSFORMATIONS

1.1 Introduction 1

1.2 Development of Crystallographic Theory 5

1.3 Development of Kinetic Theory 9

1.3.1 Classical theories 9

1.3.2 Operational theories 13

1.4 Nucleation Mechanisms 19

1.5 Thermoelastic and Stress-induced Martensite 23

CHAPTER 2 : THE TRANSFORMATION IN ALUMINIUM BRONZES

2.1 Phase Equilibria 29

2.2 Morphology and Kinetics of the Martensitic Transformation 32

2.3 Crystallography of the Martensitic Transformation 35

2.4 Relative Stability of β_1' and γ' Martensites 40

CONTENTS/Continued...

			PAGE :
CHAPTER 3 :		EXPERIMENTAL METHODS	
	3.1	Preparation of Alloys	44
	3.2	Light Microscopy	47
	3.3	Electron Microscopy	52
		3.3.1 Specimen preparation	52
		3.3.2 Observations with the microscopes	54
	3.4	Thermal Analysis	56
CHAPTER 4 :		EXPERIMENTAL RESULTS	
	4.1	The Ordering Reaction $\beta \rightarrow \beta_1$	57
	4.2	The Precipitation Reaction $\beta \rightarrow \beta_1 + \gamma_2$	67
	4.3	The Martensite Reactions $\beta \rightarrow \beta_1'$ or γ'; General Features	76
		4.3.1 Growth	80
		4.3.2 Transformation Temperatures	86
		4.3.3 Crystal Structures	91
	4.4	Thermal History and the Martensite Transformation	102
		4.4.1 The effect of quenching temperature	103
		4.4.2 The effect of quenching rate	105
	4.5	Free Surface and the Martensitic Transformation	105
		4.5.1 Bulk specimens for light microscopy	106
		4.5.2 Thin foil specimens for electron microscopy	108

CONTENTS/Continued...

		PAGE
4.6	Mechanical Stress and the Martensitic Transformation	112
	4.6.1 Plastic deformation of the β- phase	113
	4.6.2 Elastic stressing of the β- phase	114
	4.6.3 Deformation of γ' Martensite	116
4.7	Repeated Transformation by Thermal Cycling	120
	4.7.1 Light metallography	120
	4.7.2 Transformation temperatures	123
	4.7.3 Electron metallography	130
4.8	γ_2 Precipitation and the Martensitic Transformation	142
	4.8.1 γ_2 formed at high temperatures	142
	4.8.2 γ_2 formed by low temperature ageing	143

CHAPTER 5 : DISCUSSION

5.1	The effects of Ordering and γ_2 Precipitation on the Transformation	154
5.2	The Effects of Stress on the Transformation	161
5.3	Kinetic Features of the Transformation	165
5.4	Transformation Mechanisms	167

CHAPTER 6 : CONCLUSIONS AND FURTHER WORK

6.1	Conclusions	175
6.2	Suggestions for Further Study	179

CONTENTS/Continued...

PAGE

APPENDICES

1. Construction of γ' structure from γ_1 structure 182

2. A Nucleation Mechanism for γ' Martensite 184

REFERENCES 188

CHAPTER ONE : THE THEORY OF MARTENSITIC TRANSFORMATION

"The martensitic transformation constitutes an unusual metallurgical problem, for while it can usually be recognised it is not explicitly defined. And, since it is not explicitly defined, one may properly ask whether, in fact, it will usually be recognised."

J.G. Parr

Sorby Centennial Conference on the History of metallurgy (1963).

CHAPTER I. THE THEORY OF MARTENSITIC TRANSFORMATIONS

I.I Introduction

The descriptive term "martensitic" has had a successively broader application during the 75 years it has been in existence. This has unfortunately been accompanied by an increasing uncertainty as to the characteristics implied by such a description. The specific phase occurring in quenched steels, to which Osmond gave the name "Martensite"[1], was shown to be formed by a reaction having characteristics which differed considerably from those normally encountered. Similar characteristics were later found in the phase changes of other alloy systems and the term "martensitic transformation" was used to describe them,[2] their products being called "martensites".

The first comprehensive attempt to set out the characteristics of martensitic transformation was made by Troiano and Greninger[3] in 1946. This led them to classify solid state transformations as "athermal martensitic" or "isothermal nucleation and growth". The exclusiveness of their chosen characteristics has been often contested since, and different lists compiled. More significantly, their basis of the distinction between martensitic and nucleation and growth transformations was challenged two years later with

the observation of "isothermal martensite" by Kurdyumov and Maksimova[4] and Cech and Holloman [5]. As a result a strong body of opinion, led by Kurdyumov[6], has maintained that the kinetics of the martensitic transformation are fundamentally similar to any other phase change.

Structurally, the transformation is characterised by a change in shape of the transformed region which is apparent as a surface relief effect. First recorded in 1905[7] this observation was suggested 50 years later by Bilby and Christian[8] for use as the primary criterion for identifying the martensitic transformation. It is a significant characteristic because it must be produced by the co-operative movement of many atoms through small distances relative to their neighbours. This is very different from the atomic processes in "nucleation and growth" reactions and explains other characteristic differences such as high growth rates and low transformation temperatures. The name "military" has been given by Frank[9] to transformations ocurring by such co-operative movements and the approach developed in reviews by Christian[10] and Borland[11]. Thus the "discipline" required for the transformation to proceed in a military manner is imposed by the coherency of the interface between transformed and untransformed regions. This orderly arrangement is much more likely at low temperatures since less energy is required; at higher temperatures the thermal

energy of the atoms leads them to behave more independently, and "civilian" transformations of nucleation and growth by diffusion, predominate. At intermdediate temperatures a transformation of mixed military and civilian character may be possible. For example, in bainitic structures the diffusion of an interstitial solute species is the rate determining factor, but the structural change occurs by co-operative displacement of the solvent and substitutional solute atoms. In this case the transformation would show isothermal kinetic behaviour due to dependence on diffusion rates and the kinetic behaviour of the structural change is masked. This is the approach used by Kaufman and Cohen and others[12] to explain "isothermal martensite" by means of an athermal nucleation model. (section 1.3).

Change of shape produced by co-operative motion of atoms is not an exclusive criterion of martensitic transformation, since it occurs in mechanical twinning in response to a mechanical stress. The transformations are however closely related and martensitic transformations share many characteristics with twinning transformations. For example, morphological and growth features of twins and martensite plates show great similarity. More significantly, transformation to martensite in response to mechanical stress, first observed in 1938[13] is accepted as a common feature of the transformation in many systems, so that the formation of martensite crystals like twinning, may be considered to be a mode of deformation competing

with slip at low temperatures. Furthermore, electron metallography has clearly shown that a twinning deformation is an integral part of many martensitic transformations. (Twins within martensite plates were first observed, but not recognised, as long ago as 1905 by Osmond and Cortaud[14]). In the last few years, considerable interest has been aroused by the discovery of unusual "rubberlike" and "memory" effects in several alloy martensites. Though imperfectly understood as yet, the importance of the twinning deformation associated with the martensitic transformation seems paramount (see section 1.5).

It is apparent therefore that there are structural and kinetic similarities between martensitic transformations and other changes of the solid state, perhaps as significant as the differences within the group of changes labelled "martensitic". It is thought by the present author that undue emphasis on the supposed equivalence of martensitic transformations has led to much of the past controversy. It should be stated that although the martensitic transformation selected for study in this thesis appears to show many of the classic characteristics, it is not thought that the conclusions reached are necessarily applicable to other transformations bearing the description "martensitic".

1.2 The Development of Crystallographic Theory

When a structural change is brought about by a martensitic transformation a change of shape is observed in the transformed region. It is also observed that the advancing interface between transformed and untransformed crystal called the habit plane, remains approximately undistorted and unrotated during transformation. Crystallographic theory must show how these features, and the orientation relationships relate the initial and final structures.

Since the shape change is produced by a co-operative movement of all atoms in the transformed region, the first step in the analysis is to find a correspondence of atom sites between the two lattices. The assumption, made initially by Bain[15] and followed by subsequent workers, was that the relevant correspondence was the one which minimised the atomic displacements, since this would require least strain energy. From this correspondence it should be possible to obtain a homogeneous strain matrix which contains the equations defining the deformation. However it is found that, if the other features of the transformation such as an undistorted habit plane are taken into account, this is possible only in the f.c.c. to h.c.p. transformations. In the general case it has been shown[16, 17] that a lattice invariant shear (S), and a rigid body rotation (R) are required in addition to the homogeneous strain (P), to account for

the shear deformation (F). The equation of the transformation is therefore given by:

$$F = R P S \qquad (1.1)$$

where F, R, P, S all represent 3 x 3 matrices.

The prediction of the presence of a second, lattice invariant deformation had little experimental support at the time but was vindicated by later electron microscopy observations of twins and faults with in the martensite plates[18].

Equation (1.1) was the basis of the two theories published in 1953/4 by Wechsler, Lieberman and Read[19] and Bowles and Mackenzie[20] which have been applied with considerable success to many well documented transformations [21, 22]. The matrix F is constructed from measurements of the shape deformation and P from lattice correspondence. R is then uniquely defined by Euler's theorem. S is constructed from measurements of the internal shears in a martensite plate; at the time of the theories these were not well investigated and assumptions were made as to their exact nature. Later experimentation has shown that this can be quite complicated; for example, the mixed shear by twinning and slip observed in Fe-Ni martensite[23, 24]. Recently there have been a number of attempts to extend the theory to cover variations in lattice invariant shear [25-28]. These have been reviewed by Ross and Crocker[29] when presenting their own particularly adaptable theory which allows for

the combination of any two (or more) independent slip or twinning shears. Equation (1.1) thus becomes:

$$F = R P S_1 S_2 \qquad (1.2)$$

They derive possible mechanisms for an outstanding problem in ferrous martensites (the $\{225\}$ habit) and predict that the order in which the two shears are applied has a physical significance from a consideration of the nature of an interface produced by two independent shears.

The nature of the interface is the source of an alternative approach to the theory of martensite crystallography initiated by Frank in 1953[30]. The atomic distribution of the interface planes in each phase are matched by applying the necessary shear and dilatation. It is found necessary to include an array of dislocations in the interface, however, to complete the matching (Fig. 1.1). This model contains the equivalent components of the matrix formulation - a homogeneous shear of the lattice, and a heterogeneous lattice invariant shear produced by the dislocations. This model has been extended to a more general treatment by Bilby and Frank[31], and Bullough and Bilby[32], using surface dislocation concepts.

Fig.1.1 : Frank's model of the martensite interface in steels (Ref.30)

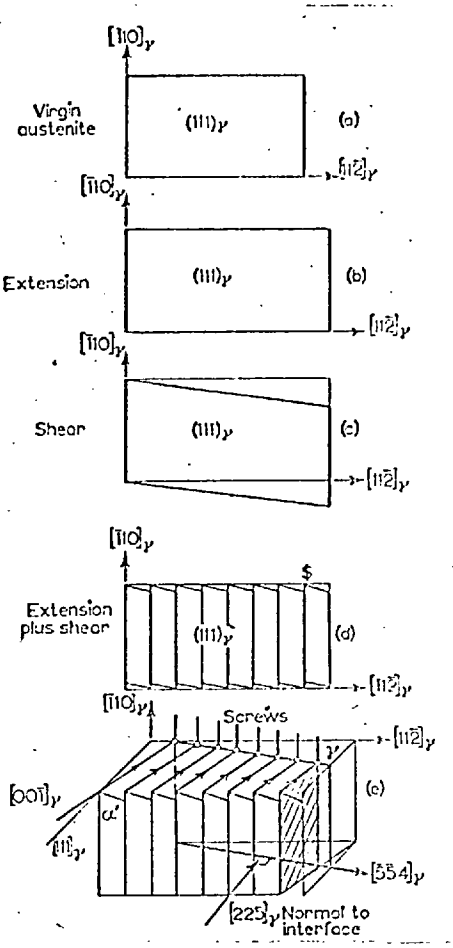
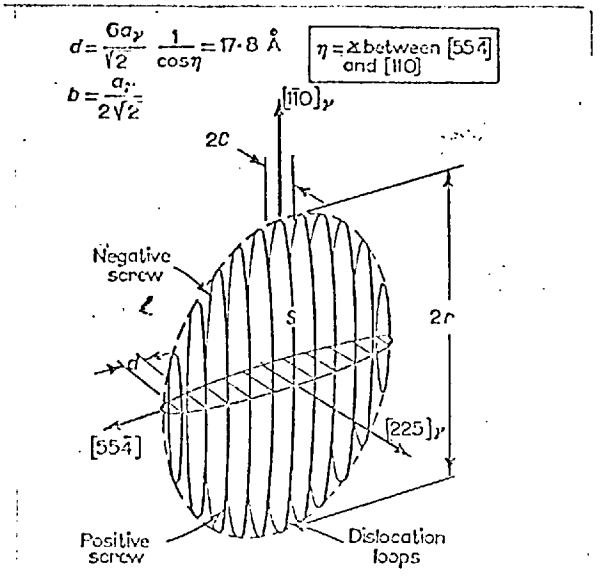


Fig.1.2 : Knapp and Dehlingers' model of a martensite embryo (Ref.39)



1.3 Development of Kinetic Theory

The kinetic characteristics of martensitic transformations show wide variations which have been reflected in the succession of theories developed to account for an increasingly comprehensive collection of observations. The purpose of the following brief review is to present the assumptions and comment on the limitations of these theories, with particular regard to the attention focused on the nature of the nucleation processes.

The chemical driving force for a change of state is given by the difference in free energy between the parent and product phase (ΔF). The formation of a new structure such as martensite, in the solid state, involves a volume change and creation of interfaces. Thus for the transformation to be thermodynamically possible the decrease in the chemical free energy must balance the sum of the strain and interfacial energies

$$\Delta F = \Delta G(\text{strain}) + \Delta G(\text{interface}) \quad (1.3)$$

1.3.1 Classical Theories

Following the observation of isothermal, "C-curve" kinetics in a martensitic transformation in Fe-Mn-C, Kurdyumov and Maksimova[4] applied the classical homogeneous nucleation theory which was later developed by Fisher et al[33 - 35]. The theory considered the variation

of the factors in equation (1.3) with the dimensions of a lenticular particle of martensite, radius r, and thickness, c. The total free energy change of the transformation on ΔW becomes:

$$\Delta W = \pi r^2 c \Delta f + 2\pi r^2 \sigma + \pi r c^2 A \quad (1.4)$$

where Δf is the chemical free energy change per cm^3 of martensite formed, σ is the surface energy per cm^2, and A the elastic constant. This function exhibits a maximum with respect to the "embryo" volume which is interpreted as the "nucleation barrier". The barrier can be surmounted by the embryos attaining a critical size ($r = r^*$) with the aid of thermal fluctuations, at which they have this maximum free energy (ΔW_*). Every atom is a potential nucleation site and the number of nuclei is given by

$$\dot{N} = (N_0 / V)\, \nu \exp.(-\Delta F_*/KT) \text{ per } cm^3 \text{ sec.} \quad (1.5)$$

where N_0/V is the number of atoms per cm^3 and ν is the lattice vibration frequency. The activation energy for growth was assumed finite, but small, in earlier theories, and zero in the later modifications, in view of the rapid growth observed at temperatures approaching zero.

The theory predicts isothermal nucleation with $\dot{N}$ showing sigmoidal variation; athermal characteristics were accounted for by identifying the martensite start temperature (M_s) with $N = 1$ nucleation event per cm^3 per sec. At slightly higher temperatures

$\dot{N}$ was assumed so small that isothermal nucleation would not be observed in reasonable times; at slightly lower temperatures $\dot{N}$ was assumed so large that isothermal nucleation would not be suppresed, even on rapid cooling. It had some success in explaining the C-curve characteristics observed in Fe-Ni-Mn-C alloys by Cech and Holloman[5] and other purely isothermal reactions, but proved unable to account quantitatively for variations in nucleation rate, for example in Fe-Ni alloys of varying nickel contents[12].

More significantly, evidence accumulated to indicate that nucleation occurred heterogenously. For example, the precise repetition of appearance of martensitic plates in successive cycles of a thermoelastic transformation, and the experiment of Cech and Turnbull [36] on very small particles of asutenite in which transformation started at widely different temperatures, are two of the more striking observations. Attempts were made to modify the classical theory to take account of this heterogeneous nature.

Holloman and Turnbull[37] proposed that compositional fluctuations frozen in from a higher temperature could provide heterogeneous nucleation sites, to be activated by thermal fluctuations. The theory appears to require dilute-solution conditions however, which are inapplicable to many transformations occurring over a wide range of composition. It has been argued, furthermore, that this should lead to random nucleation. The theory of Cohen, Machlin and Paranjpe[38]

proposed that the heterogeneities acting as embryonic nuclei were strain centres involving a dislocation arrangement ("if they exist" the paper cautiously adds !). These strain centres were assumed to pass though a series of intermediate states which gradually resembled the martensitic structure - a "reaction path", which led to a distribution of "strain embryos" of differing free energy, maximum F_m. The activation barrier to nucleation could be overcome by the formation of internal strains by applied stress, and/or thermal fluctuations. If the free energy for activation at a specific temperature T is $F_A(T)$ then the transformation can begin athermally when $F_m = F_A(M_s)$ and will procede over a range of temperatures. Isothermal transformation is also possible at temperatures within the athermal range at say, temperatures T_1 if thermal fluctuations are able to raise the energy of some embryos from below $F_A(T_1)$ to above $F_A(T_1)$. Thus the transformation is partially suppressible. Growth was again assumed to require little or no activation and proceed rapidly. The theory explained the observed effect of applied stress aiding transformation and stabilisation suppressing the transformation in terms of a stimulation and relaxation of the strin embryos, respectively. It took no account of the physical nature of the embryo, considering merely its thermodynamic significance. Nor did it consider the energy of the interface. However it provided a starting point for later theories which used more detailed models of this type of embryo.

1.3.2 Operational Theories

A general criticism of the classical theories is that they depend on atom by atom mechanisms which are obviously not significant in the characteristic growth features of the transformation. The discovery of the importance of the line defect on the mechanical behaviour of metals suggested a means of moving large numbers at high speeds and low temperatures, in accordance with experimental observations. An array of dislocations, which could behave as a surface defect, would be required to sweep though the crystal during transformation, producing the required lattice deformation. The implications of this mechanism on the kinetics of the transformation were analysed by Knapp and Dehlinger in 1956[39]. They used a model of the embryonic martensite plate which had an oblate spheroid shape and an interface based on the proposals of Frank (section 1.2), tc calculate the strain and surface energy to form and expand the dislocation loops in the interface (interfacial energy), and the energy of the displacements created (strain energy), must be supplied by the chemical driving force. It was assumed that an existing embryo will "trigger" spontaneously into a full size plate once the chemical driving force exceeds these restraining forces. An expression for the minimum of these restraining forces (Δg min) is derived in terms of the embryo dimensions and it is found

to decrease monotonically with the increasing embryo size - as shown in fig. 1.3 which identifies the critical radius r_o as that for $w = 0$. Rapid growth is then possible since the interface is mobile and the net force on it increases as the particle expands. Their calculated values for the velocity of the interface showed good agreement with experimental values.

It was assumed that there would be a size distribution of pre-existing embryos, and that only the largest would participate in the transformation at M_s. This size was calculated to be about 8×10^6 atoms in extent. As the temperature falls the chemical driving force increases and expansion of successively smaller embryos is possible. Thus athermal kinetics are expected, since thermal activation plays no role in "triggering off" the embryos.

It is clear that this theory does not consider the problem of nucleation at all since it starts with the assumption of the presence of embryos. Kaufman and Cohen [12] extended the approach to account for their existance, and for the observation of isothermal kinetics. They assumed that there would be dislocations in the matrix phase which, if incorporated into a frank-type interface, could reduce their strain energy to zero. Such a gain in energy would make it possible for embryos to exist at temperatures above T_o where $\Delta f = 0$ and they derived an expression for the optimum embryo size at temperatures within this range. This size increases with falling temperatures

Fig.1.3 :

Effect of embryo size on restraining force (Δg_{min}) and net driving force (Δw)

(39)

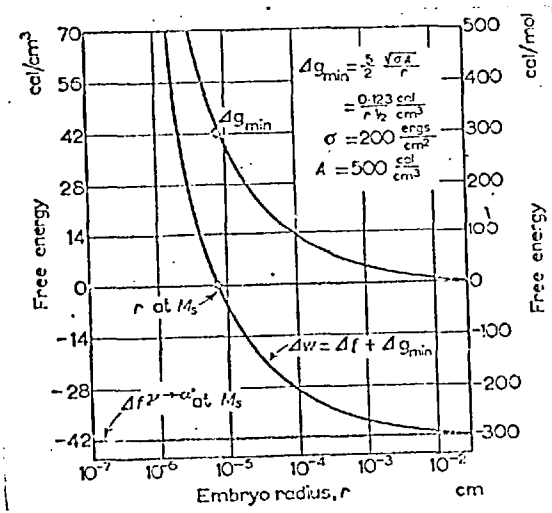
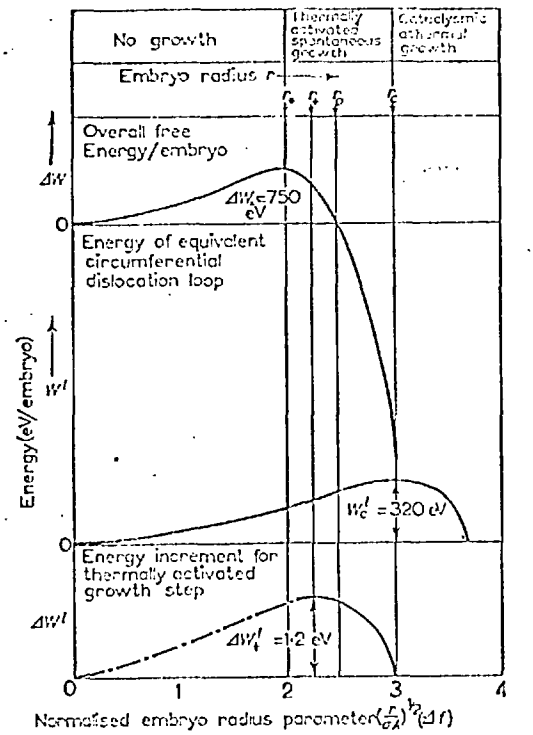


Fig.1.4 :

Effect of embryo size on overall free energy, (Δw), energy of circumferential dislocation loop (w^1) and thermal activation (Δw^1)

(12)



(Δf also increases), and it was presumed that embryos would coalesce as the temperature fell, by rearrangement of dislocations. This would depend on the dislocation mobility and it was suggested that the embryos would be "frozen in" as temperatures fell towards To due immobilisation of dislocations.

They then approached the problem of the cataclysmic growth of these embryos (the "operational" nucleation process) by assuming that the creation of new dislocation loops is the critical step, rather than the equivalence of chemical driving force and non-chemical restraining forces, assumed by Knapp and Dehlinger - a thermodynamic equation taking no account of the nature of the atomic displacements possible. By simplifying the dislocation array of the oblate spheroid embryo to a single large loop they obtained a relationship for the energy of this loop (W^L), giving a maximum value (W^L_c) at a critical radius of $r_c = 9\sigma A/\Delta f^2$ which compares with that predicted by the classical theory $r_* = 4\sigma A/\Delta f^2$, and that predicted by Knapp and Dehlinger $r_o = 25\pi\sigma A/4\Delta f^2$. Figure 1.4 shows the energy change versus embryo size for the classical and operational theories, and that of the thermal activation for the growth of loops.

The theory is able therefore to explain both athermal and isothermal kinetic behaviour: quenching to a temperature where some embryos have a size greater than r_c results in athermal

formation; holding at temperatures where the largest size embryo has radius between r_* and r_c results in isothermal formation. The size of embryo which is predicted by the theory may be as large as 1,000 Å diameter for the largest existing at M_s. Such structural features should be observable by electron microscopy, and serious doubt has been cast on the theory by the total failure to identify such features.

Magee and Paxton[40] have criticised the assumptions made in this theory about the ability of dislocations to arrange themselves into a martensitic structure (the embryo) above T_o, and the subsequent freezing of these arrangements below T_o. They point out that observations suggest a continual decrease of dislocation mobility with temperature. This factor they consider to be of prime importance in determining the driving force necessary to move the dislocations in the interface, that is, to promote growth. Their analysis predicts that a balance between reduced interface mobility and increased driving force as the temperature falls, should lead to sigmoidal, time dependent reaction kinetics.

An outstanding characteristic of the transformation is its autocatalytic behaviour which is expected to have a considerable effect on the kinetics of the course of the transformation. The preceding theories attempted to avoid these effects by limiting the calculation to the initial nucleation rates and using the experimental

results of isothermal transformations in the presence of no athermal martensite, or at least a constant amount. However, the results of Raghavan and Entwisle[43] from an isothermal transformation in Fe-Ni-Mn indicated that the autocatalytic effect is present in the earliest detectable stages of the transformation (before 0.2%) so that it is invalid to neglect embryos formed by the transformation in comparing the observed operational nucleation rates with the theoretical predictions. Assuming that the number of embryos formed by the strain generated in the matrix by the transformation is proportional to the volume of martensite formed, and that these embryos require the same activation energy as those pre-existing, they were able to derive an expression for the volume fraction of martensite as a function of time. Comparison with experimentally obtained curves show good agreement up to 10% martensite, when the transformation began to decelerate. It is at this stage that the partitioning effect of existing plates reducing the size of new plates, becomes significant, so that deviations could be due to inadequacies in the partitioning theory.

The number of embryos expected by this theory is large - $10^7/cm^3$, pre-existing and $2 \times 10^{10}/cm^3$ formed during the transformation of 1 cm^3 of material, which suggests that the process is a simple event creating small embryos.

It has been emphasised that nucleation rates used in kinetic theory can only be inferred from experimental observation of relatively macroscopic changes in structure. It is possible that these may define a critical condition not directly related to the nucleation process - so-called "operational rate"[42]. This provides a justification for the foregoing theories which have had considerable successes in explaining the overall kinetics of the phase change without any detailed model of the nature of the earliest stages - the "true" nucleation process.

1.4 Nucleation Mechanisms

From the preceding section it is clear that a model of the martensite nucleation process must satisfy a number of criteria:

(i) The initial nucleus need not have an identical crystal structure to the final martensitic phase.

(ii) Although its formation should produce a net reduction in the free energy of the system, it need not show the same kinetic features as the later stages of the transformation (e.g. cataclysmic growth).

(iii) Sites for nucleation are heterogeneous but readily available in large numbers.

(iv) The ease and sequence of retransformation suggest that this is due to a reversion of the reaction, rather than a separate nucleation process.

It was quickly realised that these considerations indicated a dislocation reaction. In 1951 Christian[43] showed how the dissociation of f.c.c. dislocations of $\{111\}$ could lead to a structure similar to h.c.p., to account for the martensitic phase change in cobalt. Since that time many other proposals have been made in a number of systems involving different changes in crystal structure. Experimental support for these suggestions has been hampered by the difficulty of arresting martensitic growth at a sufficiently early stage, although stacking faults have been identified in connection with several f.c.c. to h.c.p. transformations. The major theoretical problem has been to generate a three dimensional crystal from a planar fault.

The similarity of the transformation to twinning deformation has prompted an interest in the pole mechanism, proposed by Cottrell and Bilby[44] for b.c.c. structures and modified by Venables[45] to account for twinning in f.c.c. The elements required are a fixed dislocation (node) and a rotating screw dislocation which produces successive displacements in each atomic plane. The change in crystal structure during martensite transformations involves more complex displacements than this however. For example, the f.c.c.

to h.c.p. observed in cobalt and Co-Ni which is perhaps the simplest, can be effected by the movement of the twinning $a/6 \langle 112 \rangle$ partial dislocations on every second plane. Pole mechanisms have been constructed for a number of martensitic transformations including Cu-Al-(Ni)[46].

de Lamotte and Altstetter[47] however, considered that the large number of pole dislocations of high energy, which would be required, made this an unlikely mechanism, from their study of the f.c.c. to h.c.p. transformation in Co-Ni. The observation of the availability for the transformation of dislocations of differing Burgers vectors led them to propose a model involving the nucleation of transformation dislocations at interfaces, since the pole mechanism would produce "replica" dislocations of identical Burgers vector.

Electron metallography of the transformation in Fe-Ni (f.c.c. to b.c.c.) by Dash and Brown[48], showed a correlation between fault traces in $\{111\}_{fcc}$ and martensite plates, often connected by complex dislocation arrangements. This was taken as evidence of the mechanism of the Bogers and Burgers[49] involving $a/18 \langle 112 \rangle$ shears in $\{111\}$, and they also suggested that the necessary dislocations can be generated during the transformation. There was no attempt to relate these shears and faults to the observed habit plane of the fully grown martensite plate since this

was considered to be a macroscopic concept - an interface made up of differently oriented plates. In contrast to this a recent study of the same structural change in Fe-Cr[50] showed thin martensite plates having the same habit plane, $\{225\}_{fcc}$, as the fully grown plate, at a very early stage.

Direct evidence of the necessity of dislocations to the transformation has come from studies of small particles of iron in a copper matrix[51, 52]. These precipitates do not transform from f.c.c. to b.c.c. even when cooled 850°C below the bulk M_s temperature, unless dislocations are introduced by plastic deformations. Electron metallography clearly showed the formation of martensite in those particles that were intersected by the dislocations.

Transformations from b.c.c. to h.c.p. and closely related structures are common in copper alloys and Walimont has reviewed[53] the evidence of a low resistance to shear along $(011)[011]_{bcc}$ in β-brass and other β copper phases. This, he suggested indicates the possibility of a nucleation mechanism incorporating such a shear. One was proposed by Cohen et.al.[54] involving the dissociation of the perfect $a/2[111]$ dislocation as follows

$$\frac{a}{2}[111] \rightarrow \frac{a}{8}[011] + \frac{a}{4}[211] + \frac{a}{8}[011] \qquad (1.6)$$

This is energetically favourable, and also produces a stacking

similar to h.c.p. by the movement of the a/8 [011] partial dislocations. This proposal was used by Duggin and Rachinger[46] in developing a nucleation mechanism for the transformation in Cu-Al-(Ni) and is described in more detail in section 2.3.

1.5 Thermoelastic and Stress-Induced Martensite

During the transformation the shape and volume change must be accommodated by elastic or plastic deformation of the transformed and/or untransformed regions of the crystal. Whether the elastic limit of these phases is reached will depend on the size of the transformation shears and dilatations and the mechanical properties of the phases. If the limit is reached plastic deformation will occur which will make the continued passage of the interface more difficult, and will not, in general, be removed when the crystal is retransformed. Thus the driving force necessary for forward or reverse transformation is increased, manifest as a large temperature difference between the start and finish of the transformation, and thermal hysteresis in the reverse transformation.

If the transformation ceases before the elastic limit is reached the accommodation stress will provide a driving force for the

reverse transformation, thermal hysteresis will be greatly reduced or absent, and the temperature range of the transformation small. This behaviour was first observed in an aluminium bronze by Kurdyumov and Khandros[55] and the product called thermoelastic martensite (further details are given in section 2.2). The transformation temperatures of a thermoelastic and non-thermoelastic reaction are compared in fig. 1.5.

Cahn[56] drew attention to the similarity between these transformations and the elastic twins formed in calcite and used the results of Garber[57] on these crystals to explain the growth features of the thermoelastic martensite.

Since no work is done in plastic deformation or in overcoming the resistance to interface movement caused by it, the increase in strain energy, ΔG (strain) in equation (1.3) is available to promote the reverse transformation. Considering the growth of a particular martensite plate of fixed shape, this term will be of much greater importance than the surface energy term shortly after nucleation since it is proportional to the volume, and the latter is proportional to the surface area. The free energy promoting growth (ΔF) is also proportional to the volume of the plate so that a balance is set up between these two factors. As the plate grows however, its shape may change due to a restriction of growth in some directions, and this could lead to a rapid increase in strain

Fig.1.5 : Elastic and non-elastic transformation temperature ranges.

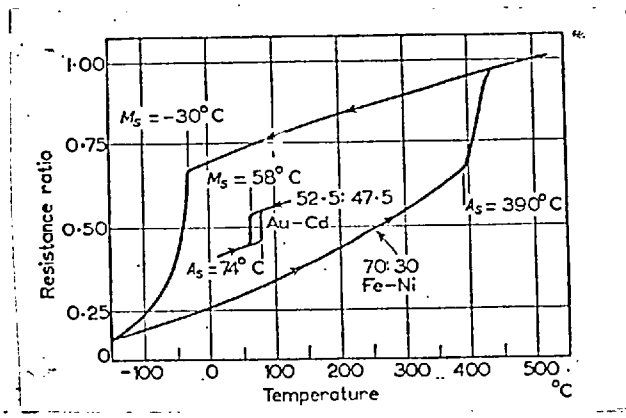
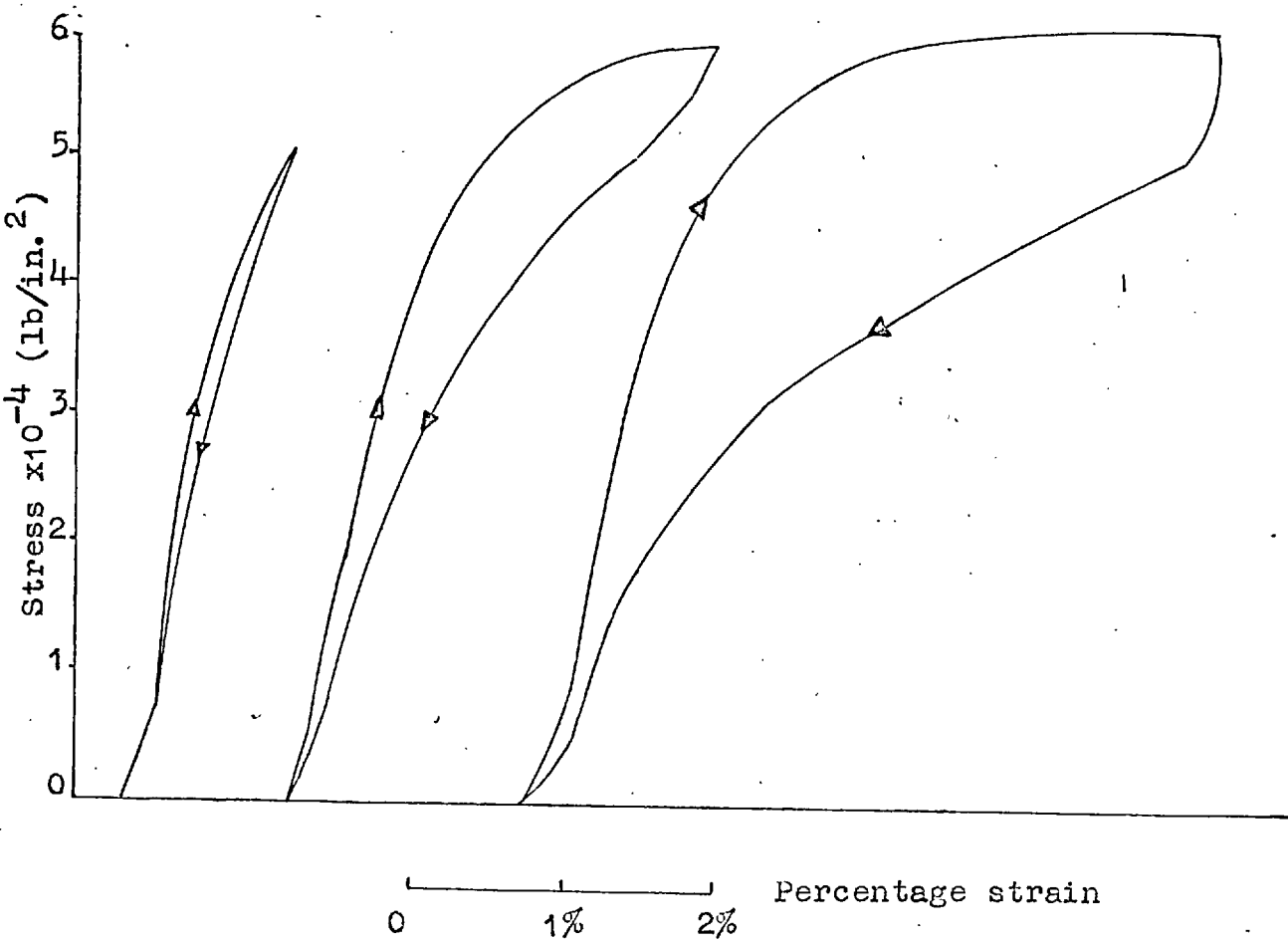


Fig.1.6 : Stress/strain readings through an elastic transformation (Cu - 14.5^{W}/o Al - 3^{W}/o Ni [63])



energy sufficient to stop the plate. The plate is thus in thermoelastic equilibrium with the matrix, since an increase in the volume free energy produced by a reduction in temperature will cause the plate to grow, and vice versa. The speed of growth or shrinkage of the plate is therefore directly dependent on the rate of change of temperature.

Since martensites are formed by a shear transformation it is clear that the application of stress may tend to promote its formation. Thus transformation may begin at a temperature higher than M_s. These effects were predicted by Schiel in 1932[58] and have been confirmed in many transformations since. The criterion for transformation by the applied stress is not that of critical resolved shear stress, however, as Schiel proposed because the formation of a new crystal structure involves a volume change in addition to shear displacements. Thus Patel and Cohen[59] obtained different effects on the M_s of Fe-Ni alloys applying tensile and compressive stresses, for which the shear components were the same (because of many available martensite habit orientations). They also observed a suppression of the transformation (lowering of M_s) on applying hydrostatic compression.

This led them to propose a thermodynamic criterion for transformation based on the assumption that M_s occurs at a certain value of the driving force (ΔF, equation (1.3)). The work done (U),

by the applied stress was calculated from a knowledge of the transformation displacements of the system. The work to form the first plates (at M_s) was designated $U_{max.}$ and this quantity simply included in equation (1.3) so that the new martensite start temperature (M_s') can be defined by

$$\Delta F \text{ at } M_s' = \Delta F \text{ at } M_s + U_{max.} \qquad (1.7)$$

The work done may aid or oppose the transformation ($U_{max.}$ + ve or - ve) depending on the nature of the applied stress and volume change of the transformation. The predicted variation in M_s agreed well with observations, including that of reduced M_s by hydrostatic pressure, since the transformation dilatations are positive.

If an external stress is applied to a phase which shows a thermoelastic transformation to martensite then removal of the stress may be expected to cause automatic retransformation. This has been observed in a number of alloy systems: Cu-Zn[60], Au-Cd[61], Cu-Al-Ni[62, 63] and Ti-Ni[64], and is extremely similar to the behaviour of the elastic twins in calcite. The effect is to increase the elastic yielding of the material in a particular temperature range and has been variously named: "ferroelastic", "super-elastic", "anelastic" and "rubberlike". The term anelastic has been suggested as appropriate, with regard to the hysteresis dysplayed in the stress-strain curves[64]. That is, the stress to

form a particular plate is always greater than the stress at which it disappears (fig, 1.6). This result is, of course, the complement to the thermal hysteresis considered previously. Reported stress-strain curves[63, 64] also show that as the maximum load increases the hysteresis also increases (fig. 1.6).

The stress-induced martensite will clearly form with a preferred orientation with respect to the applied stress, as has been observed metallographically[62] and by X-ray texture determinations[65]. This can result in a gross shape change in the stressed crystal (e.g. by bending) which can be absorbed elastically or plastically, as previously discussed. Furthermore the "elastically" strained crystal may show considerable stress hysteresis at high stress levels.

During the time ther research described in this thesis was being conducted, there has been considerable interest in a new phenomenon which is both attractive, and potentially very useful. This was the observation that certain crystals could be grossly deformed and later resume their original shape when heated, called the "shape memory" effect. It was first observed in equiatomic NiTi[66] and very recently in Cu-Al-Ni[67], Cu_3Al[68], Ni-Al[69], Fe_3Pt and brass[70]. This list includes those systems in which the thermoelastic and anelastic martensites have been observed and the structural similarities between the phases in these systems has been pointed out[67, 70]. The effect will be described and discussed in greater detail in later sections of this thesis.

CHAPTER TWO : THE TRANSFORMATION IN ALUMINIUM BRONZES

CHAPTER 2: THE MARTENSITIC TRANSFORMATION IN ALUMINIUM BRONZE

2.1 Phase Equilibria

The Cu-Al binary system has been the subject of considerable investigation and the equilibrium phase diagram is well established [71], (Fig. 2.1). In the composition range relevant to the present study the random b.c.c. solid-solution β-phase undergoes a eutectoid reaction at $565^{\circ}C$, 11.8 w/o Al. The products are the f.c.c. solid-solution α-phase and the aluminium-rich γ_2 phase. This has a γ-brass type structure based on the b.c.c. β-phase[72]. The unit cell contains 52 atoms with a stoichiometric composition of Cu_9Al_4. This unit cell is equivalent to 27 unit cells of β-phase (stoichiometric composition Cu_3Al) with 2 copper sites vacant.

If the eutectoid reaction is suppressed by rapid cooling the β-phase orders to a DO_3 structure called β_1 [73] Swann[74] has shown that the arrangement of atoms on the lattice sites of β_1 and γ_2 are closely related (Fig. 2.2). It is believed that the ordering reaction is insuppressible but the temperature of ordering has been the subject of several contradictory findings[75] (Fig. 2.3).

The influence of nickel on the binary equilibria was studied extensively by Alexander[76]. This influence is minimal in the range

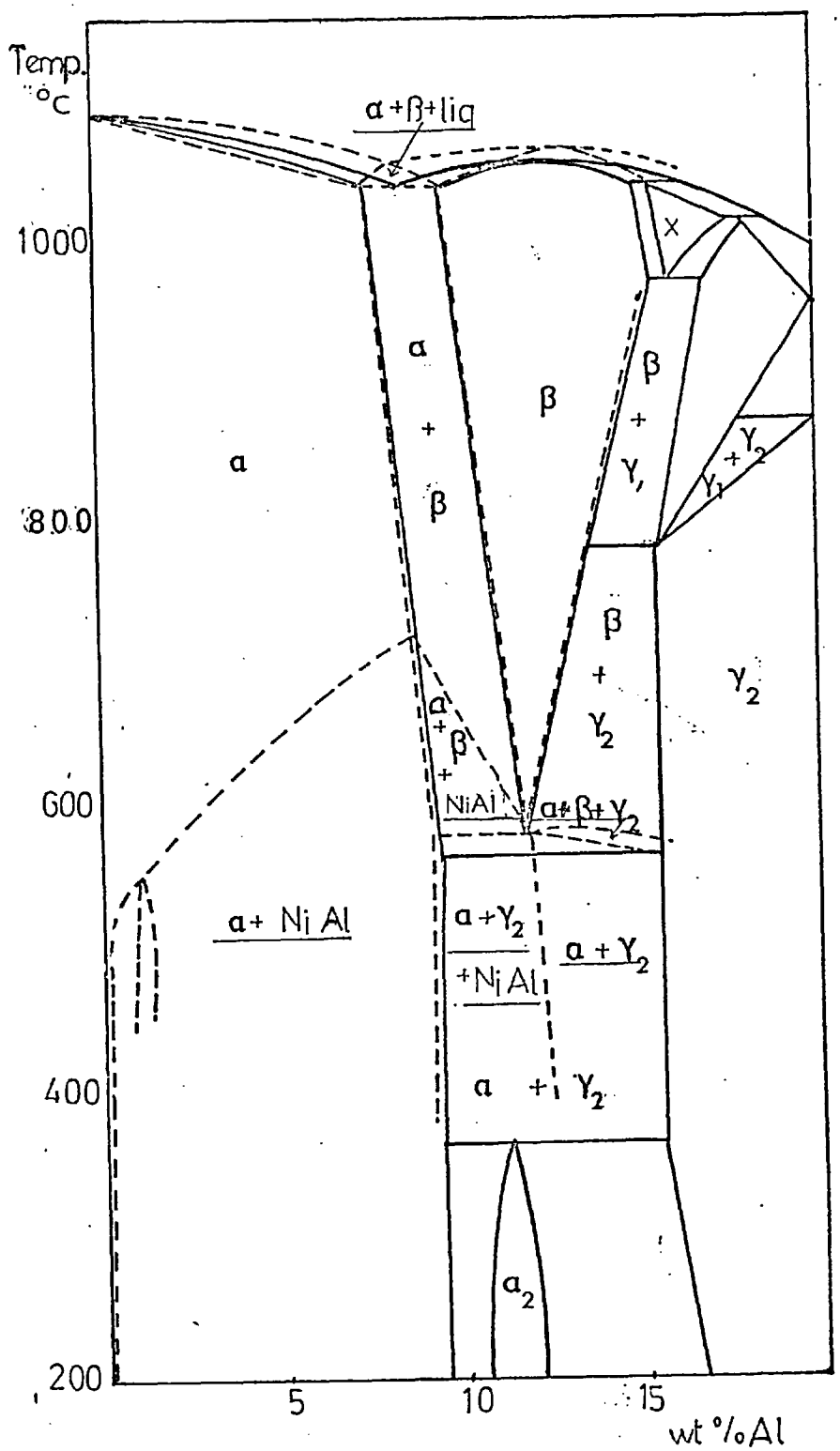
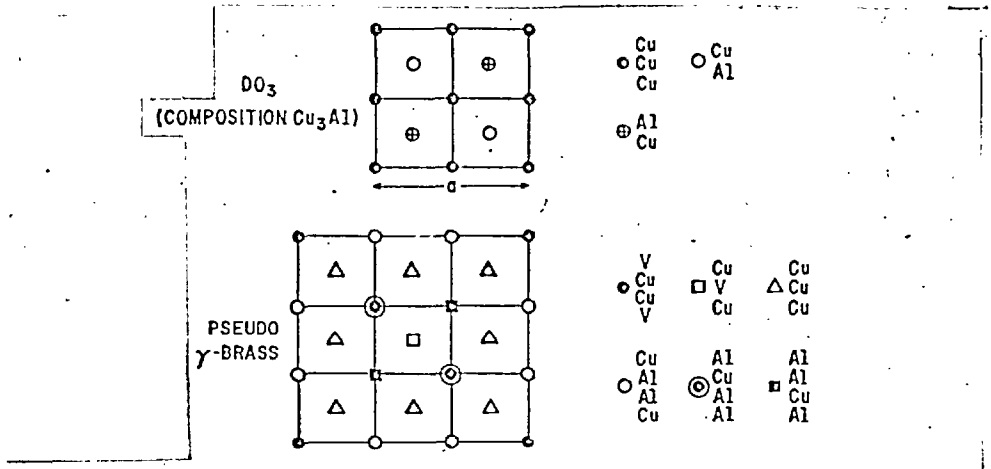


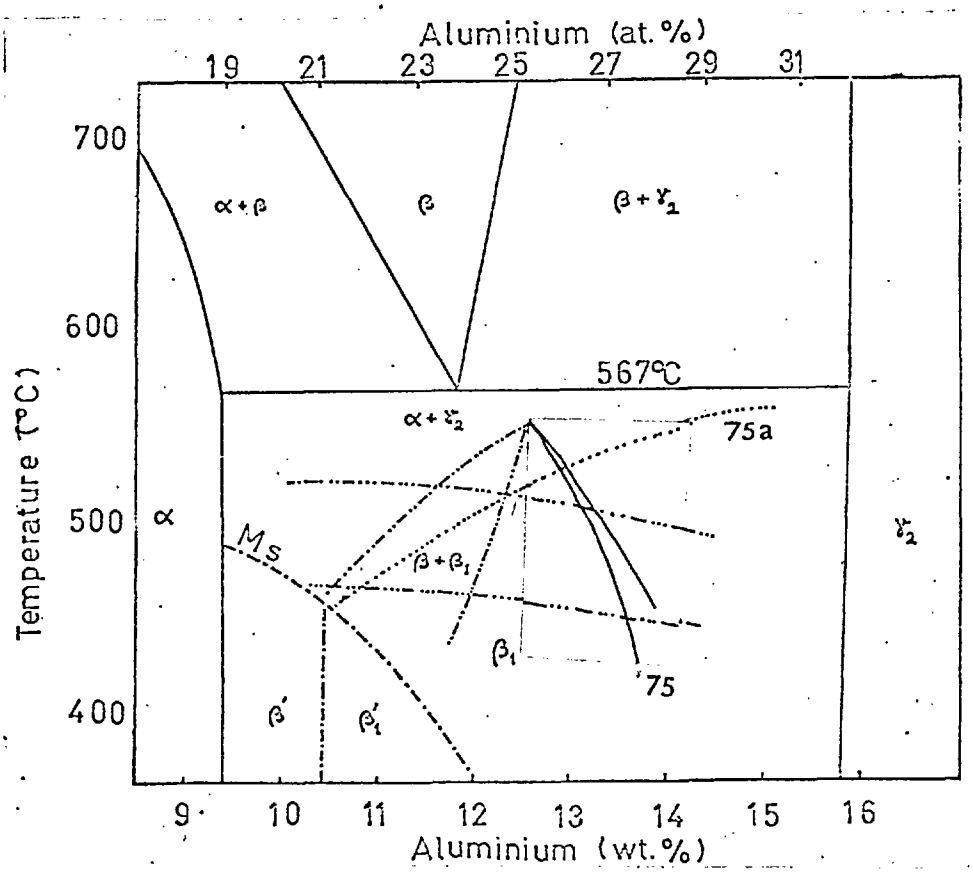
Fig. 2.1 Equilibrium phase diagrams of binary Cu-Al —— and ternary Cu-Al-3^{w}/oNi ----

Fig.2.2 : β_1 and γ_2 structural relationship (Ref.74)



The DO_3 and pseudo γ-brass structures are constructed from 8 and 27 body-centred units respectively. The symbols on the right indicate the atomic stacking sequences in columns normal to the projection. The nickel atoms in the alloy studied (not shown in the drawing) are expected to occupy 'Cu' sites randomly. The letter V indicates the position of a vacant site.

Fig.2.3 : Metastable phase diagram of Cu-Al. (Ref.75)



of compositions used in the present study (Fig. 2.1). It is expected that the nickel atoms will occupy copper sites randomly in the β, β_1 and γ_2 phases so that their stoichiometric compositions become $(CuNi)_3Al$ and $(CuNi)_9Al_4$[74].

The first observations of the martensitic transformation in Cu-Al were made by Wasserman [73] in Cu-12 w/o Al. A reversible transformation to β_1' at 280 - 300°C was noted, using X-ray methods for cooling rates greater than 1°C/sec. A second martensitic phase γ' was discovered in alloys containing more than 13.1 w/o Al with a mixture of both types in the composition range 12.9 - 13.1 % Al, as a result of the investigations of Kurdyumov and co-workers[77, 78]. This work also showed a strong dependence of the martensite start temperature (M_s) on aluminium content, falling with increasing aluminium. At aluminium contents of less than 10.5 w/o the martensitic transformation occurs before the ordering reaction and β' is formed which is a disordered version of β_1'[79,80].

2.2 Morphology and Kinetics of the Martensitic Transformation

The martensitic phases are brass coloured in contrast to the copper coloured β and β_1 phases - which aids observation of the

transformation under the light microscope. The martensites form in characteristic lenticular plates, those of β_1' tending to be narrower with very straight sides, and often forming in two interpenetrating sets[79]. γ' martensite plates are usually wider with curved boundaries, and fine parallel striations can be observed within the plates[79, 81].

Wasserman first noticed the reversible nature of the $\beta \rightarrow \beta_1'$ transformation and recorded that subsequent transformation began at similar temperatures[73]. Greninger found no such reversibility in $\beta \rightarrow \gamma'$[79] but this was reported by Kurdyumov et.al.[82] to occur with a large temperature hysteresis. For alloys containing nickel with an M_s temperature between $+10^{\circ}C$ and $-10^{\circ}C$ Kurdyumov reported[55] a reversible $\beta \rightarrow \gamma'$ transformation with no hysteresis. Later work [83, 84] has shown that a small hysteresis does exist for these alloys. These investigations also established that the extent of the transformation depended only on the temperature, and the rate of martensitic growth depended only on the rate of change of temperature.

The formation of martensite above M_s by the application of stress, and its disappearance on removal of the stress has been reported by several workers [62, 63, 83]. The increase in the stress hysteresis with increasing strain was recorded by Rachinger[63], and Kurdyumov et. al. [62] observed that in a single interface transformation

there was no reverse transformation on removal of the load. The dependence of martensite orientation on the direction of the applied stress was also recorded, metallographically; a different group of martensite plates grew when the direction of the stress was changed. Otsuka and Shimizu[67] deformed the γ' martensite in a similar alloy and observed that on heating to reverse the transformation to β-phase the original shape was restored. They proposed that the deformation was accommodated by the preferential growth of suitably oriented twins in γ', without slip, so that the reversibility of the transformation was not affected. All of the above investigations were carried out on alloys of approximately Cu-14.5 w/o Al - 3 w/o Ni as this composition has the transformation temperatures close to room temperature. They clearly indicate a thermoelastic type of transformation with little or no plastic deformation of β or γ' phases.

In contrast to this, alloys with M_s of approximately 400°C studied by Haynes[85] were reported to show an isothermal transformation to martensite. Hull and Garwood studying an alloy containing 12.8 w/o Al 7.7 w/o Ni [86] also observed isothermal transformation in addition to the athermal mode. They produced two martensites with different morphologies by different heat treatments. Quenching gave a fine acicular structure, slower cooling or "tempering" above the transformation temperature resulted in

broader plates. In view of their similar morphology to the binary martensites these were called β_1' and γ' respectively. No evidence of precipitation or solute segregation was observed and it was suggested that the γ' martensite was formed by segregation during ordering, which has some support from reports of Klier et.al (87, 88) on binary Cu-Al. This view is not substantiated however, by a later electron microscopy study of Cu-Al martensites by Swann and Warlimont(80) which indicated that the ordering process has no influence on the martensitic transformation. Furthermore γ' martensite which should correspond to the aluminium - rich martensite was observed to have a higher M_s in Hull and Garwood's work which conflicts with several other investigations showing a fall in M_s with increasing aluminium content.

2.3 Crystallography of Martensites

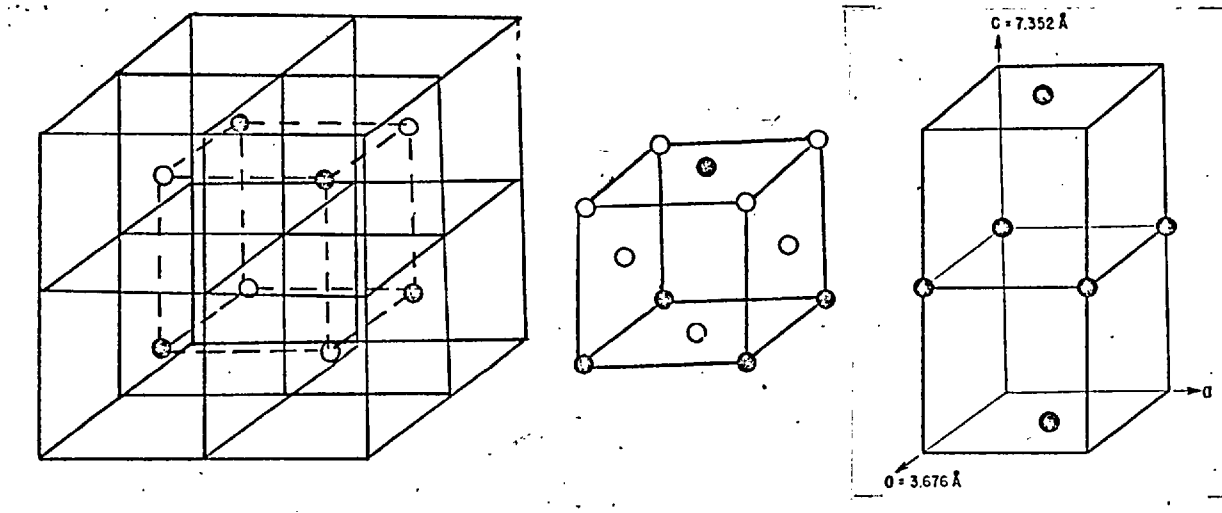
The first measurements of the martensitic structures were made by Kurdyumov et. al. (2, 89) and Greinger(79) using X-ray techniques. γ' martensite was reported to have an ordered h.c.p. structure with an orientation relationship of: $(00.1)\gamma' // (110)\beta_1$ and $[01.0]\gamma' // [1\bar{1}1]\beta_1$ and habit plane 3° from $\{122\}\beta_1$.

Kurdyumov et al.[89] on constructing the γ' from the β_1 structure from correspondence considerations discovered that although the lattice points have hexagonal symmetry the inheritance of the DO_3 ordering of β_1 results in orthorhombic symmetry of γ' structure, (appendix 1). This has been confirmed by later X-ray and electron diffraction measurements. The structure of β_1 was reported as distorted h.c.p. with habit plane 2° from $\{133\}\beta_1$. Swann and Warlimont[20] were first to examine the martensites by electron microscopy and their observations confirmed the previous results on γ'. They found β' and β_1' to be highly faulted structures giving diffraction patterns similar to an h.c.p. structure, but they proposed that the lattice was basically f.c.c. in each case. They identified internal twinning in γ' on $\{201\}$ and $\{121\}$ (orthorhombic) and faulting on $\{112\}$ in $<1\bar{1}1>$ β_1 (equiv. to 111 in $<11\bar{2}>$ β')(Fig. 2.4) in β_1' and β'. These they assumed to be the lattice invariant shear predicted in crystallographic theory. This is supported by the observation that, although the energy of stacking faults is expected to decrease with increasing aluminium content the density of stacking faults was found to be independent of composition within the β' and β_1' martensites and the twinned γ' martensite was observed at aluminium contents where the stacking fault energy is a minimum.

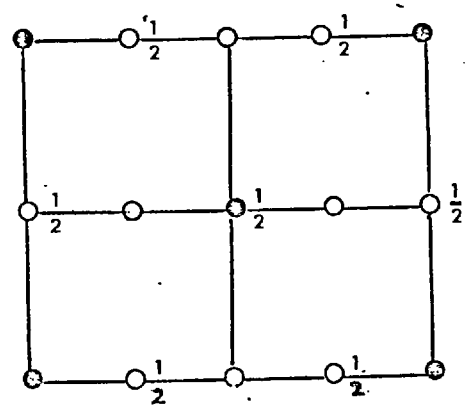
Mackenzie and Bowles[22] had earlier assumed from Greninger's metallography of γ' that the internal striations were due to twinning on $\{121\}$ or $\{201\}$ and predicted the ratio of

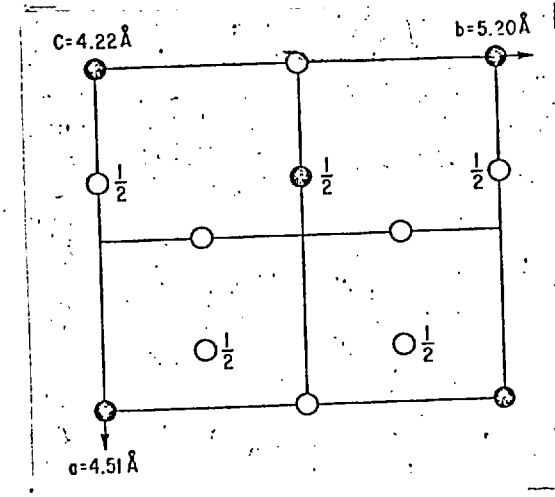
Fig.2.4 : Unit cells of Cu - Al structures.

● Aluminium atom ○ Copper atom



a) β_1 b.c.c. DO_3 order b) β' f.c.c. c) β_1' DO_{22} order structures shown before faulting





($\frac{1}{2}$ refers to the c co-ordinate)

d) DO_{22} (001) projection of c e) γ' orthorhombic (001) projection

thicknesses of the 2 twin orientations. Swann and Warlimont found some discrepancy when their experimental results were compared but pointed out that the twins were observed not to extend completely across the martensite plates as the theory assumes. They used the theory of Wechsler et. al. to calculate the extent of faulting in β' and β_1' and the discrepancy between calculation and experimental values was attributed to termination of faults in mid plate, since partial dislocations were apparent inside the plates.

Mackenzie and Bowles confirmed the habit plane of γ' observed by Greninger, using their theory, and Swann and Warlimont obtained good agreement with his measured β_1' habit plane, using the theory of Wechsler et. al.

Subsequent work on β_1' and β' has indicated that the faulting is systematic, rather than random as Swann and Warlimont proposed. Wilkins and Warlimont[90] have proposed a 22 layer structural period whereas Nishiyama and Kajiwara[91] favour an 18 layer period. Sato et. al.[92] carried out a detailed analysis of the diffraction patterns of the 3 martensites using a method they consider to have a general application to any close packed structure made up of a stacking sequence of close packed planes[93]. From this they conclude that the γ' structure is as previously determined and that β_1' β_1' have an 18 layer stacking period so that all martensites have the same basic close packed structure and the

differences are due to stacking variations in the DO_{22} structure.

The results of X-ray studies on γ' in nickel-containing aluminium bronzes[46, 55] have indicated that the structure and relations are comparable to those in the binary. Duggin and Rackinger[46] working on Cu-14.5Al-3Ni reported the lattice to be orthorhombic with cell parameters of : a = 4.41 Å, b = 5.31 Å, c = 4.22 Å, the interphase boundary to be between $\{221\}\ \beta_1$ and $\{331\}\ \beta_1$ with some scatter, and the orientation relation to be : $(101)\ [010]\ \beta_1 \parallel (001)\ [010]\ \gamma'$ giving a reconstruction identical to that of Kurdyumov et. al.[89]. This they expressed in matrix form as shown in appendix 1. Otsuka and Shimizu[94] using electron microscopy techniques on thin foil speciments of Cu-14.2Al 4.3Ni confirmed the structure of γ' but proposed an orientation relation of $(110)\ [1\bar{1}\bar{1}]\ \beta_1 \parallel (121)[2\bar{1}0]\gamma'$. which although it is produced by the same correspondence differs from that of Duggin and Rackinger by $4^{\circ}5'$ around $[\overline{7.23}\ \ 3.98\ \ 0.22]\ \gamma'$. They reported internal twinning on $\{121\}\ \gamma'$ and also that most martensite plates consisted of 2 twin related parts with the midrib or ridge being at $\{121\}\ \gamma'$ twin planes. They found the interface (habit) plane to be $\{331\}$ & reasoned that the two twin related parts existed to make possible a $\{331\}$ interface plane on both sides of the martensite plate. They also recorded faults within twins in (001) γ' planes which they suggested are not part of the

lattice invariant shear of the transformation.

Following the suggestions of Cohen et. al. (eqn. 1.6, section 1.4) Duggin and Rachinger have considered the relation between matrix dislocations and the martensite structure. Since the $\frac{a}{2}[111]$ β dislocation is no longer a perfect dislocation in the β_1 structure it is proposed that this can dissociate to produce stacking faults, one of which can create a similar atomic configuration in (110) β_1 to (001) γ'. The suggested growth of this into a plate is by a pole mechanism with an $a[111]$ β_1 as node, (appendix 2). Table 2.1 summarises the crystallographic details of the phases present in the composition range studied.

2.4 The Relative Stability of β_1' and γ' Martensites

Comparison between these martensites and ferrous martensites suggests that the transition from internally faulted β_1' to internally twinned γ' may be determined by the temperature of the transformation. Wayman[24] has shown that in iron-nickel alloys the mode of the lattice invariant deformation changes from slip to twinning as the nickel content increases and the M_s temperature decreases. It was suggested that this is in accordance with general

Table 2.1 : Crystallographic details of phases

PHASE	STRUCTURE TYPE	UNIT CELL DIMENSIONS a b c	REMARKS	REF.
α	f.c.c.(random)A1	3.61-3.66	0 to 9.0 $^{w}/_{o}$Al at R.T.	80
β	b.c.c.(random)A2	2.95	11.3 $^{w}/_{o}$Al at 672°C	80
		2.917	12.5 $^{w}/_{o}$Al	
β_1(m)	cubic (ordered) DO_3	5.84	11.9 $^{w}/_{o}$Al at 350°C, stoichometric composition Cu_3Al	80, 104
β'(m)	f.c.c.(random)A1		martensite 10-11 $^{w}/_{o}$Al	80
			stacking modulation 3R	92
β_1'(m)	tetragonal (ordered) DO_{22}	3.676 7.352	martensite 11-13.4 $^{w}/_{o}$Al	80
			stacking modulation 3R	92
γ'(m)	orthorhombic (ordered) DO_{22}	4.51 5.20 4.22	above martensite 13 $^{w}/_{o}$Al	80, 89
			finely twinned, modulation 2H	92, 104
γ_2	rhombohedral γ-brass type		stoichometric composition Cu_9Al_4	74

(m) = metastable

observations of deformation modes, which show a preference for slip at higher temperatures and twinning at lower.

The observations of faulting in the lower aluminium content martensites is surprising however, since as Swann and Warlimont pointed out[80] it is in this composition range that the stacking fault energy (of the low temperature f.c.c. α-phase) is appreciable. The transition to the internally twinned γ' martensite takes place at the composition where the s.f.e. falls to zero (approx. 13.5 w/o Al). This was explained by the assumption that the s.f.e. represents the free energy difference between f.c.c. and h.c.p. structures, so that the two coexist when s.f.e. = 0. The γ' structure is then presumably preferable on electron to atom ratio considerations. Sato et. al. developed this approach in a general theory of long period superlattices which was applied to these structures[92, 93]. The formation of such superlattices is due to the creation of Brillouin zone boundaries at the Fermi surface to reduce the energy of the electrons, they considered. In the b.c.c. β-phase alloys such as β CuAl the e : a ratio is approximately 1.5. Therefore if a transformation to a close-packed structure is to occur it cannot be to f.c.c. since the Brillouin zones so formed would increase the electron energies[95]. However the M = 1 structure which can be directly formed from the DO_3 ordered β_1 phase

is a lower energy form of a close-packed structure. The stacking order modulation of this structure is then a further effort to reduce the energy of the electrons. Thus the change in structure from $3_1'$ to γ' is seen as a change in modulation of the M = 1 structure due to changing e : a ratio. The fact that the order of appearance of several such modifications is found to be common in different alloys of this type[53] was held to support this theory.

This does however seem to be in conflict with the requirement of crystallographic theory for a heterogeneous shear which was attributed with some success to the $3_1'$ faults by Swann and Warlimont, and is present as twins in the γ' structure. The observation of partial dislocations within $3_1'$ plates also seems to point to a shear function for the faults. However the lack of agreement on the detailed structure of the $3_1'$ phase, and the observation of faults in γ' not believed to contribute to the lattice invariant shear do indicate that the relative significance of the chemical and mechanical factors is not yet completely understood.

CHAPTER THREE : EXPERIMENTAL METHODS

"Science is spectrum analysis;

art is photosynthesis."

Krans

CHAPTER 3 : EXPERIMENTAL METHODS

3.1 Preparation of Alloys

The majority of the alloys studied were made in the laboratory from electrolytic copper (99.999% purity), super-purity aluminium (99.999%) and mond-carbonyl nickel (99.95%). After surface cleaning the metals were cut into small pieces and 50 g. melts prepared. To reduce the loss of aluminium by evaporation this was wrapped in copper foil. Initially the samples were placed in silica tubes for melting by radio-frequency induction heating under continuous vacuum. This made possible a rapid quench cooling from the molten state to suppress segregation. If however, the aluminium came into contact with the silica during melting a reaction would occur and aluminium was lost as it adhered to the side of the tube. In later melts therefore an alumina crucible was placed inside the silica tube. This material is very sensitive to thermal shock and so heating and cooling had to proceed more slowly, and the crucible was wrapped with asbestos paper to prevent spillage in case of fracture.

The melting assembly was mounted vertically in the coil of the radio frequency generator which had a 25 kw 450 khz output. The temperature was raised to approximately 1250°C over 15 minutes and held there for about 20 minutes with agitation every minute since the frequency is rather high to promote good "eddy" stirring.

The melt was cooled gradually with frequent agitation to just below the solidus and then quenched in cold water. The resulting cylindrical ingots 50 mm long and 15 mm in diameter were homogenised for 20 hours at 950°C and then hot rolled to a thickness of 0.5 mm at 950°C.

Analyses of the alloys were performed in the college and are shown in table 3.1. With the exception of alloy A different samples from an ingot showed a lack of homogeneity of less than 0.1 %. Alloys C, F and H were prepared in the laboratories of United States Steel Corporation, Pittsburg, by a similar technique. Alloy G was used in work by Rachinger[63] and its preparation is described in that paper.

Heat Treatments

Discs 10 mm in diameter were machined from the hot rolled strip using a "Servomet" spark machine with copper cutting tool. Samples were mounted in Wood's metal which acts as a conducting adhesive. Solution heat treatment was performed in air, in a vertical quenching furnace built for this purpose. This had a 50 mm zone of constant temperature - (gradient $< 0.05^{\circ}C$ /mm). The specimen was held within a stainless steel heat shield to reduce heat loss during the descent into the quenching medium. Quenching was normally into iced brine, since a very fast quench is necessary to prevent γ_2 precipitation. The quenching rate was varied by the use of different media.

Table 3.1 : Composition of Alloys

CODE	w/o COPPER		w/o ALUMINIUM		w/o NICKEL	
	Est.[d]	Meas.[d]	Est.[d]	Meas.[d]	Est.[d]	Meas.[d]
A	84.4	86.5 - 85.5	14.4	12.3 - 13.3	1.2	1.2
B	84.6	85.0	14.2	13.8	1.2	1.2
C▲	82.9	83.0	14.1	13.8	3.0	3.2
D	85.8	86.0	14.2	14.0	0	0
E	82.8	82.9	14.2	14.1	3.0	3.0
F	82.9	82.9	14.3	14.3	2.8	2.8
F▲	82.6	82.9	14.6	14.3	2.8	2.8
G	82.5	82.6	14.5	14.4	3.0	3.0
H▲	81.5	81.6	14.5	14.4	4.0	4.0
J	84.3	84.2	14.5	14.6	1.2	1.2
K	82.5	82.6	14.5	14.6	3.0	2.8
L	85.4	85.0	14.6	15.0	0	0

▲ Prepared at U.S. Steel

Specimen temperature was measured by a thermocouple placed inside the heat shield, alongside the specimen .

Ageing treatments were performed in oil or salt baths capable of maintaining a constant temperature ($\pm$ 0.5°C) for long period of time. Step quenching was carried out by mounting the vertical quenching furnace over a salt bath; the specimen was then transferred by hand to iced brine for the final quench.

During these treatments it was found that the increase in surface oxidation of the specimens, over that suffered during hot rolling, was negligible.

3.2 Light Microscopy

The course of the martensitic transformation in polished specimens of these alloys can readily be followed optically due to an associated colour change.

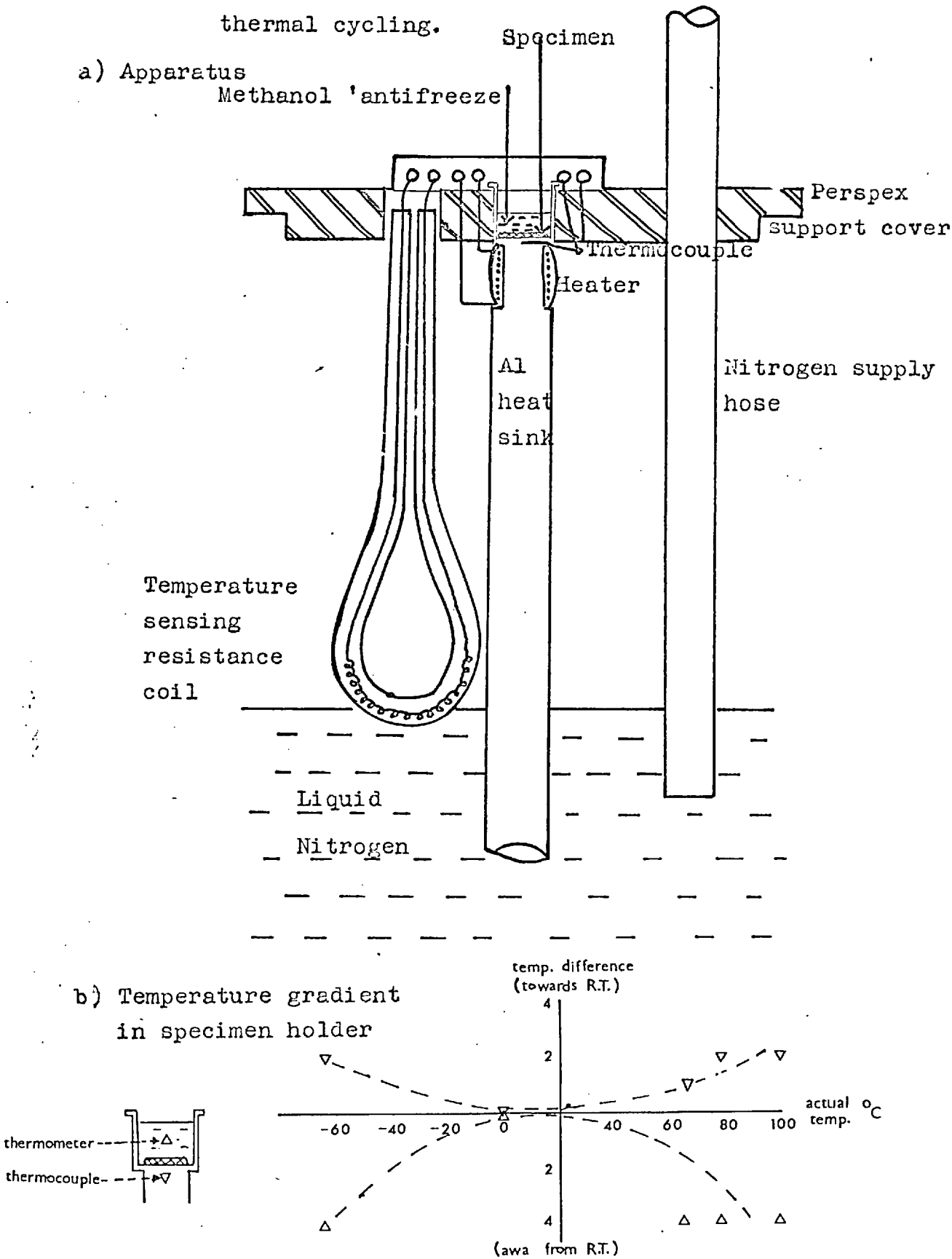
After the appropriate heat treatments the 10 mm discs were ground to remove oxide coating and the distorted layer so created removed by a chemical polish. The transformation is readily induced by deformation and this layer was always found to be martensite. Great care was necessary therefore in the handling of specimens to avoid inducing transformation in this way. The chemical polish used was an acid mixture of 50 cm^3 nitric, 25 cm^3 acetic, 25 cm^3 phosphoric

and 5 cm^3 hydrochloric. This gave a shiny but rumpled surface, which was finally prepared by electropolishing using a solution of 50 g chromium trioxide in 266 cm^3 of glacial acetic acid and 14 cm^3 water. This was used at a temperature of 0 - 10°C with a stainless steel beaker as cathode, and container for the electrolyte. The potential difference for polishing is approximately 30 v. giving a current density of 1.5 - 2.0 ma/mm^2.

Heating and Cooling Stages: Routine observations on the course of the transformation were made using a Bausch and Lomb binocular microscope having a continuous magnification range of up to X 45. A simple heating and cooling stage was built for use in these experiments; a diagram of the apparatus is shown if Fig. 3.1 a. Cooling was produced through the aluminium rod which rests in the liquid nitrogen reservoir; heating by a nichrome resistance furnace placed just below the specimen. Fig. 3.1 b shows the accuracy of temperature measurements possible with the apparatus.

This stage was also used for automatically cycling specimens through the temperature range of the transformation. The furnace was connected in circuit with a cam-operated switch such that it was on and off for alternate 30 second periods. The level of the liquid nitrogen reservoir was controlled automatically by the temperature sensitive resistance coil connected to a control unit which operated an electromagnetic relay. When the temperature rose, indicating a

Fig.3.1 : Heating and cooling stage for continuous thermal cycling.

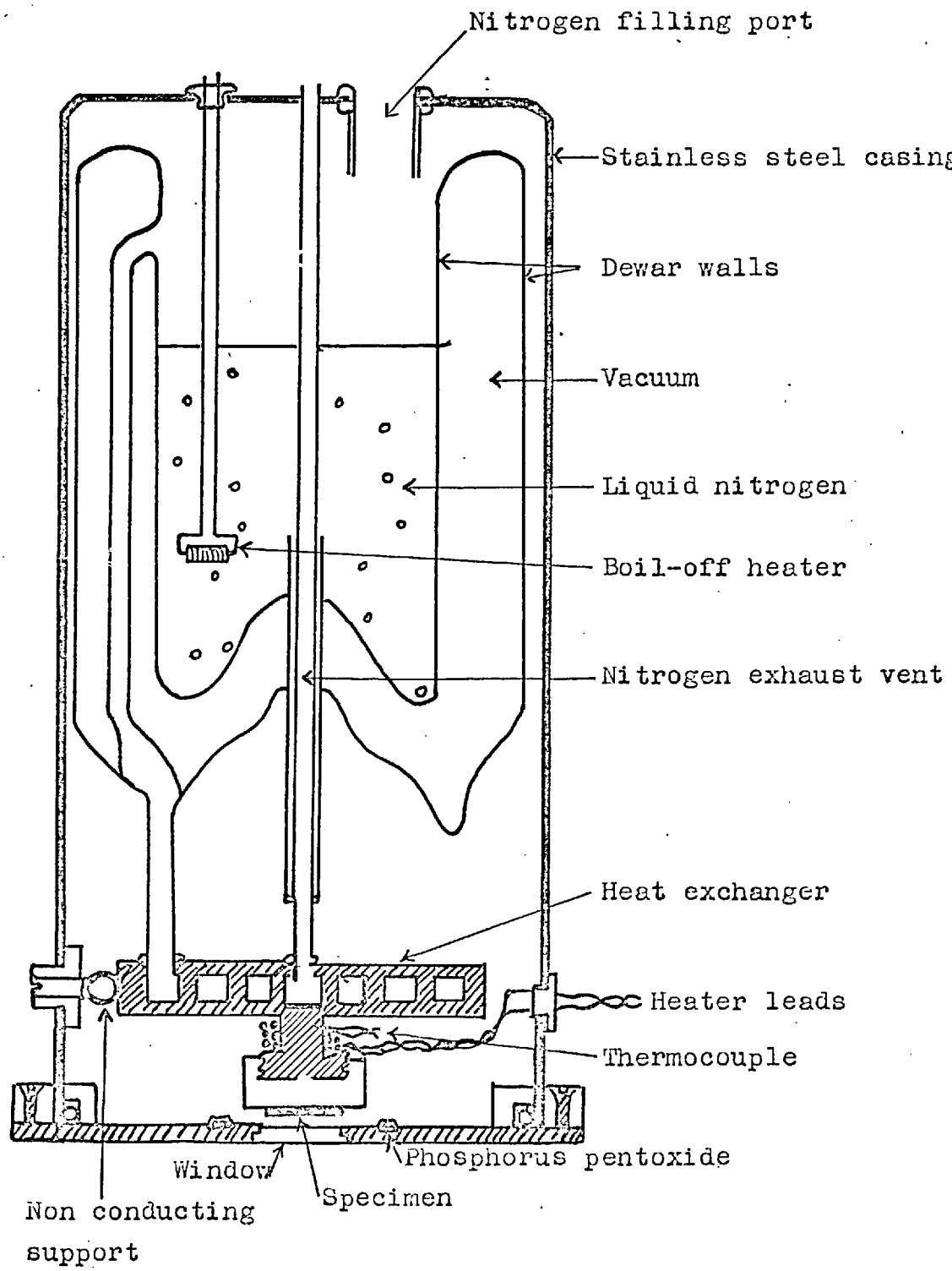


fall in the nitrogen level, the relay allowed the supply pipe from a storage cannister to open. When the level has risen sufficiently this was automatically clamped shut again.

Photography of the microstructures, and certain observations on the course of the transformation were carried out on a Reichert projection microscope, MeFI. The heating or cooling stage built for this purpose is shown in Fig. 3.2. Cooling was produced by nitrogen vapour passing though a heat exchange from a reservoir of liquid nitrogen. The rate of flow of vapour was controlled by a boil-off heater. Heating was produced by a similar furnace to the one previously mentioned. The volume of air cooled with the specimen was kept to minimum by packing; isolated from the atmosphere; and dried with P_2O_5 before cooling began, to prevent formation of ice on the specimen. The specimen, a 10 mm diameter disc, was set on an indium base with a smear of vaseline grease. It was situated 4.25 mm from the window to allow the use of a 16 X objective lens (5mm working distance) for magnifications of up to 250 X. Icing on the outside of the window was prevented by using a triple windowof cover glasses separated by teflon washers. Control of temperature was effected by a Erurotherm unit in circuit with either the specimen heater or the boil off heater for cooling.

Photography: Black and white micrographs were recorded on Ilford G30 chromatic backed plates in holders fitting the viewing port of the

Fig. 3.2 : Heating and cooling stage for projection microscope



microscope. Colour photographs were taken with daylight 35 mm colour negative strip film in a Leica back which was fitted to the microscope by standard extension pieces incorporating a reflex screen for photographing the exact area viewed. Cinefilm was taken on Ilford Mk 5 film with a Bolex Paillard camera using the same extension components.

3.3 Electron Microscopy

3.3.1 Specimen Preparation

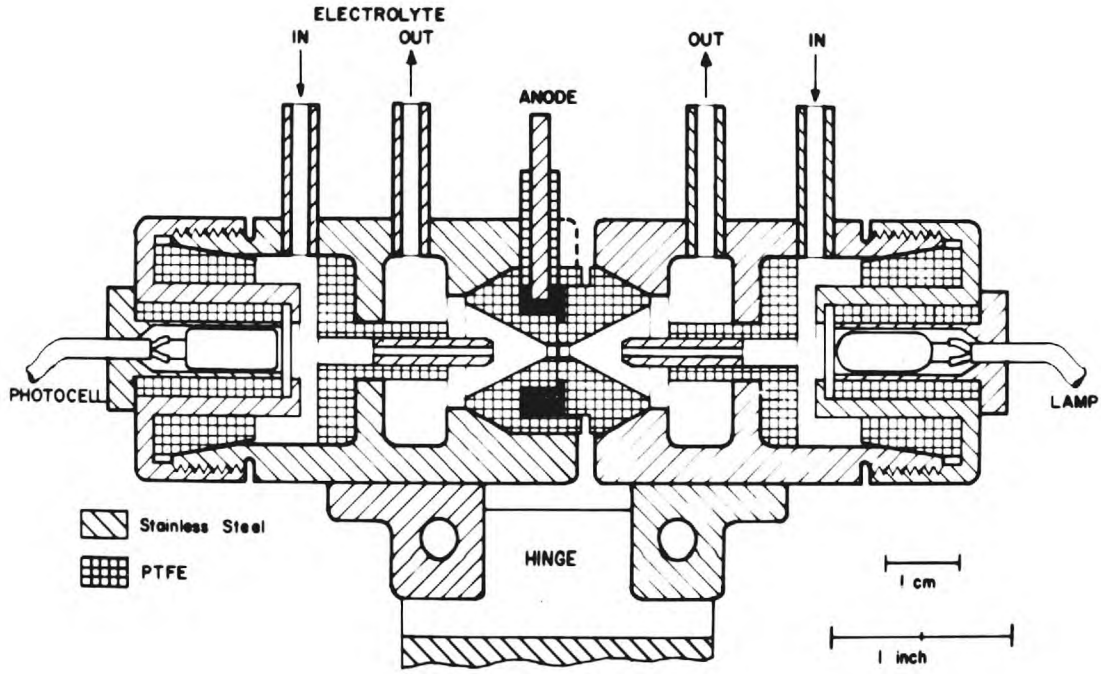
Thein foils were prepared from the bulk material by electro-polishing using either the Bollmann window technique or a jet technique. In each case the electrolyte was the chromic-acetic acid mixture used under the same conditions as for polishing the opical specimens.

Jet polishing offers a rapid, easily repeatable method of producing specimen discs which are easy to handle being much more robust than the fragments produced by the window technique. A jet polisher was developed in the group[96] for use with iron and copper alloys. It was found that the polishing conditions using the chromic-acetic electrolyte were almost identical for all alloys polished, although these conditions were very critical for production of satisfactory thin foil specimens. The instrument is shown in Fig. 3.3.

Fig.3.3 : Jet polishing apparatus



a) External appearance, with teflon specimen holder in position on the left.



b) Cross-section showing details of construction.

Discs are spark cut from the rolled strip, thinned by chemical polishing to 0.125 mm, so that they will fit directly into the specimen holder of the electron microscope (2.3 mm diameter for the Siemens Elmiskop I and 3 mm in diameter for the EM6G). The disc is then clamped into a teflon holder fitted with an electrical contact and located between the jets. The electrolyte is gravity fed and recirculated by a small pump. Perforation is detected by the photocell which is aligned with a small bulb though the jets. Detection automatically switched off the current to prevent preferential attackof the thinned regions. The specimen is removed from the holder and carefully washed in water and methanol.

A number of parameters such as flow rate, current, water content of electrolye and dimension of specimen holder govern the profile and surface of the polished disc[96] and precise setting of these is of considerable importance to produce good specimens. Once the settings have been determined however a whole series of specimens can be polished quickly. The time for polishing the alloys in this work was approximately 6 minutes. The technique is particularly valuable for multiphase structures since the jetting action removes the preferential polishing which occurs in window methods.

For the "in-situ" studies of the transformation specimens were required which contained as much of the foil as possible transparent to the electron beam. The Bollmann Window technique was used for this,

starting with the 10 cm diameter 0.5 mm thick optical specimens and a double pointed, stainless steel cathode.

3.3.2 Observations with the microscopes

Two models were available for use in the department: the Siemens Elmiskop I which was used for most of the dark field work, for example in the ordering study; and the AEI EM6G which was fitted with a double tilt cooling/heating stage during the course of the work for the "in-situ" studies of the transformation.

The Heating/Cooling Stage operated on the same principle as that described for use with the Reichert projection microscope; heating was by a small furnace located close to the specimen holder, cooling by nitrogen vapour, controlled by a boil off heater in a reservoir of liquid nitrogen mounter on the side of the microscope. The nitrogen passed into the microscope through flexible bellows and cooled the specimen through a hollow copper annulus close to the specimen holder. The apparatus has a temperature range of approximately -160°C to + 40°C and is capable of high stability of temperature and ideal control characteristics. These attachments were incorporated in a tilting stage which permitted tilts of up to 60° in 2 orthogonal directions.

(An observation of a partially transformed specimen was made using the 1 MV A.E.I. EM7 microscope which was installed in the department at the end of the period during which this research was carried out)

3.4 Thermal Analysis

Cooling and heating curves for several of the alloys were obtained using apparatus at the Royal Aircraft Establishment, Farnborough, which has been described elsewhere[97, 98]. Discs 3 mm in diameter, 0.25 mm thick were annealed in a vacuum and could be cooled at varying rates by simulataneously switching off the heater and admitting Helium at different temperatures and pressures. Cooling rates of from 25°C/sec to 1000°C/sec were used in the present work. The temperature was detected by means of a Pt -13% Rh thermocouple spot welded across the faces of the specimen, and recorded by a variable speed, ultraviolet spot recorder.

CHAPTER FOUR : EXPERIMENTAL RESULTS

"In the field of observation, chance favours only the prepared mind."

Pasteur

CHAPTER 4 : EXPERIMENTAL RESULTS

This investigation of a martensitic transformation has proceeded by studies of the effects of various factors on the course, and nature of the transformation, which might be expected to give information about the kinetic and nucleation processes occurring. Preliminary investigations were necessary however, to develop a suitable alloy, in view of the uncertainties in previous work on the metastable transformation in Cu-Al-Ni. An alloy was required with an Ms around room temperature, and in which the precipitate of aluminium-rich γ_2 phase was suppressible. The influence of the ordering reaction on the martensitic transformation was also a subject of some uncertainty.

A report of the results of investigations on the metastable phase relationships in a range of Cu-Al-Ni alloys precedes the investigations on the martensitic transformation itself.

4.1 The ordering reaction $\beta \rightarrow \beta_1$

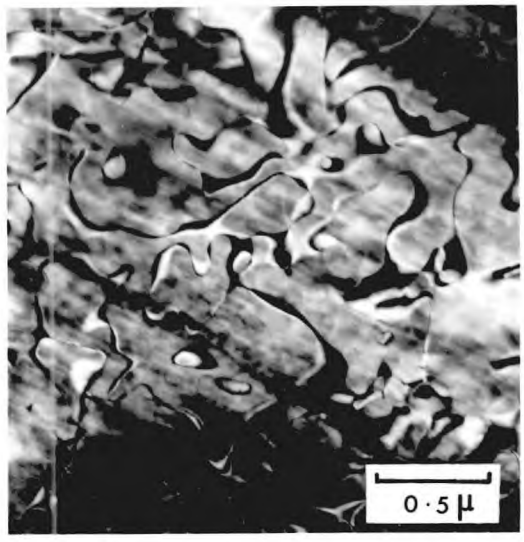
This reaction is readily studied by electron microscopy due to the contrast effects of the antiphase vector operating between

domains of order. This contrast shows up particularly well in dark field using a superlattice reflection. Domain contrast was exhibited by all alloys studied, which included alloys quenched at rates up to 1000 ^{o}C/sec.

Two types of displacement are possible between the domains of an ordered DO_3 structure. These are a/4 <111> and a/2 <100> and have been designated[74] as B2 and DO_3 antiphase boundaries respectively. This is because the a/4 <111> type displacement is present as antiphase boundaries in the B2 ordered structure. Since these two displacements give different antiphase angles, reflections can be selected which show up one type and not the other. Superlattice reflections of the type: h, k, l all odd (S_1) will produce contrast from both types of boundary, whereas reflections of the type: hkl all even but (h + k + l)/2 odd (S_2) produce contrast only from the a/4 <111> B2 type displacements. [Reflections of the type khl all even and h + k + l /2 even do not produce any domain boundary contrast since they are not superlattice reflections.] Fig. 4.1.1 shows the domain structure exhibited under the two types of reflection. It will be noticed that the B2 boundaries are fewer (B2 interboundary distance $\simeq$ 2X DO_3 interboundary distance); and also that it is difficult to distinguish the two types of boundary in an S_1 reflection micrograph.

The ordering temperature can be investigated by electron

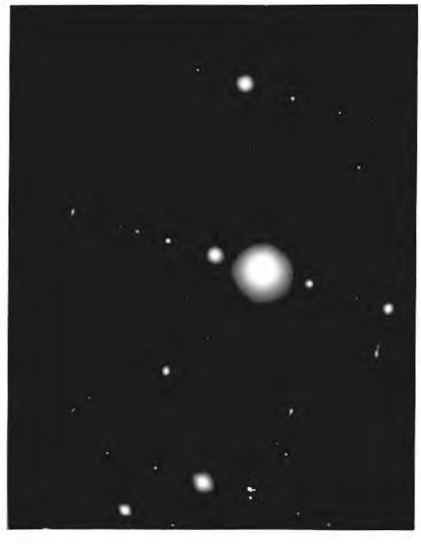
Fig.4.1.1 B2 and DO_3 type domain boundaries
(Alloy F, 1 hour at 950°C - Q in iced brine)

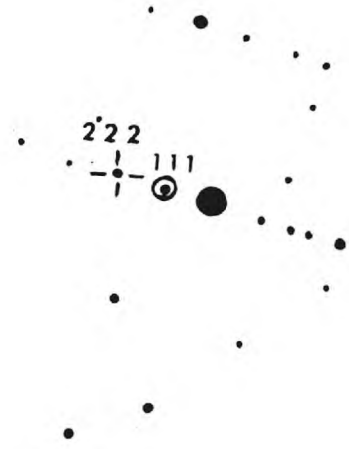


a) Dark field (D.F.)
g =<222> B2 type



b) Field as a)
g =<111> DO_3 and B2 type





c) Selected area diffraction pattern (S.A.D.P.) of a) and b)
showing reflections used in a) ⊣⊢ and b) ⊙

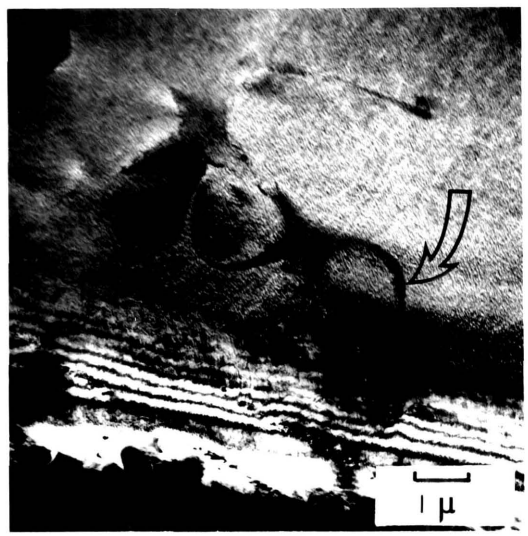
microscopy if specimens are made of step quenched alloys. If the alloy is held just below the ordering temperature then quenched, the domains will be large with few domain boundaries visible under the microscope, since considerable growth will have occurred. Holding just above the ordering temperature on the other hand, results in very small domains and many boundaries. The ordering temperatures in Cu-Al-Ni alloys close to Cu_2AlMn have been determined to an accuracy of better than $\pm$ 5 °C by Bouchard[99] using this technique.

Applied to the present alloys the technique led to the discovery that the ordering to DO_3 from disordered β (bcc) takes place in two stages, not one as previously assumed.

Fig. 4.1.2 shows the appearance of a specimen quenched from 950 °C to 520 °C, held for 10 seconds and then quenched into iced brine. 4.1.2 a using S_2 type shows that the B2 b'dies have almost completely disappeared due to complete ordering to B2 and growth of the domains. 4.1.2 b however shows a similar density of DO_3 boundaries to that in specimens quenched directly from 950 °C. It is concluded that these have formed during the second quench, i.e. below 520 °C, whereas the ordering to B2 occurs above 520 °C.

Extensive use of this technique is prevented in these alloys, however, by the rapid precipitation of γ_2, and confirmation of the

Fig.4.1.2 Two stage ordering in step quenched specimen (Alloy H; 1 hour at 960°C - 10 s at 520°C - Q)



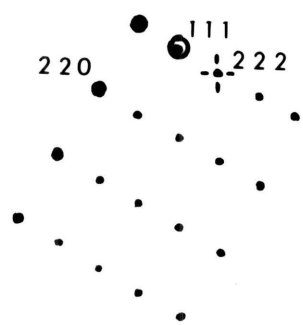
a) High resolution dark field (H.R.D.F.) **g** = <222> isolated B2 boundary

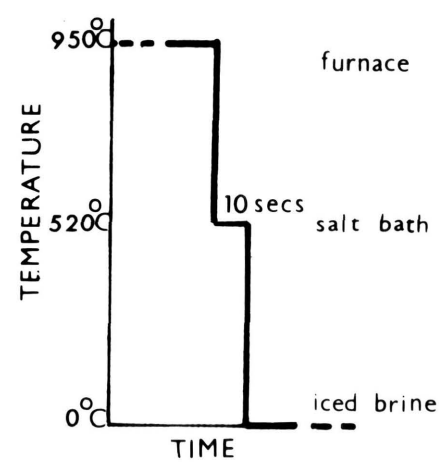


b) Field as a) g = <111> DO_3 boundaries and B2(→)



c) S.A.D.P. of a) ⊹ and b) ⊙





d) Step quench heat-treatment

above observation was sought by thermal analysis.

Nine alloys containing 0-4 w/o Ni and 13.3-15.0w/o Al were heated and cooled at varying rates. A typical heating and cooling cycle is shown in Fig. 4.1.3.

The results were again complicated by precipitation of γ_2 in some alloys, as shown by subsequent examination of thin foils made from the specimens. Table 4.1 shows the thermal arrest temperatures. The DO_3 ordering arrests, which are plotted against aluminium content, in Fig. 4.1.4. Several arrests were recorded for each specimen. The arrrests due to the precipitation of γ_2 and the martensite transformation could be identified by electron and light metallography. All specimens examined showed an arrest in the range 500 - 550 °C and those of aluminium contents greater than 13.8 w/o showed a second arrest at a temperature between 600 °C and 720 °C. The latter temperatures, which are believed to indicate the ordering to the B2 structure, increase with increasing aluminium content. The arrests in the 500 - 550 °C range are then identified with the ordering to the DO_3 structure, from B2 order in higher aluminium alloys. Although the results for a particular alloys are consistent there is a variation in the recorded temperature arrests which cannot be related to aluminium or nickel content of the alloys (the results from alloys B and C containing 13.8 w/o Al, 1.2 and 3.2 w/o Ni respectively, were

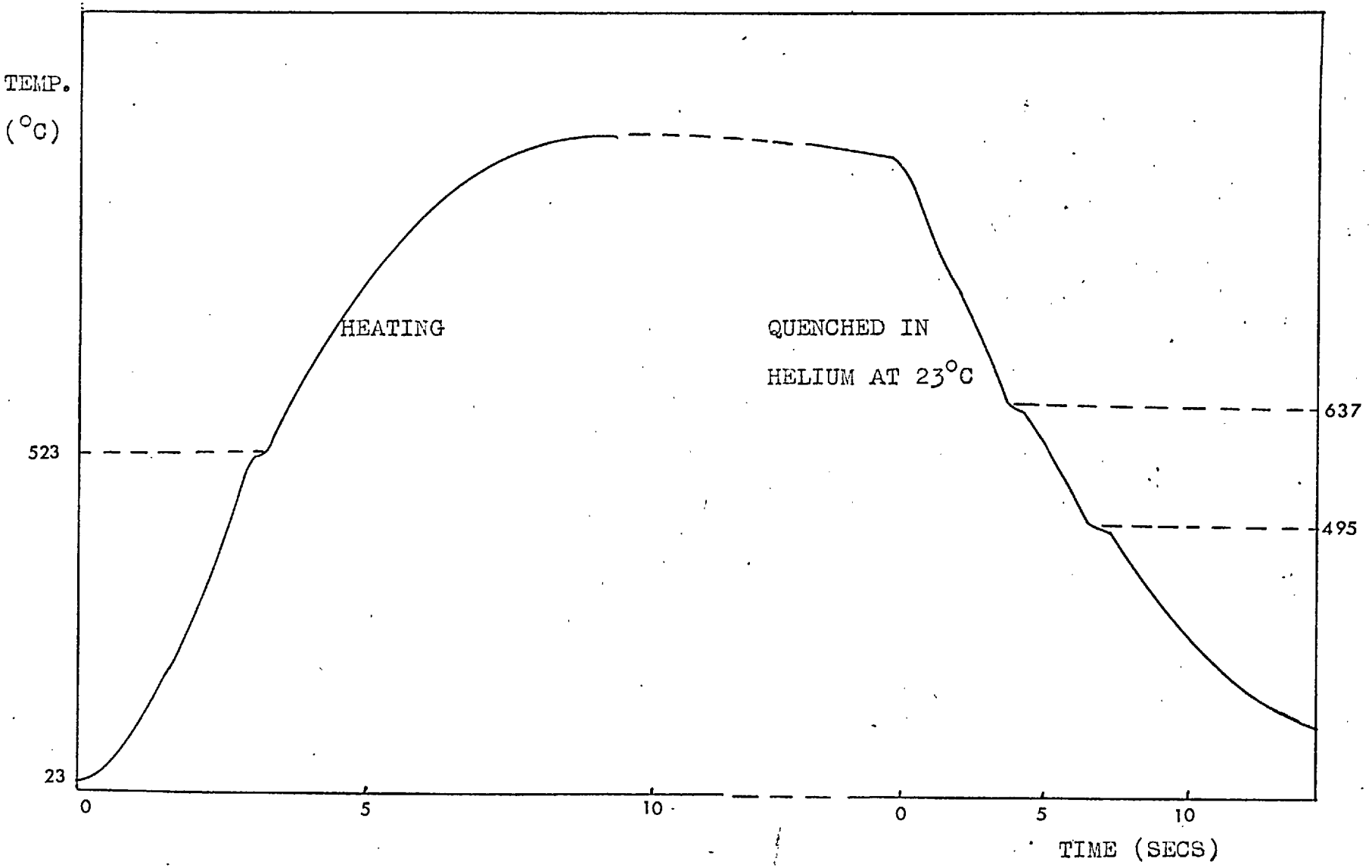
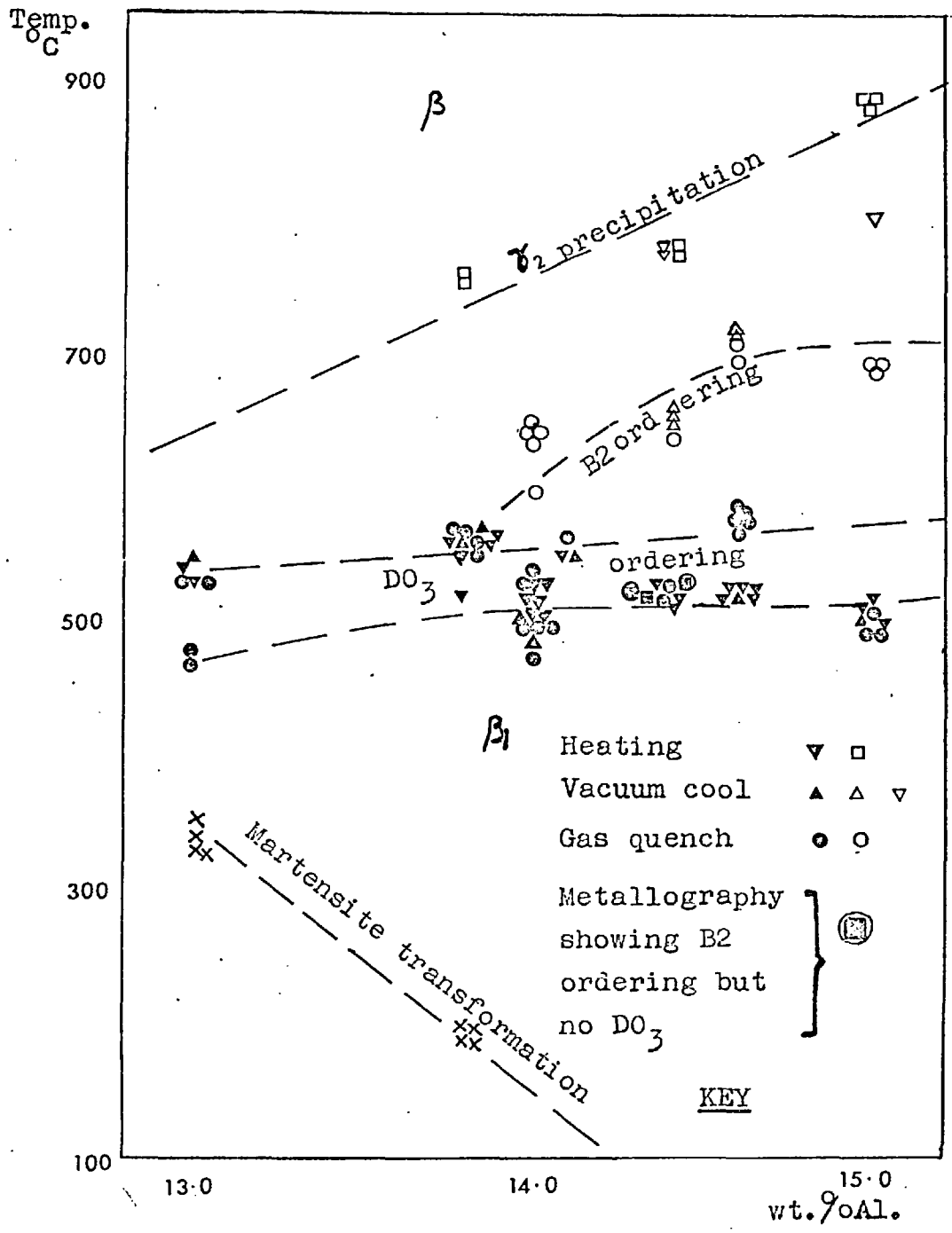


FIGURE 4.1.3: Thermal Analysis of alloy D.

TABLE 4.1 : THERMAL ARREST TEMPERATURES

ALLOY Al w/o	Ni w/o	CODE	γ_2 precipitation GAS QUENCH	γ_2 precipitation COOL (VACUUM)	γ_2 precipitation HEATS	θ_2 ordering GAS QUENCH	θ_2 ordering COOL (VACUUM)	θ_2 ordering HEATS	DO_3 ordering GAS QUENCH	DO_3 ordering COOL (VACUUM)	DO_3 ordering HEATS	Martensite transformation GAS QUENCH	Martensite transformation COOL (VAC.)	Martensite transformation HEATS
15.0	0	L		800	889 889 881	684 684 680			502 493 493	499	507 498 517			
14.6	1.2	J				(709) (675)	715 718		580 575 568 568 562	516	516 521 514 513 523	 (90) (92)		
14.4	4.0	H		(769) (766)	(784) (768)	(615	642 628 617		512 525		511 509 (525)			
14.1	3.2	E							556	550	550			
14.0	0	D				637 643 593 637 633			495 537 470 499 499	504 492	523 523 507 517 523 507			
13.8	3.2	C			(756) (752)				552 551	553	(543) 552 551			
13.8	1.2	B							561 561	561	516 557 557	~90 ~185	185-207 190 190-213	
13.0	1.2	A							462 457 525 525	542	525 530	~330 ~340 339-309 329-293	~324	~45 ~36

Fig.4.1.4: Thermal analysis results on the β-phase ordering reactions.



identical, within the limits of experimental error). Nor, in general, did the cooling rate affect the arrest temperature. The metallographic observations on the step-quenched specimens are in agreement with these interpretations of the thermal arrests; plotted on Fig. 4.1.4 they lie between the upper (B2) and lower (DO_3) temperatures so that no B2 domain boundaries are seen, due to complete ordering and the DO_3 ordering occurs during the quench to 0 °C so that the domains are the same size as those in directly quenched specimens.

The DO_3 ordering temperatures recorded by these alloys are in agreement with the results of Kurdyumov[75 a] obtained by high temperature X-ray measurements, rather than those of Elo[75] from light metallography of isothermally transformed specimens. The latter technique must however be used with caution in these alloys since the speed of the ordering and precipitation reactions and the similar morphologies of different phases can produce misleading effects.

The present observations, though not extensive have confirmed that the ordering reaction to DO_3 is insuppressible even at cooling rates approaching 1000 °C/sec; that it occurs in the temperature range 500 - 550 °C, rising slightly with increasing aluminium content, and independent of nickel content; and that a two-stage ordering reaction involving the formation of a B2 structure occurs in alloys of higher aluminium content. This is

similar to the ordering reactions reported in Fe-Al near Fe_3Al (100) and Cu-Al-Mn near Cu_2AlMn(99).

It should be emphasised that the presence of a/4 <111> type antiphase domain boundaries does not imply initial ordering to B2 structure, since these can be produced during direct ordering to DO_3 structure. Nor is it possible to determine from the morphology of the domain structure at room temperature whether the formation of DO_3 order occurred in one or two stages. Although in the formation of DO_3 from disordered B.C.C. there are four possible site permutations whereas in forming B2 there are only two, from each of which there are two possibilities for further ordering to DO_3, it can be shown that the resulting proportions and shapes of boundaries with a/2 <100> and a/4 <111> displacements are identical.

4.2 The Precipitation Reaction $\beta \rightarrow \beta_1 + \gamma_2$

The β phase exists over a narrow composition range, the hypereutectoid limit being a steeply rising boundary marking the start of γ_2 precipitation (Fig. 2.1).

Quenching from a series of temperatures determined the $\beta / \beta + \gamma_2$ boundary in alloy F (14.3 w/o al, 2.8 w/o Ni) to be 840 °C ± 10 °C in agreement with Alexander(76). After solution treatments

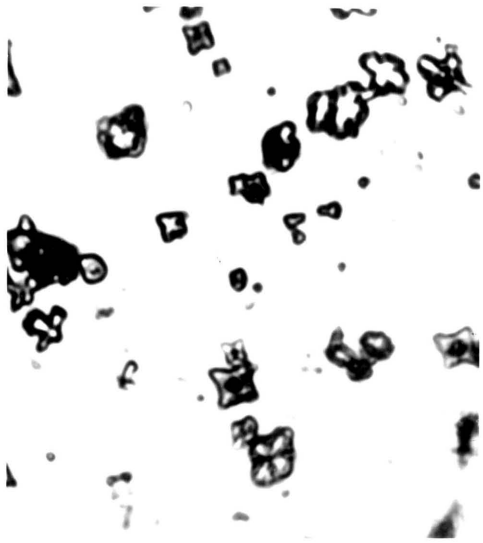
at 960 °C, the temperature at which has maximum composition range, quenching into iced brine suppressed the precipitation in all but alloy L (15 w/o Al) as expected. It was found that these very fast quench rates (> 1000 °C/second) were necessary to suppress γ_2 precipitation in the alloys of higher aluminium content; the quench rate becomes less critical for alloys approaching the eutectoid composition (Table 4.2).

QUENCHING MEDIUM	ALLOY	B	E	F	K	J	L
	ALUMINIUM CONTENT w/o	13.8	14.1	14.3	14.7	14.7	15.0
Vacuum ~30 °C/sec		β_1					
CCl_4 at 20 °C			$\beta_1 + \gamma_2$	$\beta_1 + \gamma_2$	$\alpha + \gamma_2$	$\alpha + \gamma_2$	
Water at 60 °C			β_1	β_1	$\beta_1 + \gamma_2$	$\beta_1 + \gamma_2$	$\alpha + \gamma_2$
Brine at 0 °C			β_1	β_1	β_1	β_1	$\beta_1 + \gamma_2$

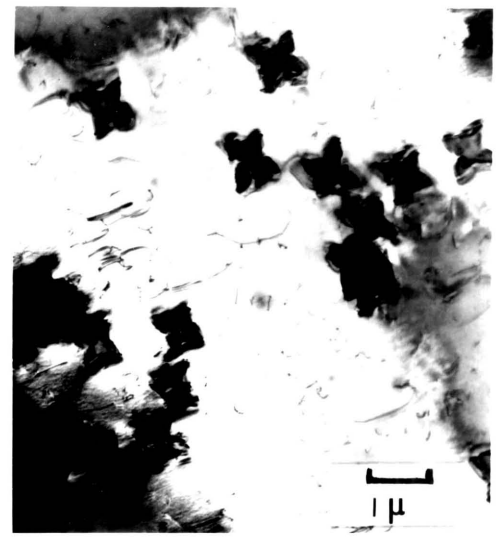
TABLE 4.2

The γ_2 precipitates formed during the quench were commonly found to have a "rosette" shape (Fig. 4.2.1 a) although more irregular shapes were found after slower cooling (Fig. 4.2.2). The structure

Fig.4.2.1 : γ_2 precipitation



a) Light micrograph (LM) Alloy K - Q H_2O at 60°C from 950°C. (x750)



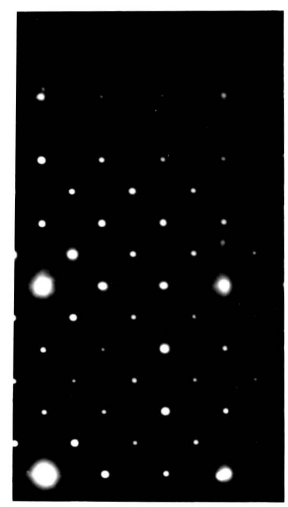
b) B.F. Alloy G γ_2 precipitation in the microscope by beam heating

γ_2 precipitation during quench.

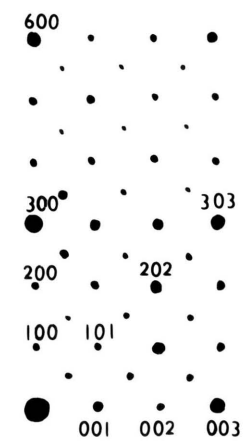
Fig.4.2.2 : Structure of γ_2



a) B.F. Alloy H vacuum cooled from 950°C. Massive γ_2 precipitation.



b) S.A.D.P. γ_2 in a)



was determined, by diffraction analysis, to be cubic with lattice parameter a $\simeq 9$ Å (Fig. 4.2.2 b) which is 3 X the lattice parameter of the disordered β - phase. This is in agreement with the pseudo γ-brass structure proposed by Swann[74] (Fig. 2.2.) Fig. 4.2.3 a is a bright field micrograph of a rosette of γ_2 in β_1 matrix and Fig. 4.2.3 b is a dark field picture of the same area taken using an S_2 type superlattice reflection to show the B2 domains. It is apparent from the diffraction pattern (Fig. 4.2.3 c) that:

$$a(\gamma_2) \quad = \quad 3a(\beta) \; = \; \frac{3}{2}\, a\,(\beta_1)$$

and that the orientation relationship is of parallelism between similar lattice vectors.

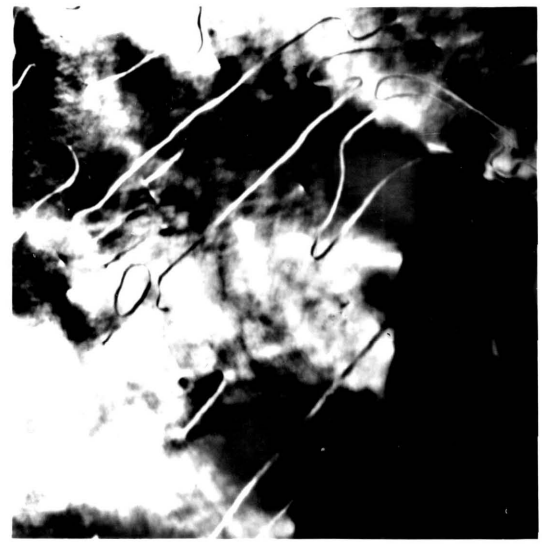
The tips of the rosettes point in <110> directions which is understandable as these are the close packed directions in the close packed {111} planes of b.c.c.

A study was made by electron metallography of the development of the γ_2 precipitates in aged β_1-phase specimens. The reaction was found to proceed rapidly at low temperatures as would be expected from the foregoing results on precipitation during cooling. The first stage which was detectable metallographically was a very fine distribution of particles on the order domain boundaries, although M_s measurements indicated a change in solute distribution at earlier stage than this (section 4.8)

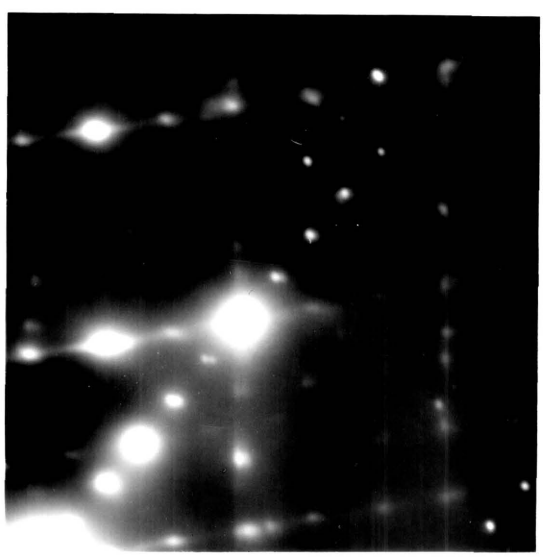
Fig.4.2.3 : γ_2, β and β_1 relationships (Alloy H)

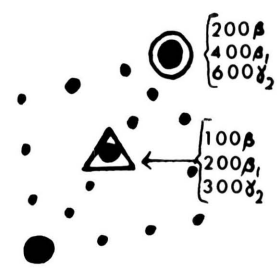


a) BF g = <400> β_1 Large γ_2 rosette in β_1 matrix.



b) DF as a). g = ⟨200⟩ β_1 β_2 domains contrast in β_1 matrix.





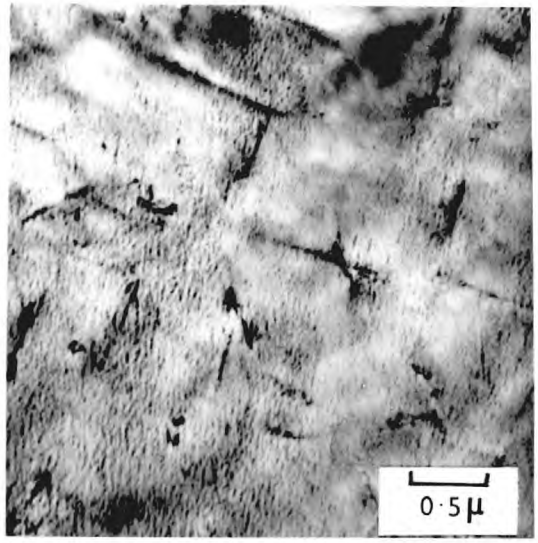
c) S.A.D.P. of γ_2/β_1 boundary showing β_1 F reflection ⊙ as in a), β_1 S_2 reflection △ as in b) and γ_2 reflections.

Precipitation on domain boundaries was observed after 1 hour at 150 °C, in agreement with observations of Swann[74] on a similar alloy. At 200 °C precipitation was observed on ageing for only 10 minutes (Fig. 4.2.4). The particles then rapidly developed into linear clusters and can be observed associated with similarly shaped dislocations, to produce a "shadow" effect (Fig. 4.2.5 a). Subsequent coarsening of the particles occurred (Fig. 4.2.5 b) and the rows became less predominant until a fairly random arrangement of cuboid precipitates was observed on dislocations after 16 hours at 200 °C (Fig. 4.2.5 c). Atlonger times and higher temperatures the "rosette" shape developed (Fig. 4.2.5 d). The development of the γ_2 precipitates with time and temperature is shown schematically in Fig. 4.2.6 for specimens of alloy H.

Similar rosette shaped morphology was observed in γ_2 precipitated in thin foil specimens by the heating effect of the electron beam of the microscope (Fig. 4.2.1 b).

The effect of the precipitation reaction on the martensitic transformation is considered in section 4.8.

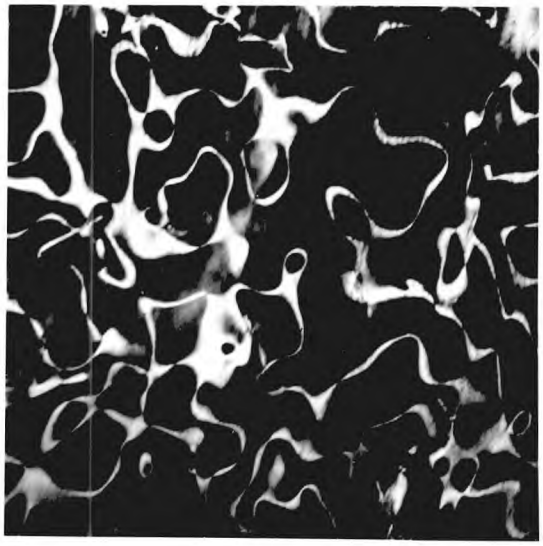
Fig.4.2.4 : γ_2 precipitation at domain boundaries.
(Alloy H, 1 hour at 950°C - 10 mins at 200°C).



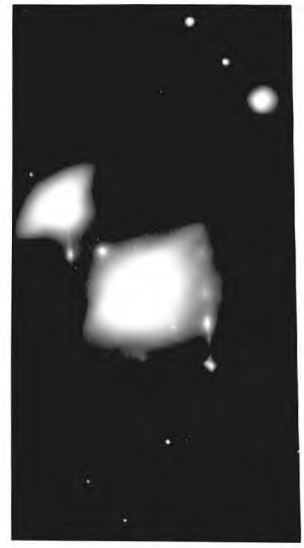
a) B.F. g = <400>
very fine γ_2 particles and dislocations.

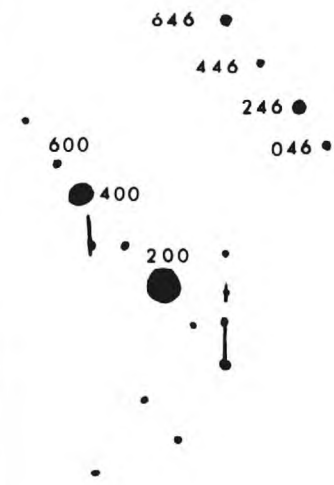


b) B.F. as a) g = <200>
B2 domains



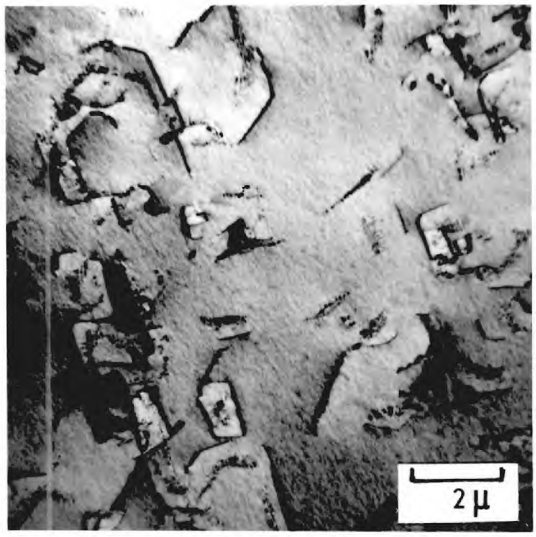
c) H.R.D.F. as b) g = <200>
B2 domains



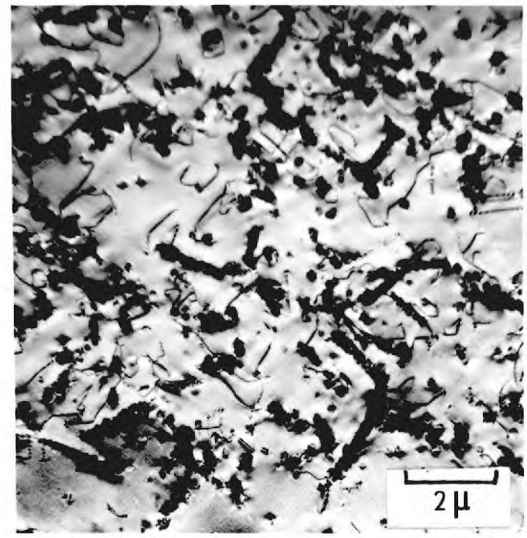


d) S.A.D.P. of a), b) and c).

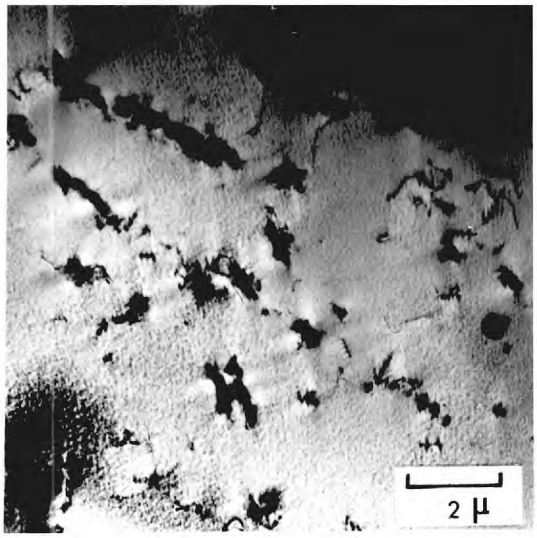
Fig.4.2.5: Y_2 precipitate growth morphology (Alloy H, 1 hour at 950°C)



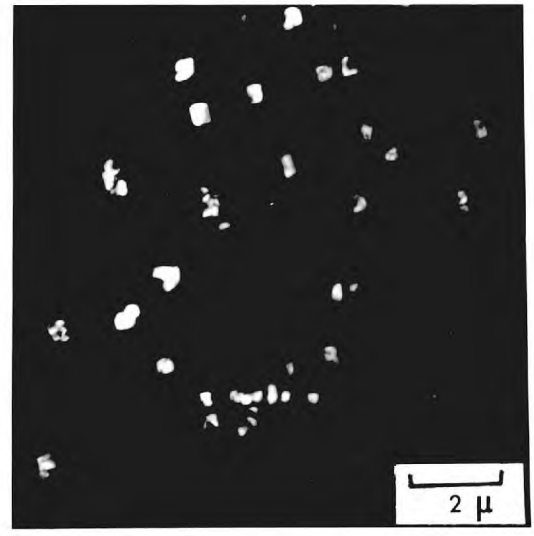
a) B.F. aged 2 hours at 200°C. Clusters of fine Y_2 particles "shadowing" dislocations.



b) B.F. aged 4 hours at 200°C. Lines of coarse particles, with some isolated particles



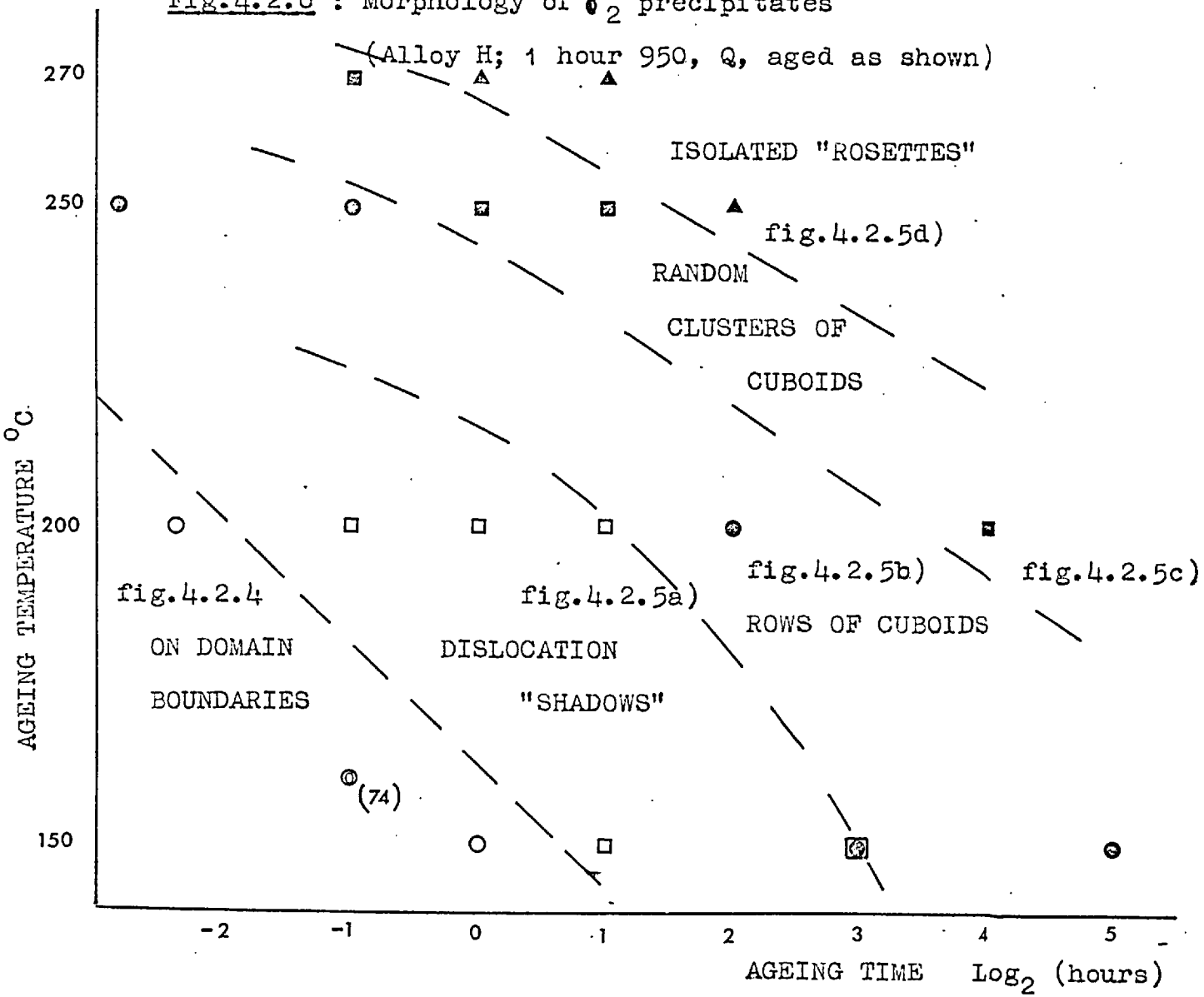
c) B.F. aged 16 hours at 200°C. Random distribution of cuboid particles.



d) D.F. aged 4 hours at 250°C. Particles developing rosette shape.

Fig.4.2.6 : Morphology of γ_2 precipitates

(Alloy H; 1 hour 950, Q, aged as shown)



4.3 The martensite reaction $\beta_1 \rightarrow \beta_1'$ or γ' :General Features

The colour change of the transformation and the change in external morphology of the martensite plate with composition are illustrated in Fig. 4.3.1. In the alloys containing 13.8 w/o Al or less, a fine network of acicular martensite is formed which differs markedly from the broad plates of the martensite in alloys with higher aluminium content. In these plates there is usually a "midrib" separating two sections of the plate with different orientations. Within the plates fine striations can be seen which are usually parallel but often irregular at the junction of plates (Fig. 4.3.1 d).

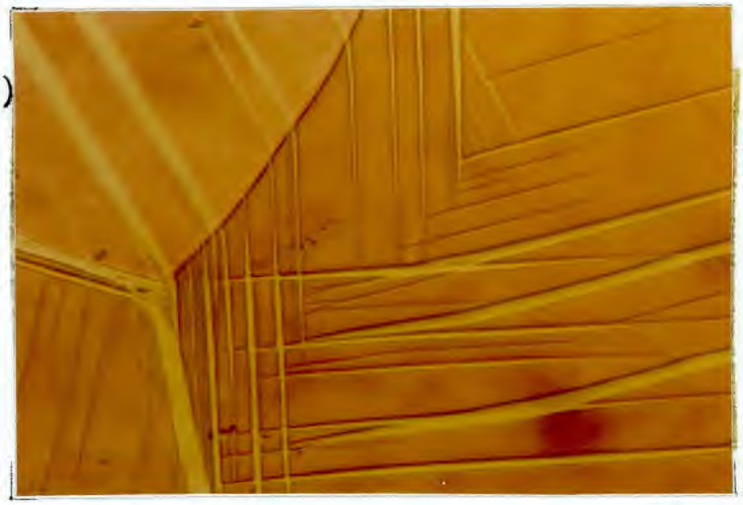
These morphological differences are more readily apparent under the electron microscope (Fig. 4.3.2). In the alloys of lower aluminium content the clusters of narrow, parallel-sided plates show numerous parallel striations of varying contrast. The broad plates of alloys of higher aluminium content by contrast. show twinning on a fine scale, changes in direction being accomplished by twins of more than one system in a particular plate.

The size of the martensite plates shows great variation. The largest (up to 5 mm in length) are those formed first since they then partition the matrix and so a continual reduction in plate size occurs as the transformation proceeds (Fig. 4.3.1 d).

Fig.4.3.1 : Martensite Morphology

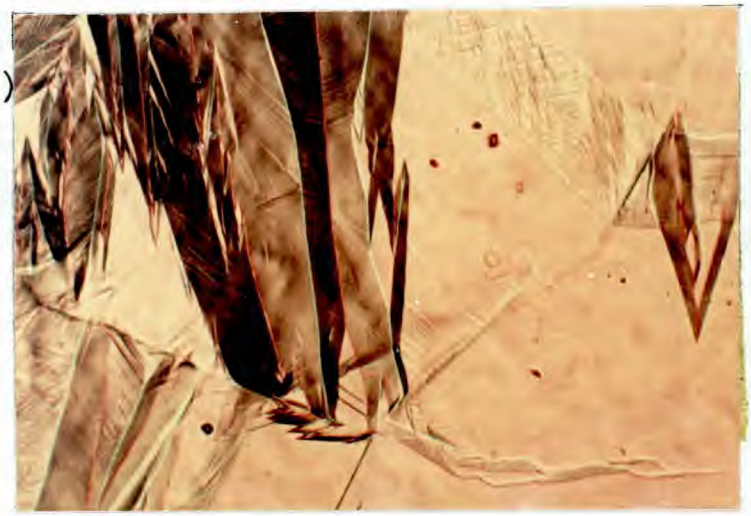
a) Alloy B ($13.8^{W}/_{o}Al$)

X250



b) Alloy F ($14.3^{W}/_{o}Al$)

X110



c) Alloy F :

martensite plates with long and short axes perpendicular to the surface.

X110

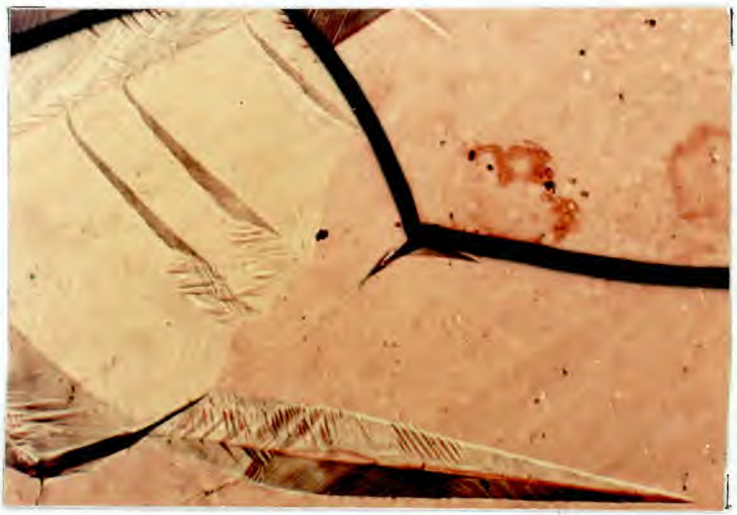


Fig.4.3.1: Martensite morphology



d) L.M. Alloy B (13.8 ^{w}/o Al) X48

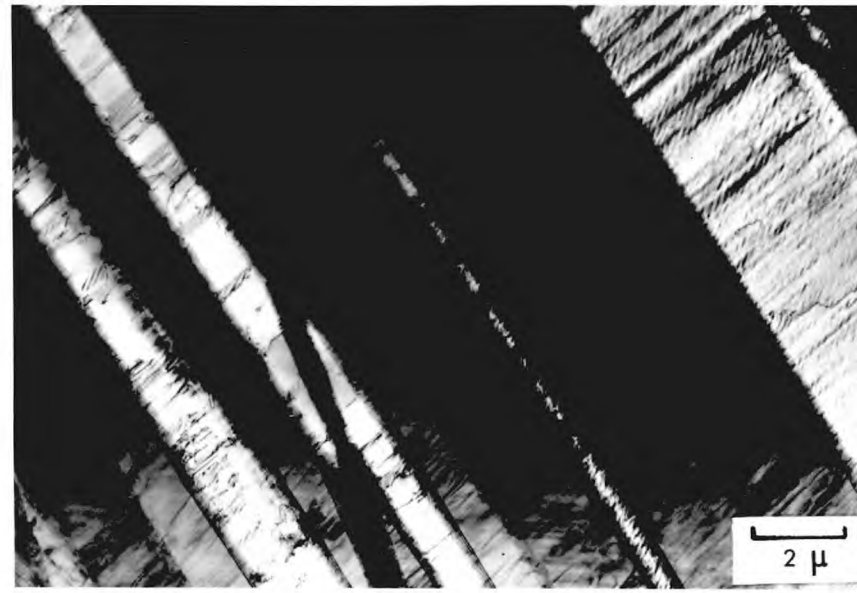
Fine parallel needles.



e) L.M. Alloy G (14.4 ^{w}/o Al) X32

Broad plates with internal striations.

Fig.4.3.2: Electron metallography of martensites



a) Alloy A (13 $^{W}/_{o}$ Al) : parallel faults in parallel plates.



b) Alloy J (14.6 $^{W}/_{o}$ Al) : sets of twins in a large plate.

4.3.1 Growth

Both the forward ($\beta \rightarrow \beta_1'$ or γ') and reverse (β_1' or $\gamma' \rightarrow \beta$) transformations were observed to occur only under conditions of changing temperature. The sensitivity to change of temperature and independence of time at a temperature of the transformation was confirmed by both light and electron microscopy. The β-phase/martensite interfaces could be advanced or retarded at will be small temperature fluctuations, although many specimens, partially transformed at room temperature were observed to retain their structure indefinitely (Figs. 4.3.3 4,5). The transformation was observed to be extremely autocatalytic; very rarely after the initial plates had formed were any plates nucleated at sites removed from existing plates (the isolated plate in Fig. 4.3.3 b was formed during the reverse transformation). Growth proceeded across grain boundaries after a slight arrest (depending on the speed of the approaching plate). The direction of growth was often observed to change due to the new crystal orientation (e.g. Fig. 4.3.1 b).

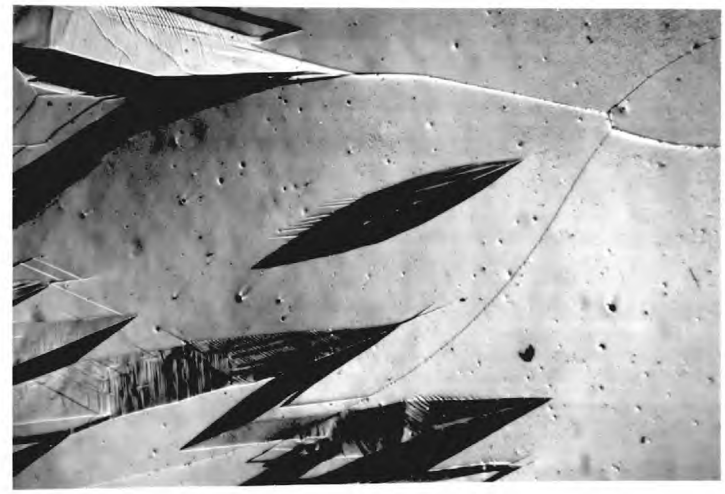
Growth rates of a particular martensite plate depended only on the rate of change of temperature. For example, quenching from room temperature into liquid nitrogen produced transformation "cries" due to the speed of interface motion, whereas an interface

Fig.4.3.3 : Disappearance of Martensite Plates
(Alloy G; light micrographs X 40)

a) -36°C



b) -34°C



c) -31°C

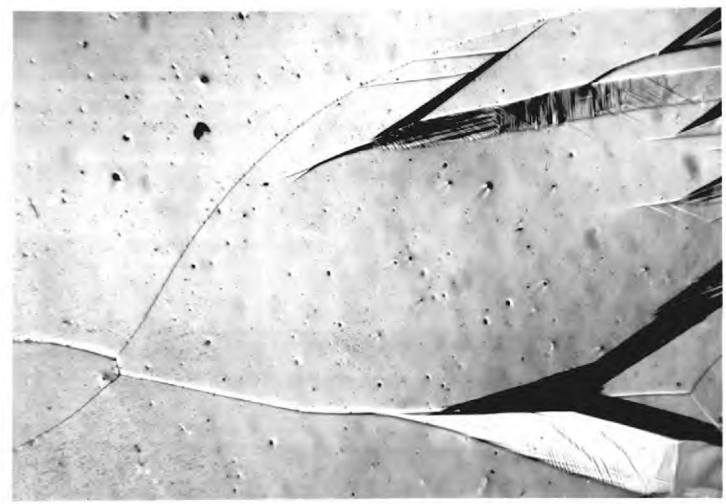
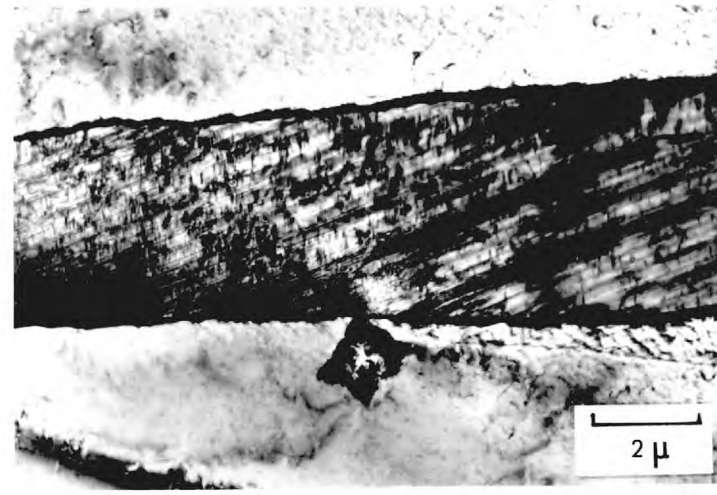
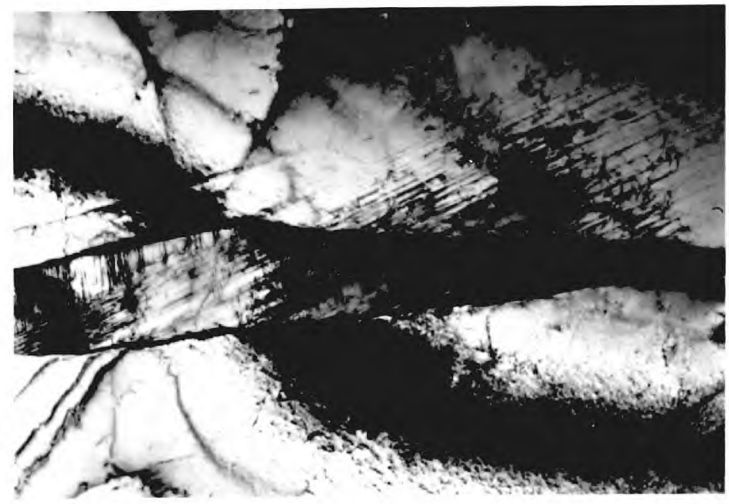


Fig.4.2.4 : Shrinkage of a martensite plate (Alloy K, electron micrographs)

a) -72°C



b) -57°C



c) -38°C



Fig.4.3.5 Growth and Shrinkage of a martensite needle (Alloy G; Electron micrographs)



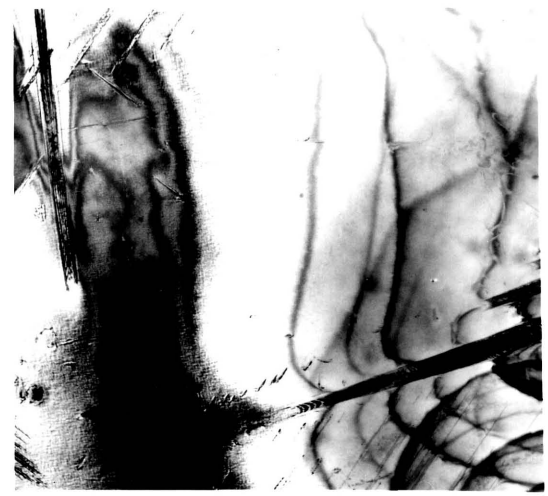
a) 20°C



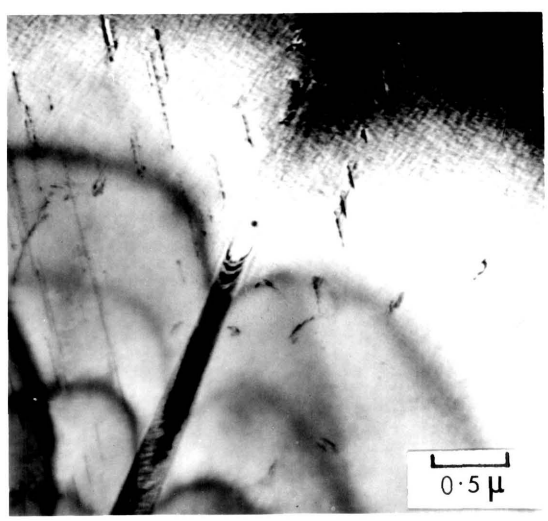
b) As a) after 19 hours.



c) cooled to -60°C



d) heated to -3°C



e) heated to +3°C



f) heated to 22°C

could be moved slowly across the electron microscope screen in thin foil specimens at magnifications of up to 30,000 X under conditions of almost constant temperature. Within a transformation however the growth rates of all crystals showed wide variation. The initial appearance of a plate was usually marked by a high growth rate; thickening and further longitudinal growth was slower. One example, recorded with a film speed of 24 f ps during a temperature fall of 1 ^{o}C showed that during the initial appearance of the plate which grew to considerable extent during the exposure of 1 frame of the film:

longitudinal growth rate was greater than 6 mm/ ^{o}C

lateral growth rate was greater than 40 mm/ ^{o}C

whereas over the next second the average lateral growth rate was only 2 mm/ ^{o}C.

The same relative interface motion rates were observed during the disappearance of a plate in the reverse transformation. This is shown in Fig. 4.3.6. It can be seen that the two sections of the plate separated by the "midrib" split, and shrink at different rates. Plates growing into untransformed matrix early in the transformation may continue at a fairly constant growth rate until the grain boundary is reached.

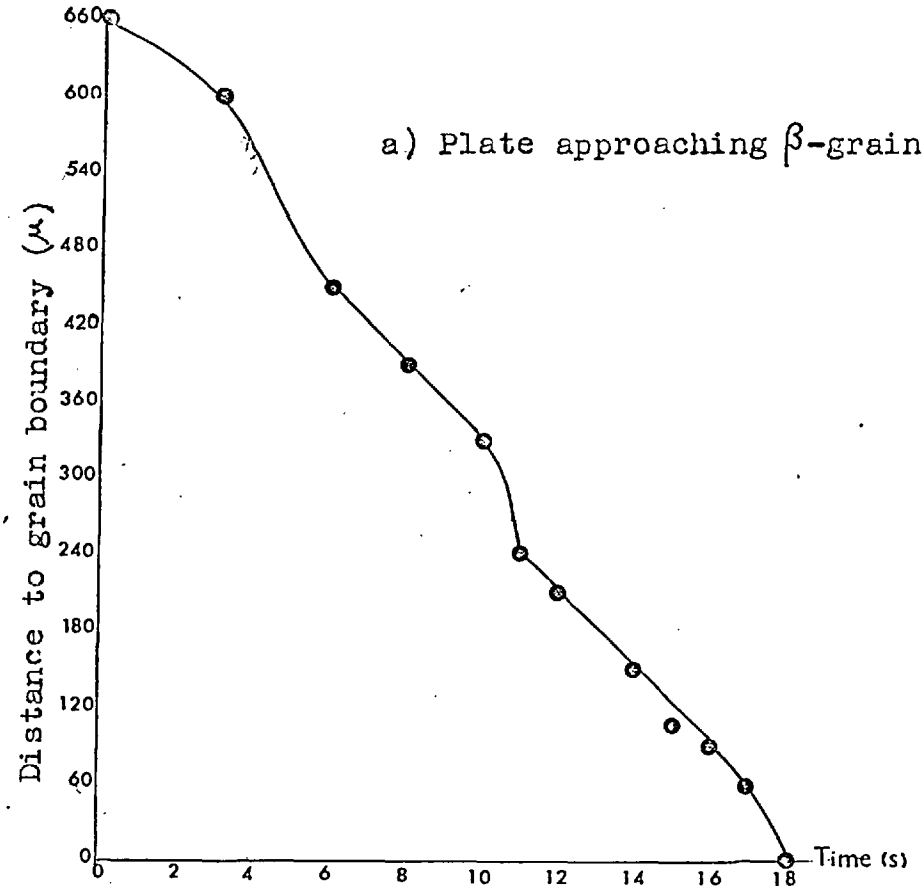
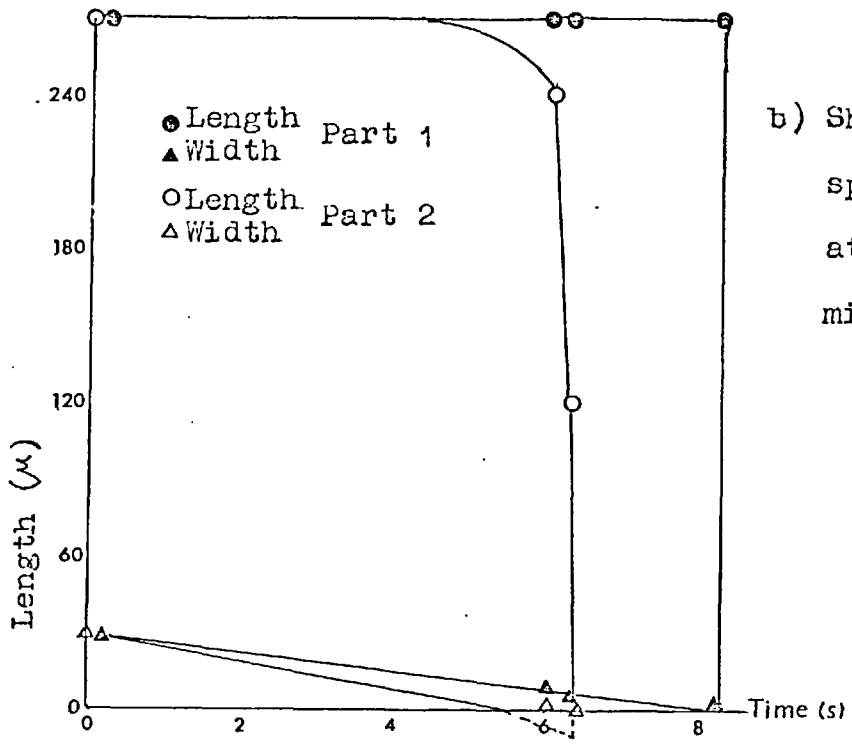


Fig.4.3.6 Growth and shrinkage of martensite plates (recorded on cine-film). Temperature change $1^{\circ}C/s$



b) Shrinking plate splits into two at central midrib

4.3.2 Transformation temperatures

The temperatures of the start and finish of the forward martensitic transformations were measured metallographically using the heating/cooling stages for the low power stereo-microscope and the Reichert projection microscope, to observe the changes in the 10 mm diameter discs. These transformation temperatures are designated M_s (start of forward transformation), M_f (finish of forward transformation), ϑ_s (start of reverse transformation) and ϑ_f (finish of reverse transformation). Direct observation is possible due to the colour change and surface tilting which accompanies transformation. Detection of the first martensite to form (M_s) and the last to disappear (ϑ_f) is particularly easy since these were usually amongst the largest of martensite plates formed and grew or disappeared very quickly to or from a linear dimension of 1 mm or more. Extreme care had to be exercised to prevent much damage of the specimens, especially at the edges, since this can produce transformation. As the transformation usually began or ended at the specimen edges anyway there was no certain method of identifying the presence of mechanical strain, although the martensite formed in the strained regions usually showed little ability to catalyse the transformation in the bulk of the specimen (see section 4.6).

Doubtful readings from a particular specimen were always repeated with several other specimens of the same alloy. The last martensite to appear (M_f) and first to disappear (β_s) were more difficult to detect, due to the partitioning effect during transformation. This leads to a progressive reduction in the size of plate formed. Furthermore it is far easier to detect a small tilted region in a flat surface, than vice versa. In all the measurements of M_f and β_s readings were continued until there was certainty that the final martensite and initial β had in fact been observed.

All specimens for the metallographic observations were solution treated for 40 minutes at 960 °C and quenched into iced brine.

Errors The stages used had an accuracy of temperature determination of at least ± 1 °C. Limitations in the observation of the transformation discussed in the previous paragraph reduce this accuracy to approximately ± 2 °C. However comparisons between specimens of the same alloy with identical thermal history did show fluctuations in the transformation temperatures recorded. All results quoted are the mean of several readings taken on from 2 to 5 specimens of the alloy and include fluctuations of up to ± 5 °C from the value given.

A summary of the results is presented in table 4.3, which shows that increasing amounts of both aluminium and nickel reduce

TABLE 4.3

VARIATION OF TRANSFORMATION TEMPERATURE WITH COMPOSITION

ALLOY CODE	COMPOSITION w/o Al	w/oNi	TRANSFORMATION TEMPERATURES ^{o}K M_s	M_f	A_f	A_s	METHOD OF MEASUREMENT
B	13.8	1.2	~190	~180	~210	~185	Thermal arrest
C	13.8	3.2	+75	+14	+100	+35	Direct Observation
J	14.6	1.2	+54	+21	+69	+46	"
E	14.1	3.0	+32	+4	+60	+15	"
F	14.3	2.8	+9	-34	+50	-7	"
K	14.6	2.8	-23	-56	-13	-50	"
G	14.4	3.0	-20	-68	+2	-46	"
H	14.4	4.0	-63	-133	-20	-94	"

the transformation temperatures. These results were used to calculate the change in transformation temperatures per unit weight % in the range of alloys studied. Starting with a comparison of alloys containing equal amounts of aluminium or nickel," best fit" curves were constructed for the transformation temperatures of all alloys. The temperature hysteresis of the transformations ($\theta_f - M_s$ and $\theta_s - M_f$) and temperature range of the transformations ($M_s - M_f$ and $\theta_f - \theta_s$) were found to be approximately constant throughout the range of compositions (30 °C to 50 °C for both hysteresis and range). The effect of change of composition was also found to be constant throughout the range. The composition/transformation temperature curves therefore are a series of parallel straight lines with gradients:

$-175\ ^{\circ}C \pm 15\ ^{\circ}C$ per unit w/o Aluminium

$-60\ ^{\circ}C \pm 10\ ^{\circ}C$ per unit w/o Nickel

These are plotted in Fig. 4.3.7 alongside the experimental values of table 4.3 standardised according to the above formula on a composition of 14.3 w/o Al or 0 w/o Ni to separate the effects of aluminium and nickel.

In the thermal analysis experiments to determine ordering temperatures, arrests due to the martensitic transformation were observed. It was not possible to quench to lower than about

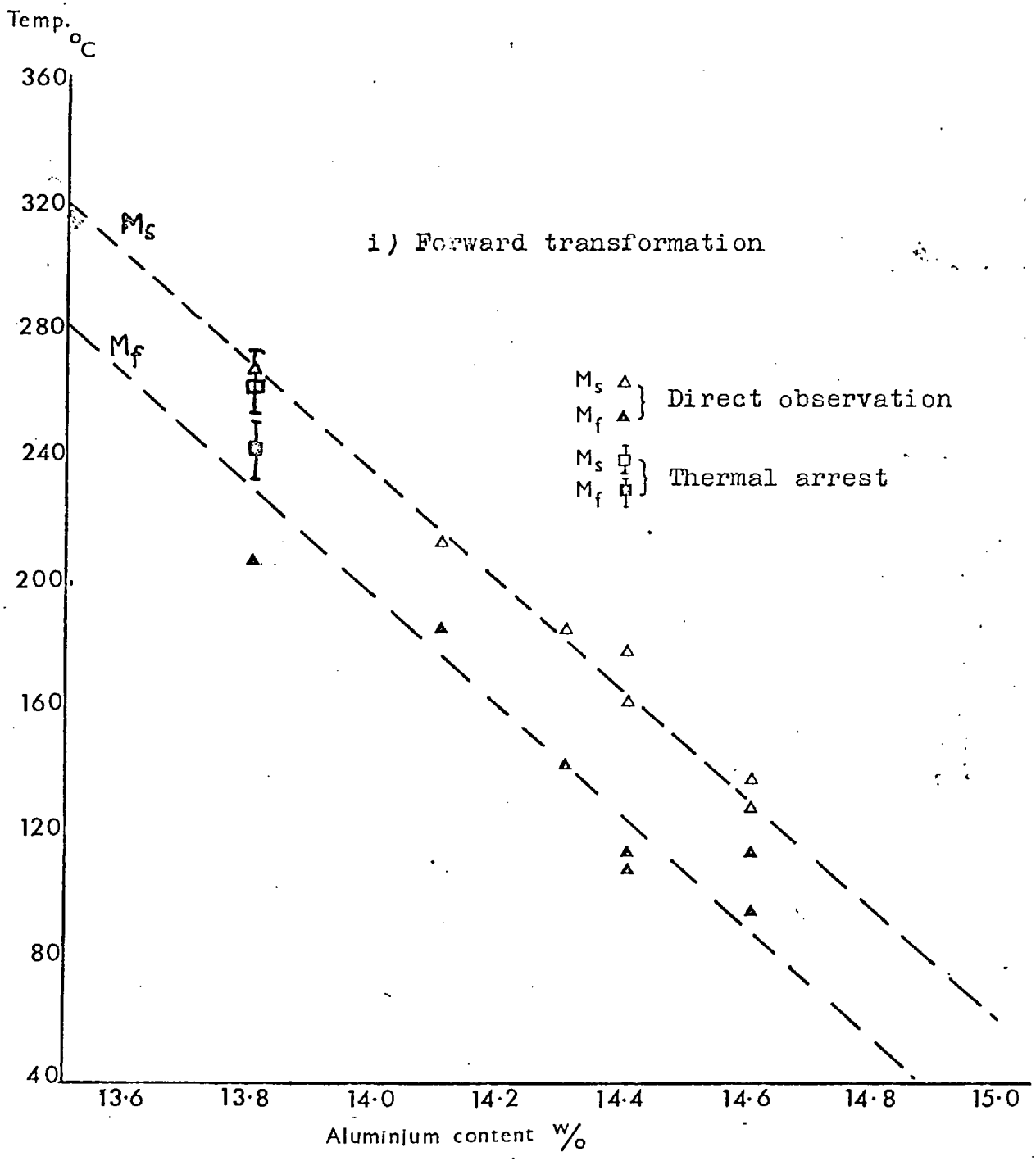


Fig.4.3.7a Effect of aluminium content on transformation temperatures.

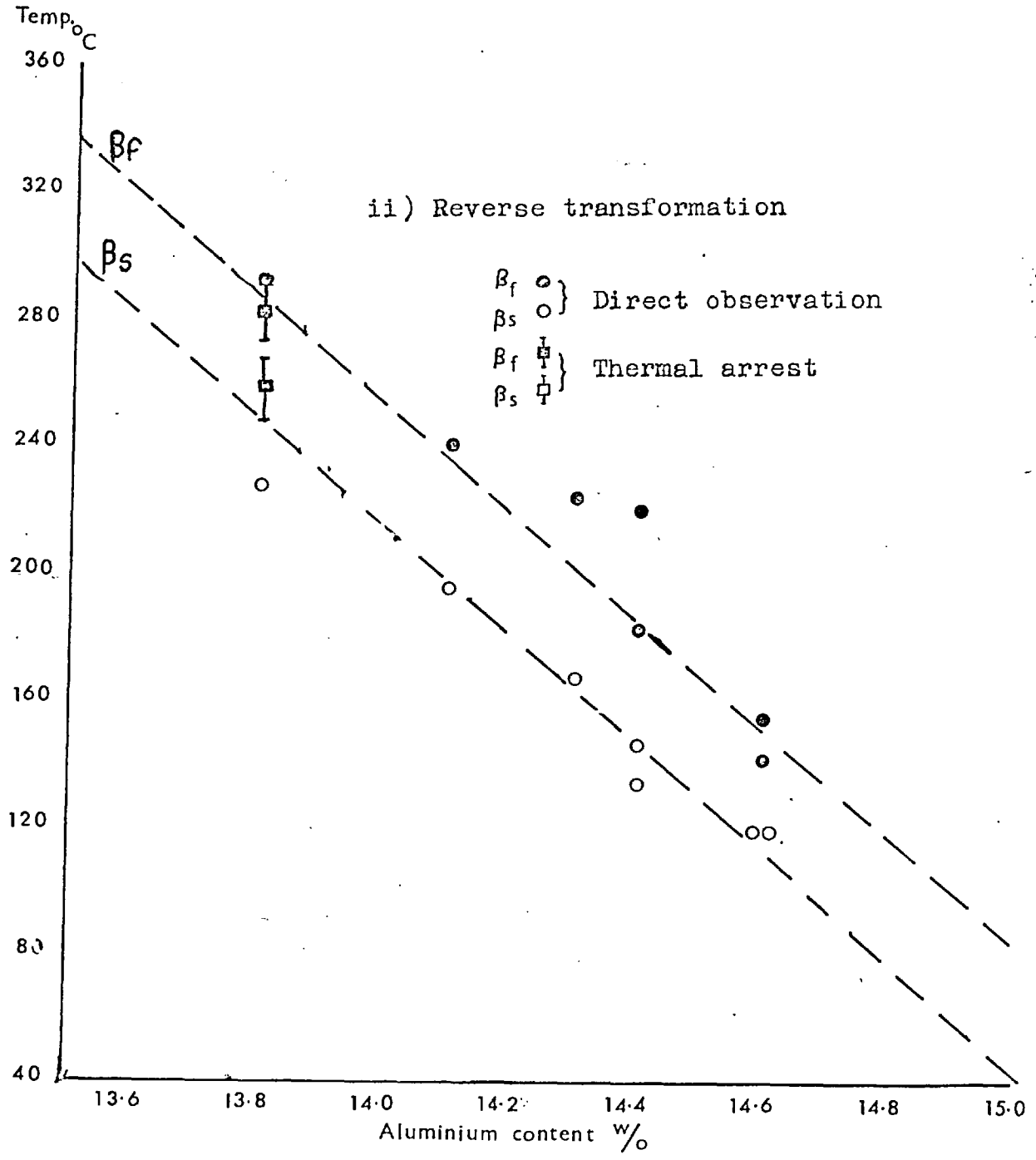


Fig.4.3.7a Effect of aluminium content on transformation temperatures.

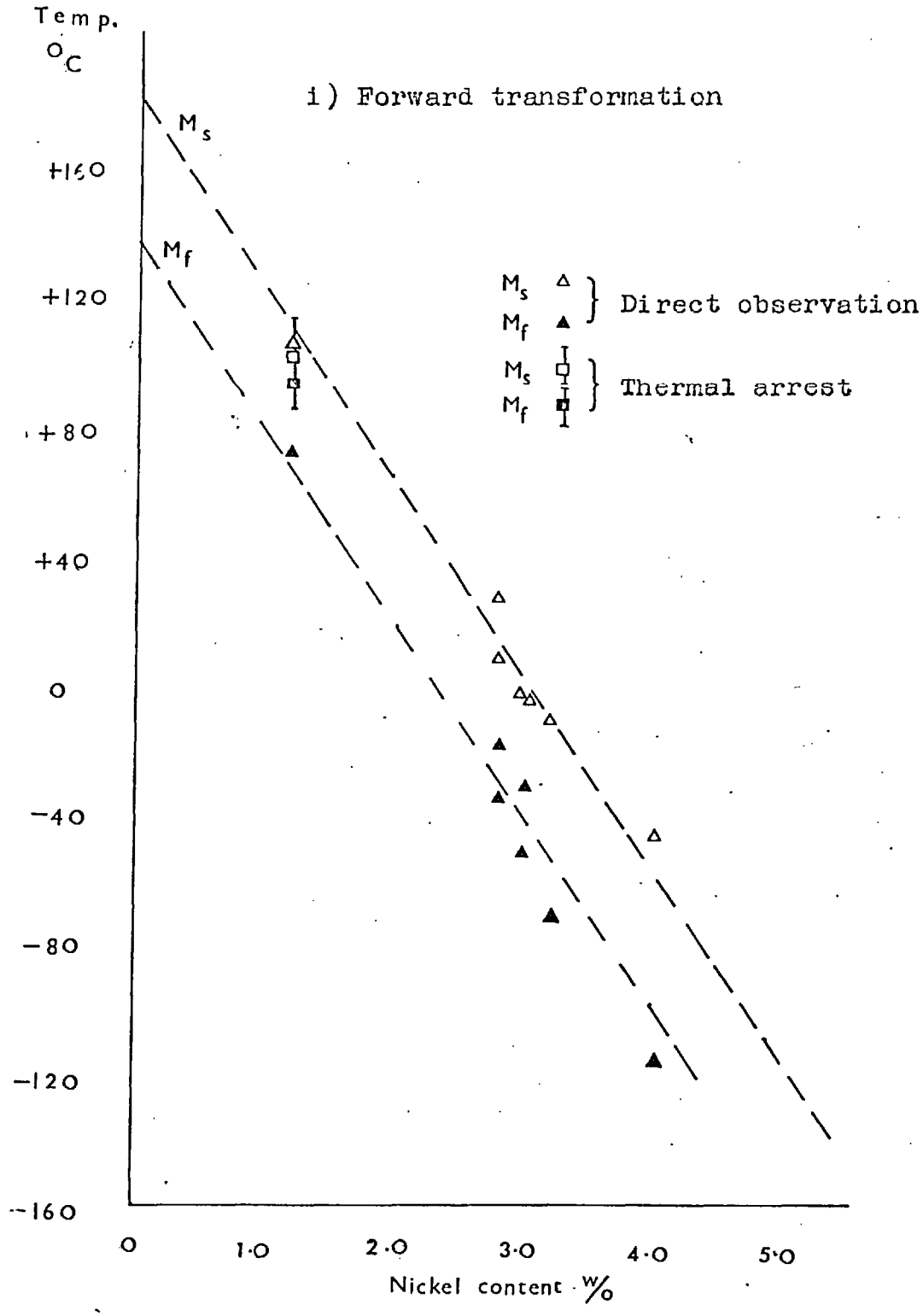


Fig.4.3.7b Effect of nickel content on transformation temperatures.

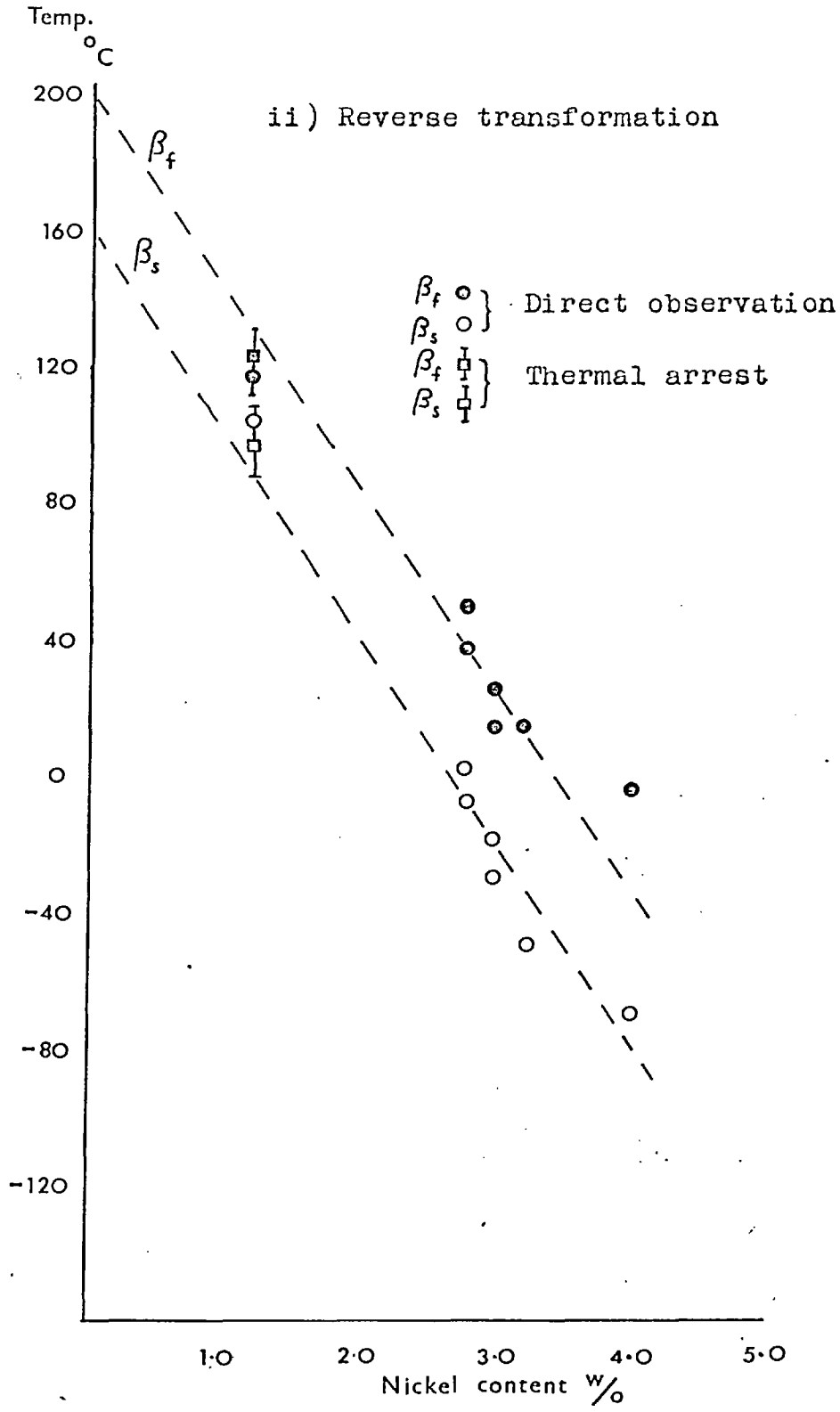


Fig.4.3.7b Effect of nickel content on transformation temperatures.

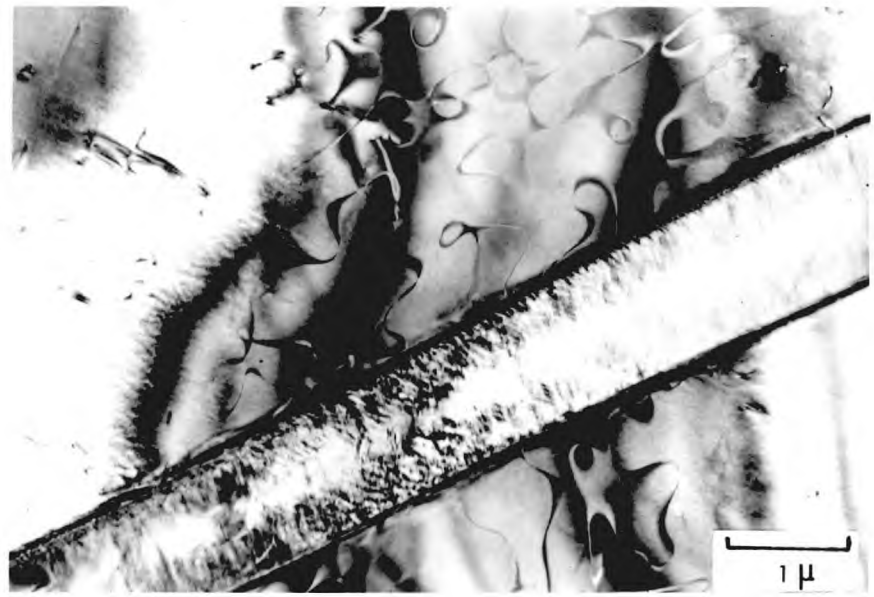
-10 °C with the apparatus however, so that the cooling rate was insufficiently rapid to detect the transformation with any degree of accuracy, except in alloy B containing the lower aluminium and nickel contents. Even in this alloy the accuracy is probably no greater than ± 10 °C but the results showed good agreement with the metallographic determinations (see Fig. 4.3.7).

4.3.3 Crystal Structures

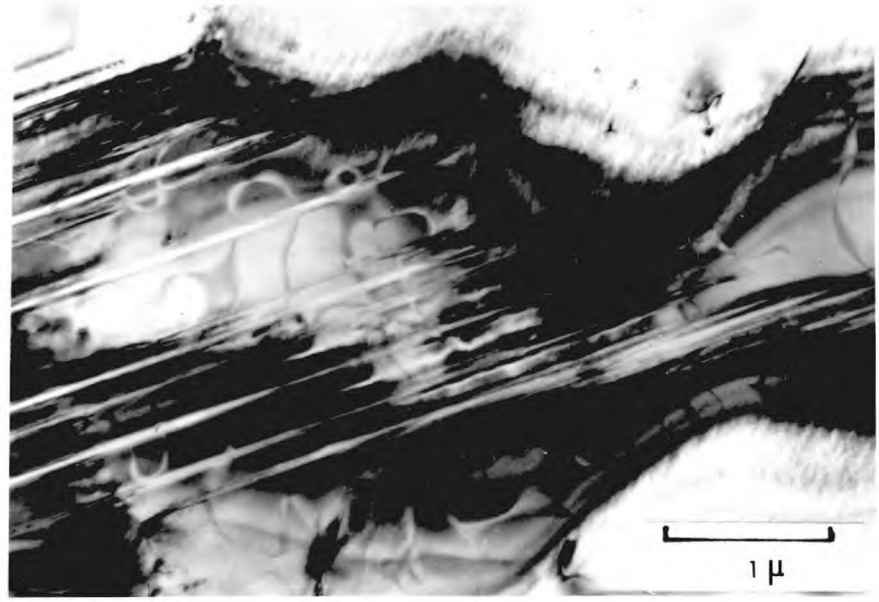
The ordering reaction occurs before the martensitic transformation in all alloys studied so that β' martensite was not observed. The antiphase contrast at superlattice domain boundaries can be observed within the γ' and β_1' martensites but this is often obscured by internal faulting (Fig. 4.3.8).

The structure of γ' martensite was found to be orthorhombic with lattice parameters approximately 4.5 Å, 5.2 Å and 4.2 Å in agreement with previous workers. Twinning was identified as $\{121\}_{\gamma'}$, the fineness of the twins often producing streaking of the diffraction pattern in directions perpendicular to the twins, as recorded by Swann and Warlimont[80]. The orientation relationship between β_1 and γ' has been determined by diffraction

Fig.4.3.8 : Order domains in martensite (Alloy G; Bright field micrographs, with S_2 type reflection)



a) B2 -type domains, largely obscured in Y' plate.



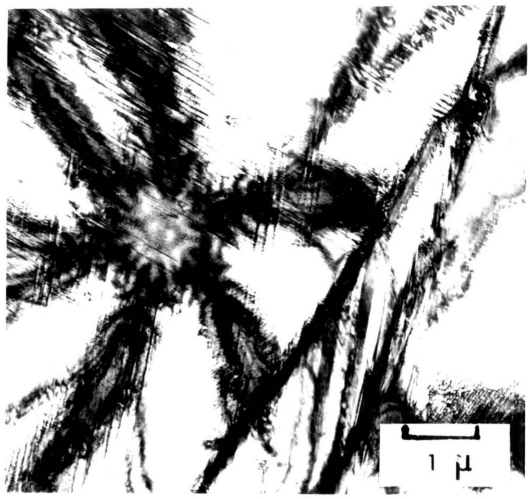
b) B2 domains in region transforming back to β_1. Domain boundaries pass through the isolated Y' twin filaments.

pattern analysis to be $(\bar{1}10)\,[111]_{\beta_1} // (\bar{1}21)\,[210]_{\gamma'}$ in agreement with previous measurements (Fig. 4.3.9). Further streaking of the diffraction patterns was observed in a direction perpendicular to faults within the twins. This direction was normal to the basal plane $(001)_{\gamma'}$ and so it was concluded that the twins contained stacking faults on this plane in agreement with the observations of Otsuka and Shimizu[94] and with the implications of the analysis of Sato et al.[93].

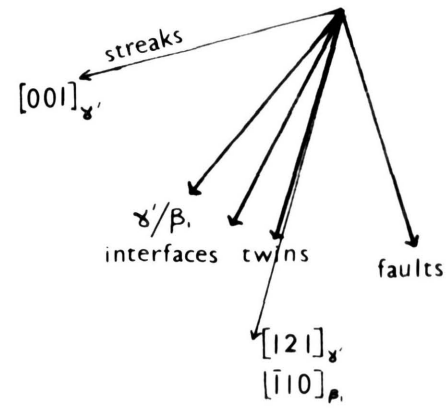
During the reverse transformation in thin foil specimens striations were often left in the β_1-phase by the disappearing γ' plates. These were particularly apparent in specimens polished in the electrolyte 50% Nitric Acid/50% Acetic Acid (Fig. 4.3.10). The striations disappeared without trace after a short period of time during which the temperature seemed of lesser importance. An analysis of the orientation of the traces is presented in Fig. 4.3.11, an adjacent area to the previous sequence. The foil surface is parallel to (111) and the traces are parallel to $[1\bar{2}1]$ (narrow) and $[1\bar{1}0]$ (broad). The $1\bar{1}0$ are perpendicular to (111) and cut the plane along $\langle 1\bar{2}1\rangle$ whereas the 110 are inclined at 35.26° to (111) and cut the plane along $\langle 1\bar{1}0\rangle$. A comparison of widths of traces x and y (Fig. 4.3.1 d) shows that these are compatible with the above inclinations. However the $\{110\}_{\beta_1}$ are equivalent to the $\{121\}_{\gamma'}$

Fig.4.3.9 : γ' martensite crystallography

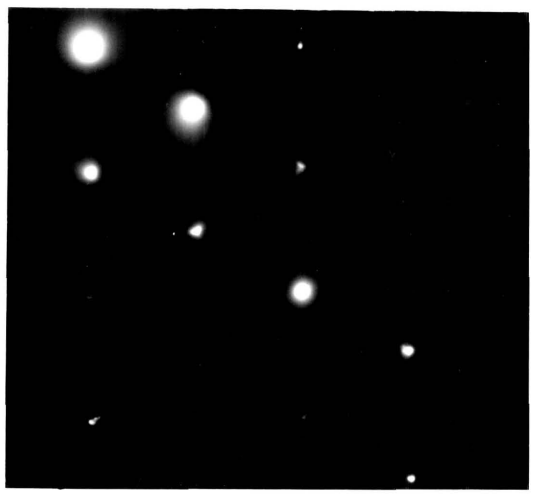
(Alloy F)



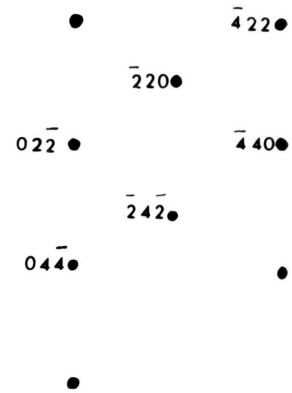
a) β_1 + γ' $[11\bar{1}]_{\beta_1}$ zone axis



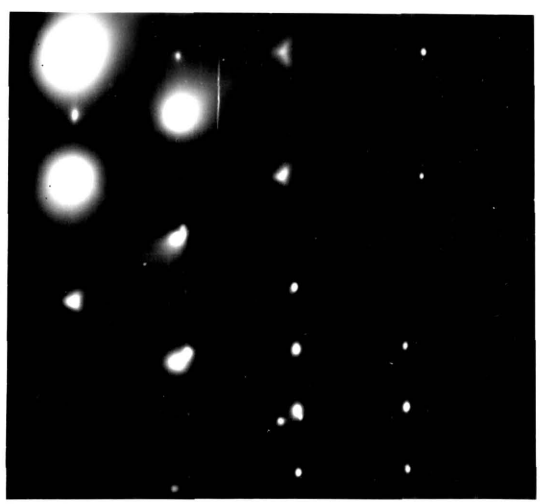
b) Trace analysis



c) S.A.D.P. β_1



d) β_1 $[11\bar{1}]$ zone



e) S.A.D.P. γ' + β_1



f) γ' $[20\bar{1}]$ zone

Fig.4.3.10 : Surface traces left by retreating γ' interface (Alloy K)

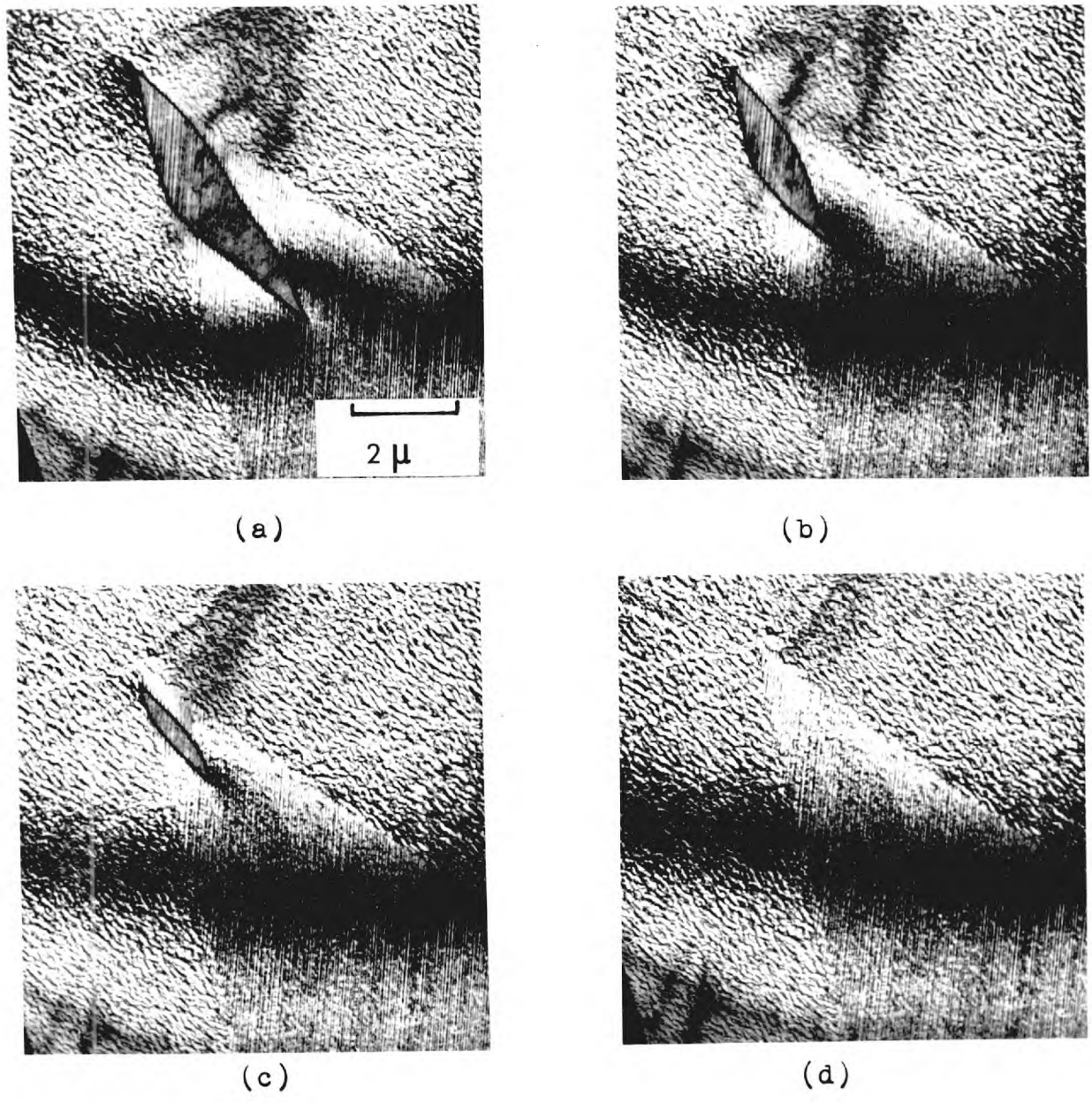
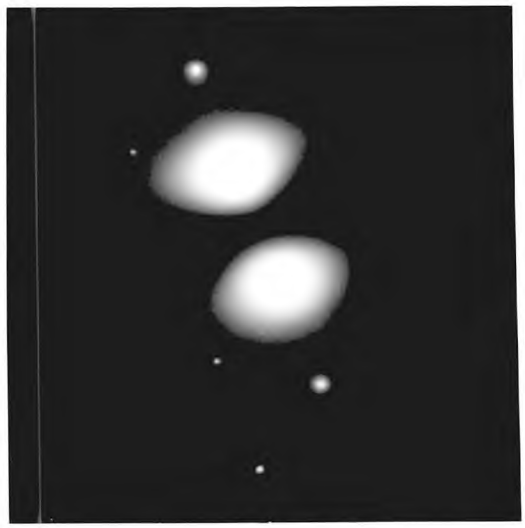
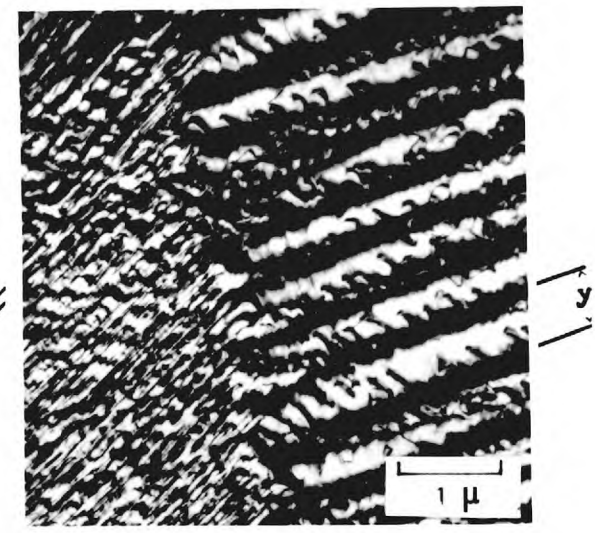


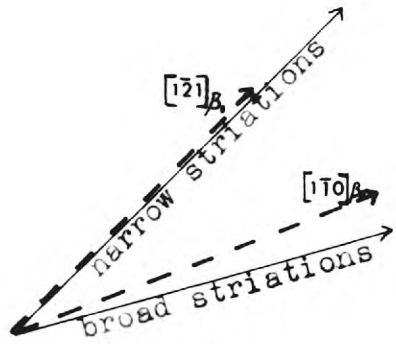
Fig.4.3.11 : Analysis of surface traces.



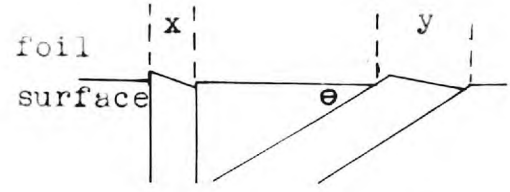
b) S.A.D.P. $[111]_{\beta_1}$ zone



a) B.F. striated β_1 surface



c) Trace analysis of a)



$\frac{x}{y} = 0.5 = \sin\theta$

Inclination of broader striations is 30° to surface

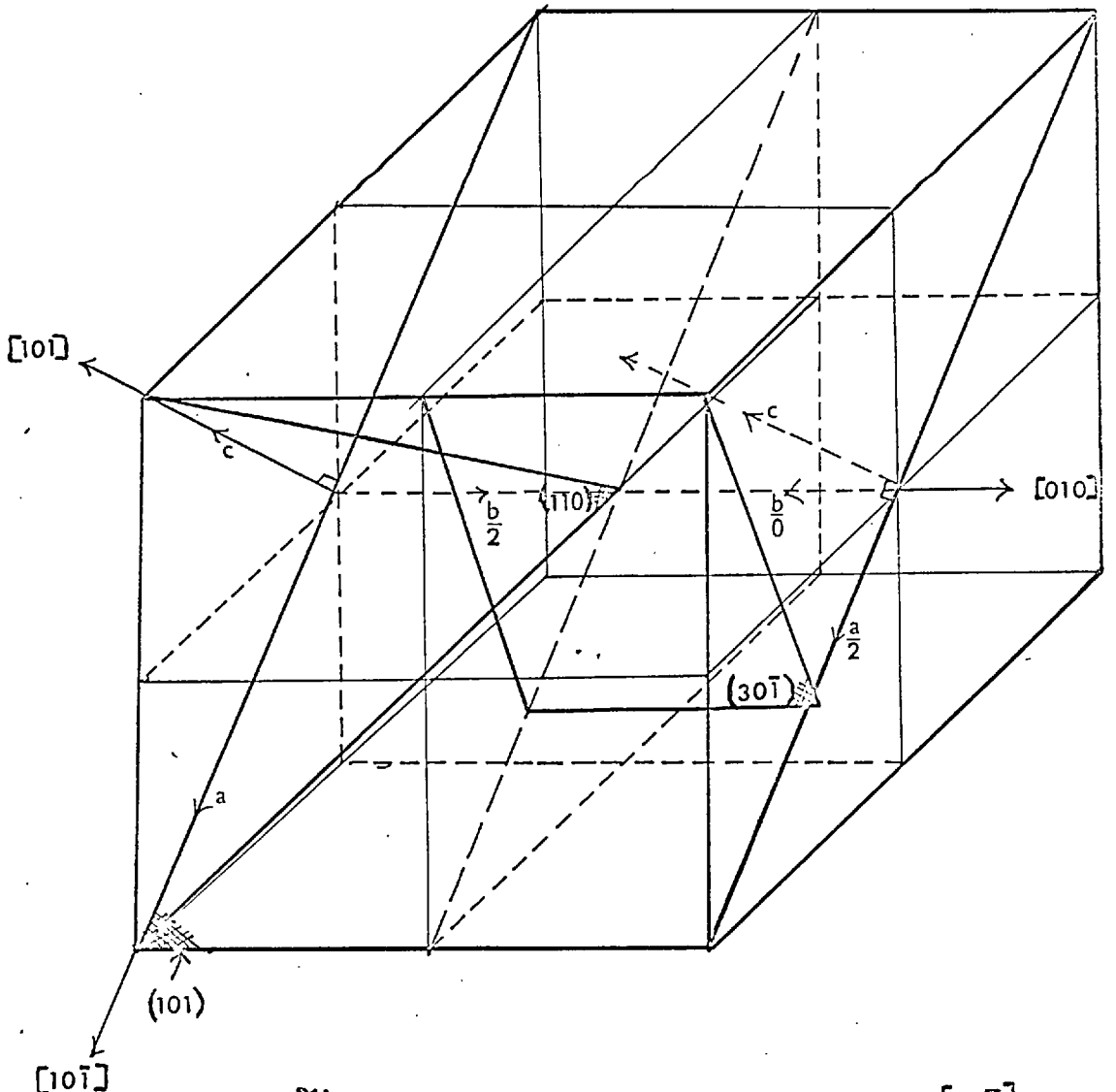
d) Inclinations of (removed) γ' twins.

(Fig. 4.3.12) which is the γ' martensite twin plane. It was therefore concluded that these traces were due to rumpling of a surface film that had been created by electropolishing, by twinning within the martensite plates. The contrast proved quite useful in identifying retransformed areas during the "in situ" experiments.

The interfaces between martensite and ϑ- phase showed wide variation of orientation, both in specimens transformed in bulk, and thin foil specimens (Fig. 4.3.13). The interface was often not a continuous plane, but contained individual traces moving ahead into ϑ-phase in the forward transformation and trailing behind in the reverse transformation (see Fig.4.3.13 a). Under the electron microscope these were identified as individual "twin" filaments of γ'. In the thin foil specimens a retreating γ' interface appeared to contain these fragments much more frequently than an advancing one; in some cases an interphase boundary could no longer be specified (Fig. 4.3.13 c).

Planar interfaces have been observed in specimens transformed in the thin foil, for example in Fig. 4.3.9 where the straight interface traces are close to $\{331\}_{\vartheta}$ and $\{332\}_{\vartheta}$. But observations failed to substantiate the findings of Otsuka and Shimizu[94] that the γ' plates always consist of two parts, twin related about a central $\{121\}_{\gamma'}$, midrib, with both sides of the

Fig.4.3.12 : Twinning planes in γ' martensite referred to β_1



Axes of γ' orthorhombic unit cell are a = $[10\bar{1}]_{\beta_1}$, b = $[010]_{\beta_1}$, c = $[101]_{\beta_1}$. Twin planes $\{121\}_{\gamma'}$ and $\{201\}_{\gamma'}$ become $\{110\}_{\beta_1}$ and $\{30\bar{1}\}_{\beta_1}$.

Fig.4.3.12 : Non-planar interfaces of γ' martensite.

a) L.M. X 40
(Alloy E,4 min.960°C,Q)
γ' growing into β_1



b) B.F.
β_1 growing into γ'



c) B.F.
γ'/β_1 interface
breaking up during
reverse transformation

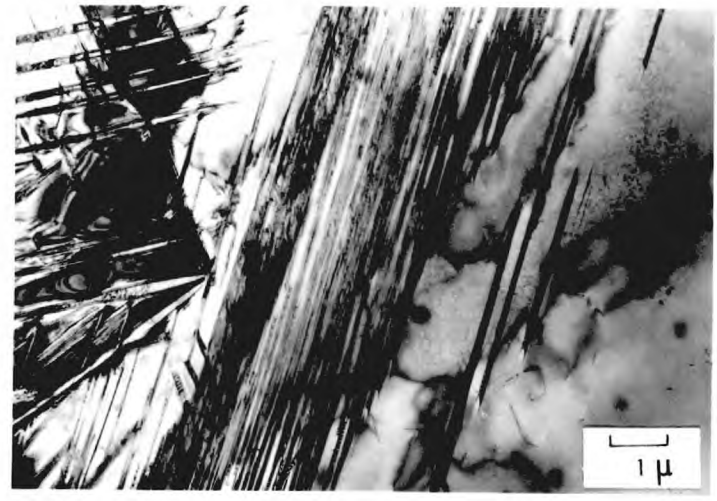


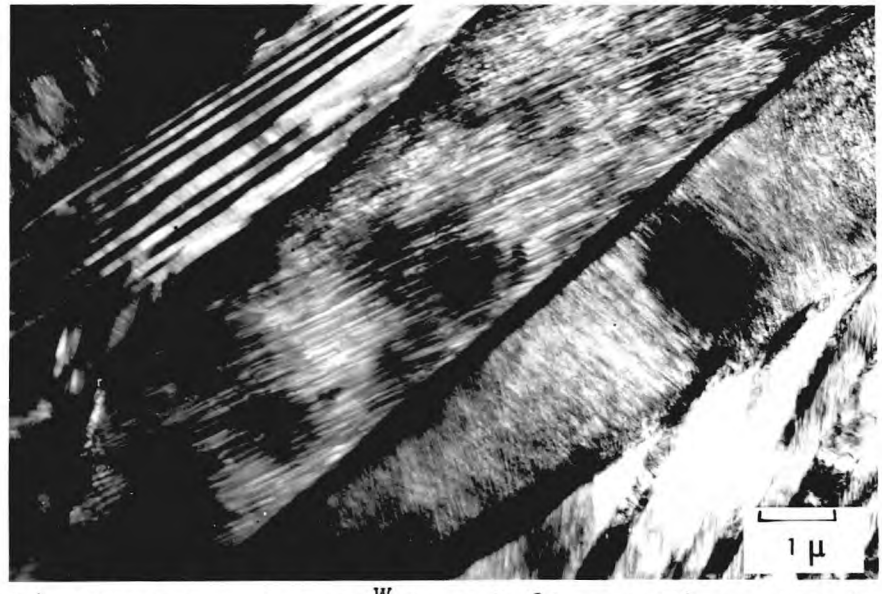
plate having $\{331\}_\beta$ - $\{441\}_\beta$ habit. As explained in that paper, it is difficult to find the midrib of most plates in thin foil specimens, due to their large size. Many of the small plates observed in the present study, having irregularly shaped interfaces and no central midrib, had formed in the thin foil so that the relief of elastic stresses, held to be the reason for that morphology, would no longer be an important factor. Similar morphologies were observed in bulk-transformed specimens however, and as section 4.3.1 described, the growth and shrinkage of the two parts of midrib plates which were observed, did not appear particularly dependent on each other.

$3_1'$ martensite was observed in alloys A, B and C (having aluminium contents of 13.8 w/o or less). The martensite needles were found to contain a high density of parallel striations which did not always extend completely across the crystal. Fig. 4.3.14 shows an example in which the faults in some of the needles are approximately parallel to the foil surface. Analysis of the diffraction data is made very difficult by this continual faulting which extends the reflections in the reciprocal lattice, causing a shift in diffraction spot maxima, dependent on the orientation. This has been discussed in considerable detail (80, 90 - 93) and the exact sequence of the faulting (on close-packed planes) is still a subject of some controversy. The alloys containing $3_1'$ martensite

Fig.4.3.14 : β' martensite



a) Alloy B. Faults with terminating partial dislocations, one set approximately parallel to the foil surface.



b) Alloy A - (13.0 $^{W}/_{o}$ Al) β' and γ' martensites.

proved unsuitable for the "in situ" observations of martensite formation, by electron microscopy in this work, since their M_s is so high as to cause γ_2 precipitation during the transformation. Insufficient data was collected therefore to make any detailed comment on the nature of the faulted structure.

In all these three alloys γ' martensite was observed in addition to $3_1'$ (Fig. 4.3.13 b) which is in agreement with observations on Cu-Al showing mixed martensite crystallography in Cu-13 w/o Al and Cu-13.7 w/o Al.[80]

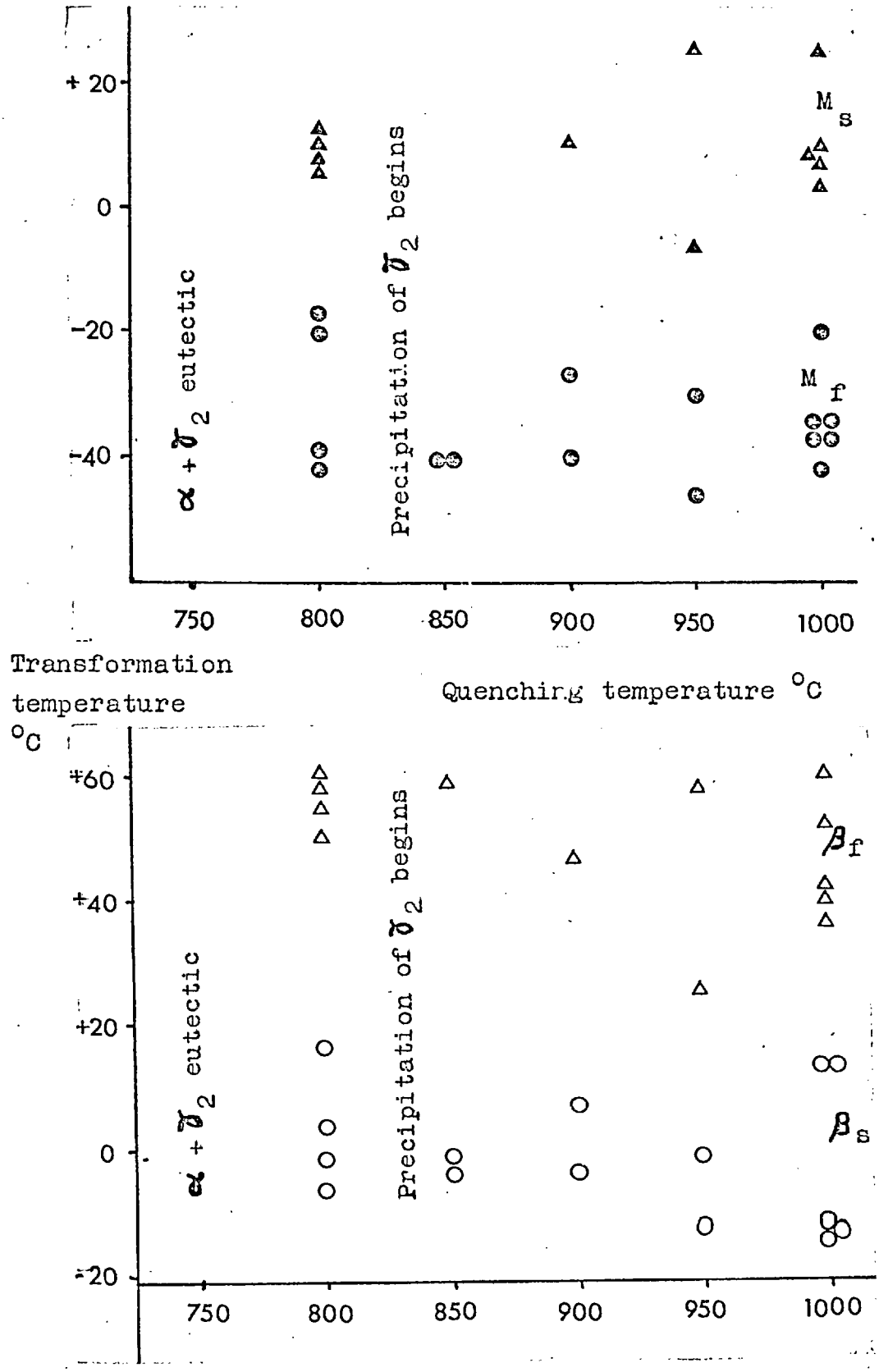
4.4 Thermal History and the Martensitic Transformation

According to the theory of Kaufman and Cohen[12] (section 1.3) martensite plates are nucleated by pre-existing "embryos" produced by dislocation reactions at higher temperatures and "frozen in" as the temperature falls. These embryos have a range of sizes, the largest producing martensite at M_s since they are predicted to have lowest activation energy. Changes in the thermal history, should therefore, be reflected in the formation of martensites.

4.4.1 Effect of Quenching Temperature

The transformation temperatures were measured metallographically, of a series of specimens of alloy F (14.3 w/o Al. 2.8 w/o Ni.) quenched from different temperatures. There was a considerable scatter of results in some cases, but the only consistent trend which appeared was a slight rise in all transformation temperatures at or below quenching temperatures of 850 °C (Fig. 4.4.1) This corresponds to the limit of single phase (according to Fig. 2.1) and in fact γ_2 precipitation was observed by light metallography in the specimens quenched from 800 °C and no martensitic transformation was recorded in those specimens quenched from 750 °C. Thus the rise in transformation temperatures can be explained as resulting from the creation of regions of low aluminium content adjacent to the precipitating γ_2, in which transformation will occur preferentially. The observation that the range of transformation $(M_s - M_f)$ is not substantially changed is consistent with an extremely autocatalytic reaction- the presence of martensite plates compensates for the increased activation energy needed for transformation in the regions richer in Aluminium. (The effect of γ_2 precipitation on the transformation is considered in more detail in Section 4.8)

Fig.4.4.1: Variation of transformation temperature with quenching temperature: alloy F



4.4.2 Effect of Quenching Rate

The transformation temperatures of alloys E, F, J and K were measured metallographically after quenching in brine at 0 °C, water at 60 °C and carbon tetrachloride at 20 °C. No significant change in the temperatures of the transformation was observed when the β phase was completely retained, in the alloys containing least aluminium at the higher quench rates (see table 4.2). The transformation temperatures were all increased when γ_2 was precipitated during quench; in the alloys containing higher aluminium concentrations and at slower quench rates. Diffusion of aluminium would again seem to be the critical factor influencing the formation of martensite.

4.5 Free Surface and the Martensitic Transformation

The transformation does not occur when the free energies of the martensitic and matrix phases are equal; an additional driving force is required to provide for the surface and strain energy produced by the development of a new crystal structure in an existing one. If these can be reduced in a particular specimen then the transformation may be expected to begin at higher

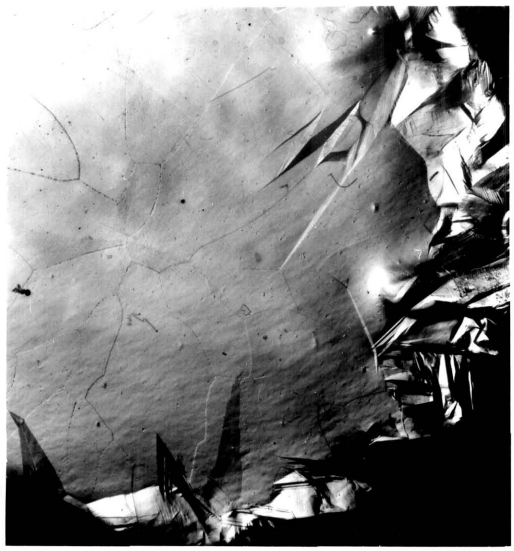
temperatures in those regions of the specimen where one or both show a minimum. The free surface of a specimen offers a situation for the reduction of both surface and strain energies, over the bulk of the specimen.

4.5.1 Bulk Specimens for Light Microscopy

The first martensite plates were invariably observed to have been nucleated at a region of high surface to volume ratio. Thus the edges of the specimens ususally transformed first (Fig. 4.5.1 a). More particularly, those parts of the edge where there was a projection or re-entrant portion which would further increase the surface/volume ratio would be the sites of the initial plates to form (Fig. 4.5.1 b) Often such initial sites were where a grain boundary met the specimen edge (Fig. 4.5.1 c). Grain boundaries within the bulk specimen were not observed to be nucleation sites except when they opened up by grain boundary cracking (often due to repeated transformation and electron-polishing). Plates between two free surfaces, for example the specimen edge and a cracked grain boundary, were found to be particularly stable (β_f temperature greatly increased for the specimen). Nucleation could often be

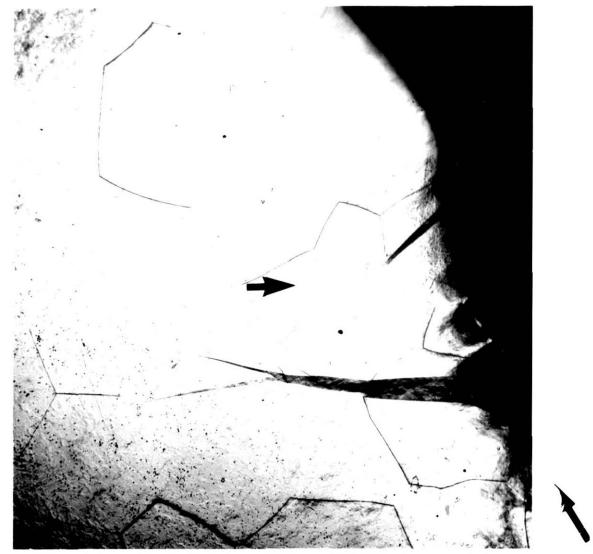
Fig.4.5.1 : Martensite formation at free surfaces.

(Light micrographs, specimen edge shown ⟶)



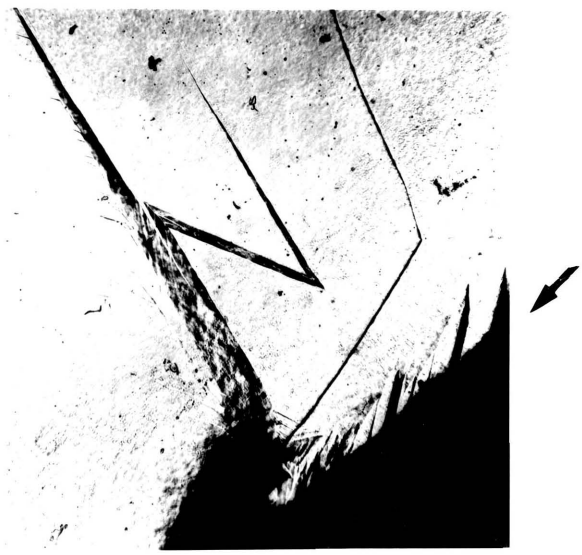
a) Alloy G X 8

Initial plates around specimen edge.



b) Alloy G X 10

Initial plate at a very thin part of specimen edge.



c) Alloy F X 40

Initial plate at grain boundary intersection with specimen edge.



d) Alloy G (as a).) X 8

Initial plates at sharp corners of specimen.

initiated in a particular area by creating a large surface/volume ratio, for example by polishing or spark cutting the edge to a particular shape (Fig. 4.5.1 d). Attempts were made to remove the free surface of a specimen by copper plating the regions where the first nuclei formed or oxidising the surface. There was no observed effect on the initial sites, the temperature at which they transformed, or the subsequent progress of the transformation. It was concluded that the copper plating was not sufficiently adhesive to exert any stress on the matrix, and that an insufficiently strong oxide film could be built up before ageing of the structure complicated the interpretation of results.

4.5.2 Thin Foil Specimens for Electron Microscopy

The reduction of bulk constraints and consequent raising of the transformation temperatures was apparent in the production of thin foil specimens. In those which had M_s just below room temperature, martensite plates could be observed to form around the rim of the perforation produced on thinning (Fig. 4.5.2). The increase in M_s was about 20 °C in most cases. On the other hand, thin foil specimens were not infrequently observed to be incompletely transformed at the lowest temperature reached by the cooling stage (-150 °C)

Fig.4.5.2: Alloy F X48

Preferential martensite formation around perforation in a thin foil specimen for electron microscopy.

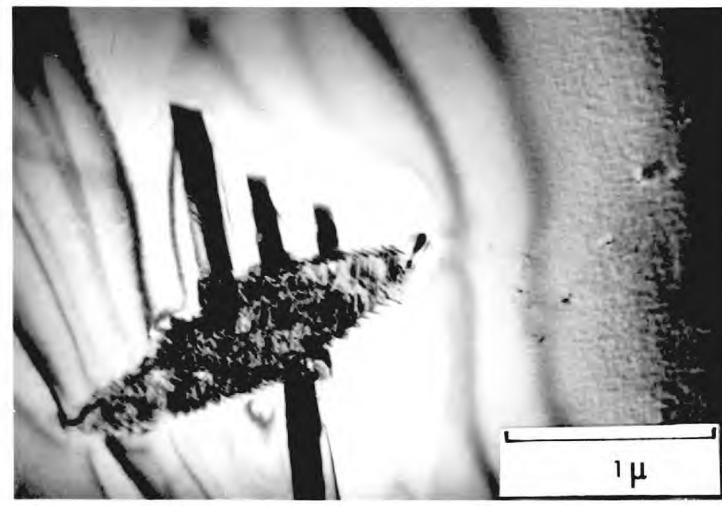


which represented a depression of the M_f temperature of over 100°C in some alloys, from those recorded in bulk specimens. Fig. 4.5.3 (a) and (b) show stages in the confused growth of a martensite plate which has formed in a preferentially thinned region of a specimen of alloy G ($M_s \sim -20$, $M_f \sim -68$ °C). The characteristically lens-shaped martensitic region was initially observed at room temperature. The analysis of the diffraction pattern of this region (fig. 4.5.3 c) shows the γ' structure with $\langle 112 \rangle_\gamma$, twin traces and streaking of the pattern caused by faults in $[001]_{\gamma'}$. Immediately the electron beam fell on this region several filaments of martensite grew from the plate (Fig. 4.5.3 a) on planes analysed as $\{201\}_{\gamma'}$ which are also known to be a twin planes for martensite. Growth appears to have proceeded in a number of directions subsequently (Fig. 4.5.3 b) on cooling to -115 °C, predominantly on second set of $\{112\}_{\gamma'}$ planes perpendicular to the foil surface. It would seem that each growth filament is arrested by the increasing constraints it is subjected to as it proceeds from the nucleating plate into the thicker foil. The temperature of -115 °C is well below the bulk M_f temperature for this alloy and so it appears that the multiplicity of growth habits has had a net retarding effect on the transformation in this region. The locking of the interfaces is confirmed by subsequent observations of the region at temperatures between - 150 °C and room temperature which

Fig.4.5.3 : Martensite growth in a very thin region (Alloy G)

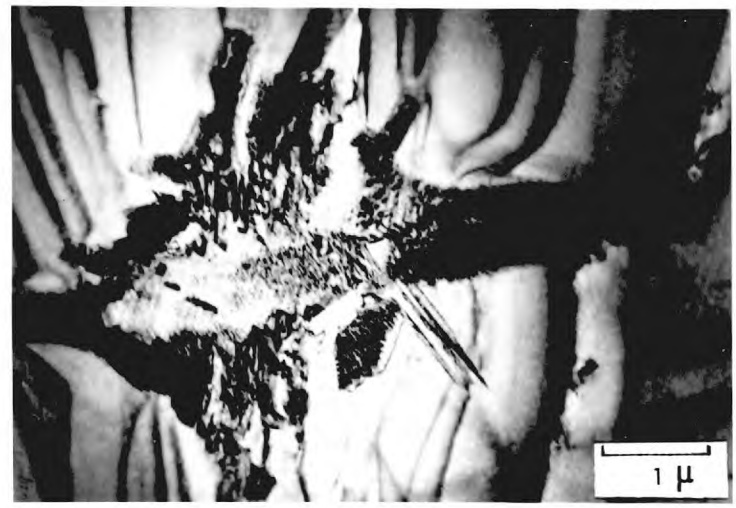
a) Initial growth

+ 20°C



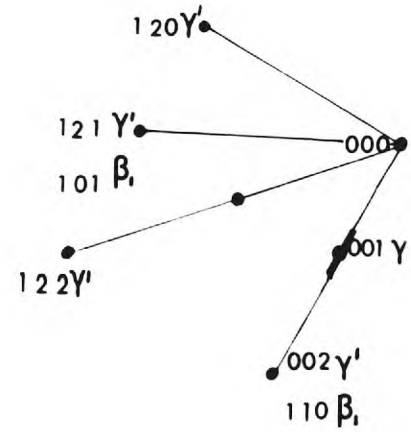
b) Maximum growth

- 115°C



c) S.A.D.P. indexed for γ' & β_1





showed a structure apparently unchanged from that pictures in Fig. 4.5.3 b.

This large temperature hysteresis was observed only at thin foil edges, and at features such as the one described but it does indicate that in the thinnest regions of the foil unusual growth mechanisms may be adopted to give complex martensitic structures not encountered in bulk specimens.

4.6 Mechanical Stress and the Martensitic Transformation

The effect of mechanical stress on the transformation in these alloys is simply observed - a scratch on the copper-coloured surface of β - phase appears brass-coloured; the transformation has been locally induced. This result imposes the precautions which were mentioned in section 4.3.2 on the preparation of specimens for the measurement of the transformation temperatures of the alloys. The initial chapter reviewed some of the evidence pointing to the importance of dislocations in nucleating martensitic transformations; in chapter 2, mention was made of the experiments of Kurdyumov et al.[62] which convincingly demonstrated the equivalence of mechanical stress and temperature as a thermodynamic driving force for the thermoelastic transformation in a similar alloy to

those used in this investigation: Cu - 14.44 w/o Al - 4.75 w/o Ni. Extreme care was taken to remove and avoid stresses both above and below the elastic limit, and a limited investigation was carried out to investigate their significance in the transformation.

4.6.1 Plastic Deformation of β-phase

The preparation of specimens for optical and electron microscopy is facilitated by surface grinding. In these alloys such deformation induces the transformation in the surface layer which can be seen to be removed by the colour change during eh subsequent electrothinning and polishing. In order to ensure that this transformation had not affected the remaining untransformed regions, specimens so prepared were compared with ones chemically polished only, after heat treatment. This method gives a poor metallographic finish but confirmation was obtained of identical transformation temperatures.

The effect of local plastic deformation was observed by indenting a specimen with a Vickers hardness machine (loads of 2.5 - 50 kg). The indented and adjacent regions transformed to martensite but subsequent cooling showed that these plates did not grow significantly or catalyse the growth of newplates, since transformation of the

bulk of the specimen proceeded at the normal rate to produce a M_f temperature similar to an undeformed specimen (Fig. 4.6.1). It was concluded therefore that the inductive effects of plastic deformation on the transformation were very local. It was not possible to examine the nature of the martensite/matrix interface but it is speculated that the absence of the autocatalytic effect is due to lack of interface coherence.

4.6.2 Elastic Stressing of β-phase

Stress was applied to several specimens of different alloys simply by bending thin strips. It was possible to induce the transformation at room temperature in alloys normally totally β-phase (e.g. alloy F: M_s = + 9 °C; alloy G: M_s = - 20 °C). The transformation could be detected visually and audibly ("cries") and commenced on the inside knee of the bend, that is where the stress concentration, notably the compressive stress, is the greatest. This is understandable as the volume change of the transformation is about 1% decrease, according to ref. 46. At low stress levels, removal of the stress results in automatic reversion of the transformation demonstrating the elastic nature of the phase change. As the

Fig.4.6.1

Martensite formation in an indented specimen.



stress increased a critical level was reached beyond which some martensite was retained after removal of the stress. The specimen remains bent due to the preferential growth of favourably oriented martensite plates. Interrupting the application of stress did not appear to affect the course of the induced transformation.

In contrast to the martensite plates formed during plastic deformation, those formed by elastic strains were observed to grow readily when the temperature was reduced.

4.6.3 Deformation of γ' martensite

If the bent specimen containing the preferentially oriented γ' martensite was heated the transformation reversed, and so did the shape, to give a flat, β-phase specimen. This is an example of the "shape-memory" effect.

A sample of 50 w/o Ni - 50 w/o Ti alloy was prepared in the laboratory (by arc melting) for comparison with the behaviour of the aluminium bronzes being studied. Specimens of this alloy, deformed at room temperature reverted to their original shape in boiling water (the β_s temperature is approximately 90 ^{o}C). In addition it was discovered that re-cooling to just below room temperature (20 ^{o}C) which is close to the M_f temperature, caused a

partial reforming of the deformed shape. Further cooling to temperatures approaching -200 °C produced no further shape change.

Several alloys of aluminium bronze with and without nickel, showing a wide range of transformation temperatures were investigated and the shape memory effect was observed in all of them. The results are summarised in Table 4.4. The deformation is more easily carried out on the γ' phase which is more ductile. Most alloys were deformed therefore at temperatures below the M_f. Reversion to β-phase and the original shape took place exactly simultaneously at temperatures in the normal β_s to β_f range. The correspondence between shape change and transformation could be closely followed by the colour change, and the frequently large surface tilts. Fig. 4.6.2. shows three stages in the "remembering" of a deformed specimen of alloy J. The colour definition is rather poor, but Fig. (a) can be seen to be totally γ', in Fig. (b) the left half has transformed to β and in Fig. (c) the specimen is all β except for a few isolated plates associated with inter-granular cracks (caused by an over zealous demonstration of the shape-memory effect).

No reversion to the deformed shape was observed on re-cooling the specimen to below M_f. The memory is one way, therefore, but the effect can be repeated by applying the deformation for a large number of cycles. Care must be taken not to exceed the "elastic limit"

ALLOY	Al w/o	Ni w/o	TRANSFORMATION TEMPERATURE M_s	M_f	β_s	β_f	DEFORM-ATION TEMP.	STRUCTURE DEFORMED	REMEMBERING TEMP. RANGE °C
E	14.1	3.0	34	4	15	60	0	γ'	15-60
"	"			"			20	$\beta + \gamma'$ (β initially stress induced to γ')	"
J	14,6	1.2	54	21	46	69	20	γ'	45-70
L	15.0	0	$\gg 0$				Below M_f	γ'	Below room temp.
D	14.0	0	~150				20	γ'	~200°

Table 4.4 : "Shape-memory" effect in Cu - Al -(Ni)

4.6.2 The "shape-memory" effect, alloy J X1.5

a) Deformed specimen γ'-phase.



b) Left hand side to about 70°C, straightened, β-phase.



c) Whole specimen heated, straightened, β + some γ' retained at cracks.



of the γ' or strains are built up which hinder retransformation and can lead to the grain boundary cracking observed in Fig. 4.6.2.

4.7 Repeated Transformation by Thermal Cycling

Direct observation was made by light and electron microscopy, of successive transformations to martensite and back to β, under conditions of changing temperature between β_f and M_f. Metallographic observation was also made of specimens which had been automatically cycled through the transformation temperature range, a large number of times.

4.7.1 Light Metallography

The characteristic surface tilts were observed on cooling a flat-surfaced specimen through the transformation range. Reversing the transformation by heating always restored the flat surface of the high temperature phase.

Exact replication of the site and shape of the initial martensite plates was observed to occur for a large number of successive

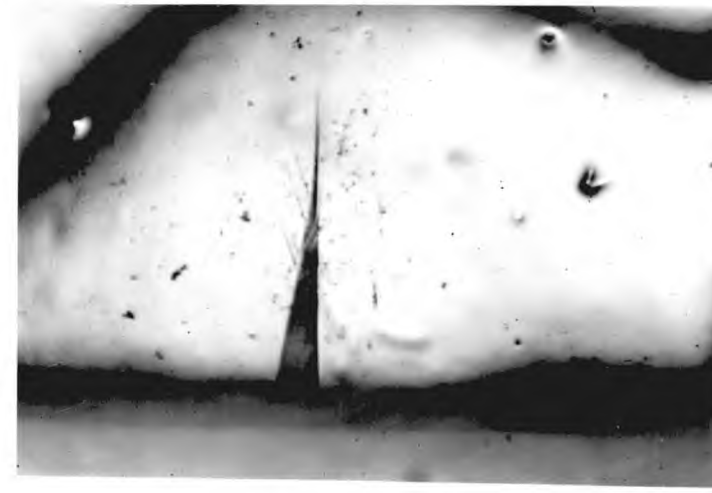
transformation cycles (up to 40 in one specimen). Wide variation of the extent of replication at this early stage in the transformation was observed, however, between specimens. Often several sites appeared preferential for the nucleation of the first plate and the operating site in a particular cycle would fluctuate between several possibilities. These sites were usually contained in the same small volume of the specimen indicating a preferred volume within which there were a number of favourable nuclei. Fig. 4.7.1 shows the initial plate to form in three successive cycles; the site changes slightly and then reverts to the original one. The site and shape of the first plate to form was observed to be more likely to show a change in the next cycle, the greater the proportion of martensite formed in the previous cycle. The formation of other martensite plates in the vicinity of the first plate, either induced by its presence, or having grown across from another part of the specimen, could affect its capacity to reverse its growth sequence and/or repeat its formation in successive cycles.

The replication of transformation displacements in any particular volume of material was observed to depend on the proportion of the specimen already transformed when <u>it</u> transformed. This is understandable in the light of the autocatalytic nature of the transformation: very few martensite plates actually form at any distance from existing plates. A change in the site and shape of

Fig.4.7.1 : First martensite plate to form in three successive cycles. (Alloy G X 85)

a) first cycle
- 32°C

specimen edge →



b) second cycle
- 32°C



c) third cycle
- 32°C



a plate at any stage in the transformation will therefore tend to affect the sites and shapes of all plates which form subsequently (Fig. 4.7.2.). This effect can be observed most clearly if the displacements of two successive cycles are produced on the same specimen surface. This can be done by polishing flat a martensite specimen. Heating through the transformation range produces β with surface tilts which are the reverse of those produced in the β to martensite change. Cooling back to martensite produced further tilts; unlike the forward then reverse transformation sequence, the flat surface is not restored, except in the regions where the first plate tilts have occurred. Fig. 4.7.3 shows surfaces produced in this way. Specimen (a) is partially re-transformed to martensite so that the tilted β - phase surface can be observed. In (b) fine parallel tilts can be observed both in γ' and β regions. These are due to the internal twins of the previous γ' plates. Specimen (c) is totally re-transformed and shows a wide variation between the displacements of two successive transformations.

4.7.2 Transformation temperatures

Many of the morphological features were reflected in the transformation temperatures (T.T's) recorded for successive cycles, as

Fig.4.7.2 : Mid-transformation martensite plates in four successive cycles. (Alloy G X 48)



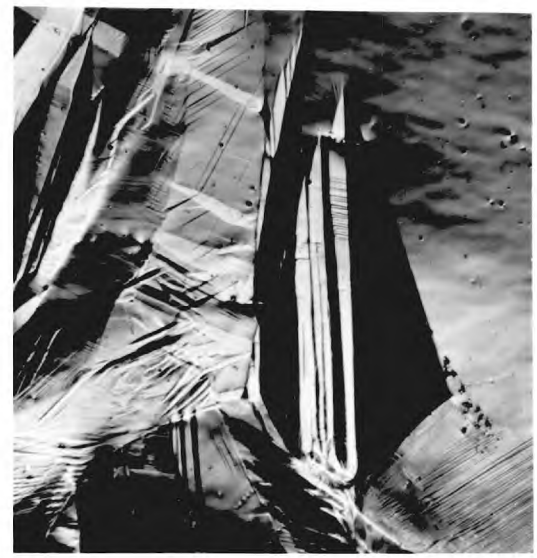
a) first cycle -46°C



b) second cycle -45°C



c) third cycle -48°C

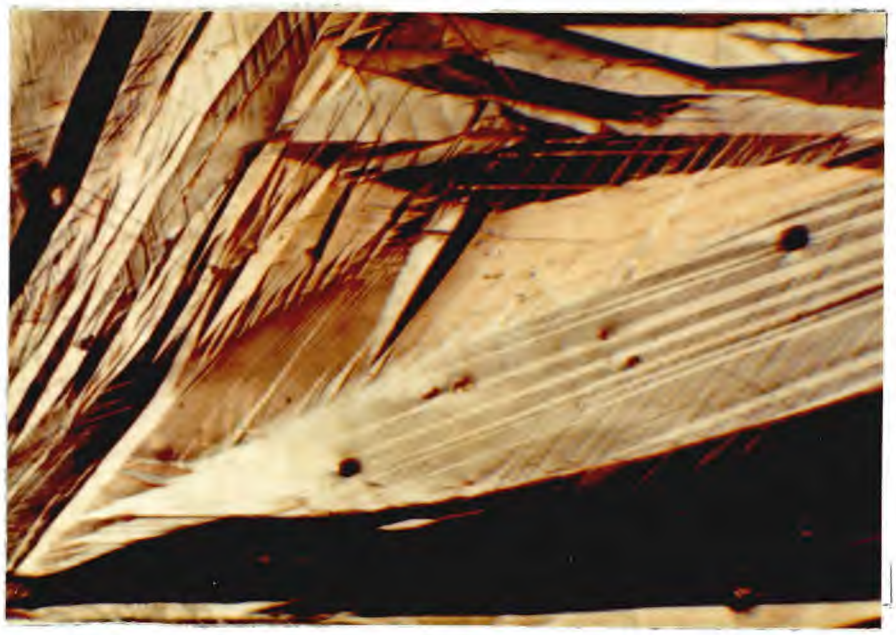


d) fourth cycle -46°C

Fig.4.7.3 : Non-replication of reversed transformation

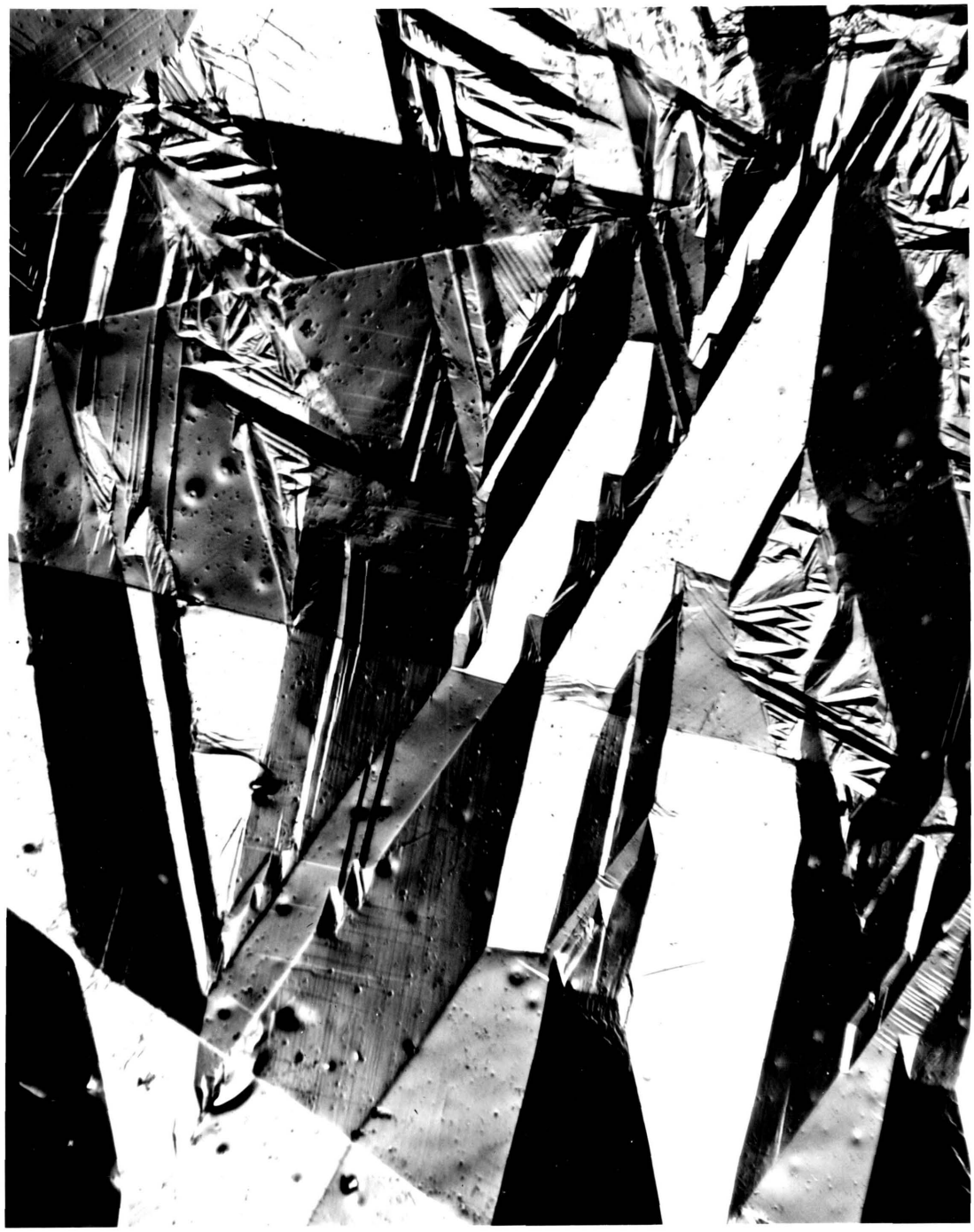


a) Alloy J Surface tilting of β and γ' X250



b) Alloy J Surface tilting in β and γ' of fine internal γ' twins X250

Fig.4.7.3c) : Total retransformation to martensite - two complete sets of surface tilts.



Alloy E

X 100

shown in Fig. 4.7.4. The time for a temperature cycle to grow the first plate and remove it ($\vartheta_f \rightarrow M_s \rightarrow \vartheta_f$) was approximately one minute; the time for a cycle through the complete transformation ($\vartheta_f \rightarrow M_f \rightarrow \vartheta_f$) was approximately 4 minutes. Interruptions in this sequence are shown in the figure. The following features may be observed:

(a) Approximately constant values for M_s ($\pm$ 2 °C) and ϑ_f ($\pm$ 1 °C) during the first 20 cycles. These values refer to the appearance and disappearance of an identical plate.

(b) Suppression of M_s after cycling through the complete transformation. This was followed by a burst of martensite growth to restore the constant relationship between temperature and volume fraction of martensite. In the case marked (L.b) this burst was correspondingly larger.

(c) An adjacent plate formed at M_s; variations in M_s between cycles increased ($\pm$ 5 °C).

(d) After 50 unobserved cycles through the transformation (each cycle taking $\frac{1}{2}$ minute) the original plate again formed at M_s. The T.T's were little changed. Cycling through ($\vartheta_f \rightarrow M_s$) range appears to favour the initial nucleation site.

(e) A further 100 rapid cycles severely suppressed transformation at this site and led to a second quite separate nucleation point. The alternation between these two sites for initial plate formation is shown.

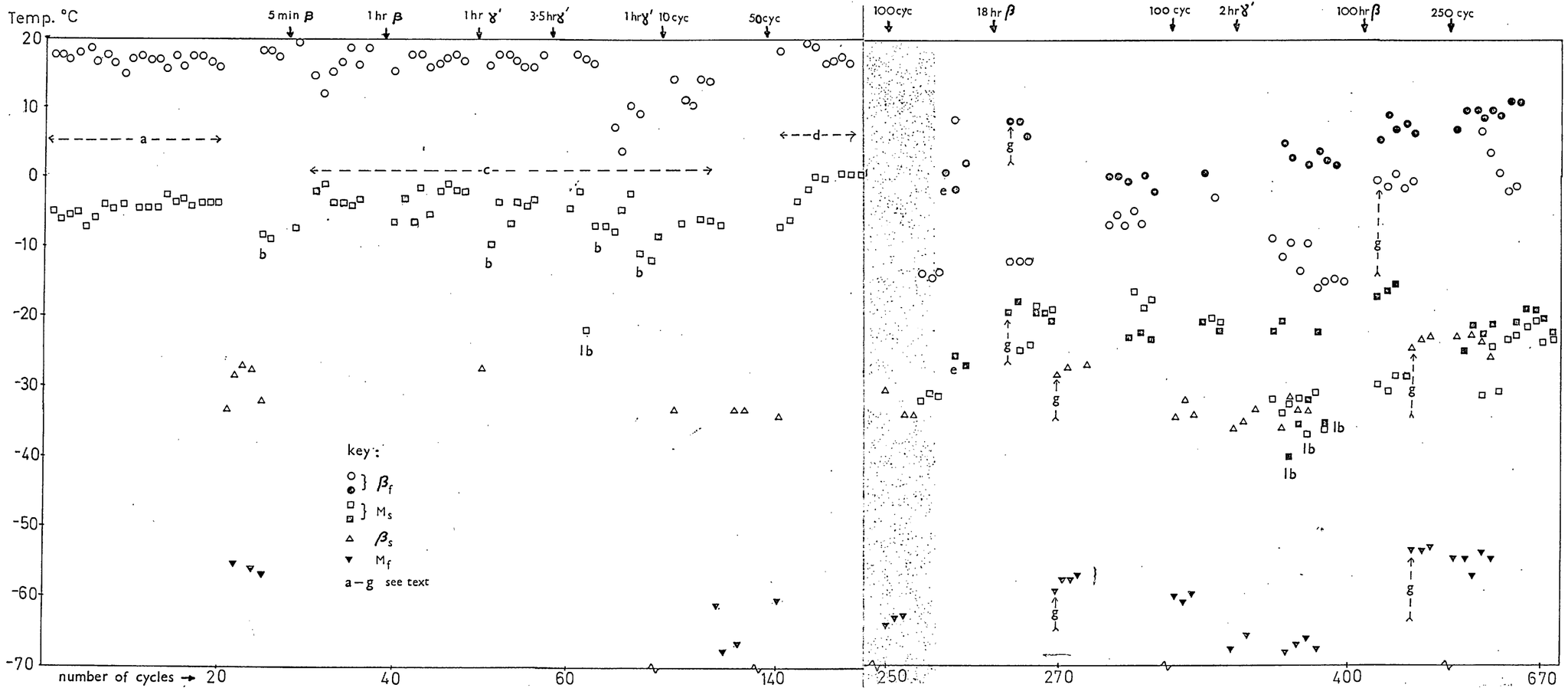


Fig.4.7.4

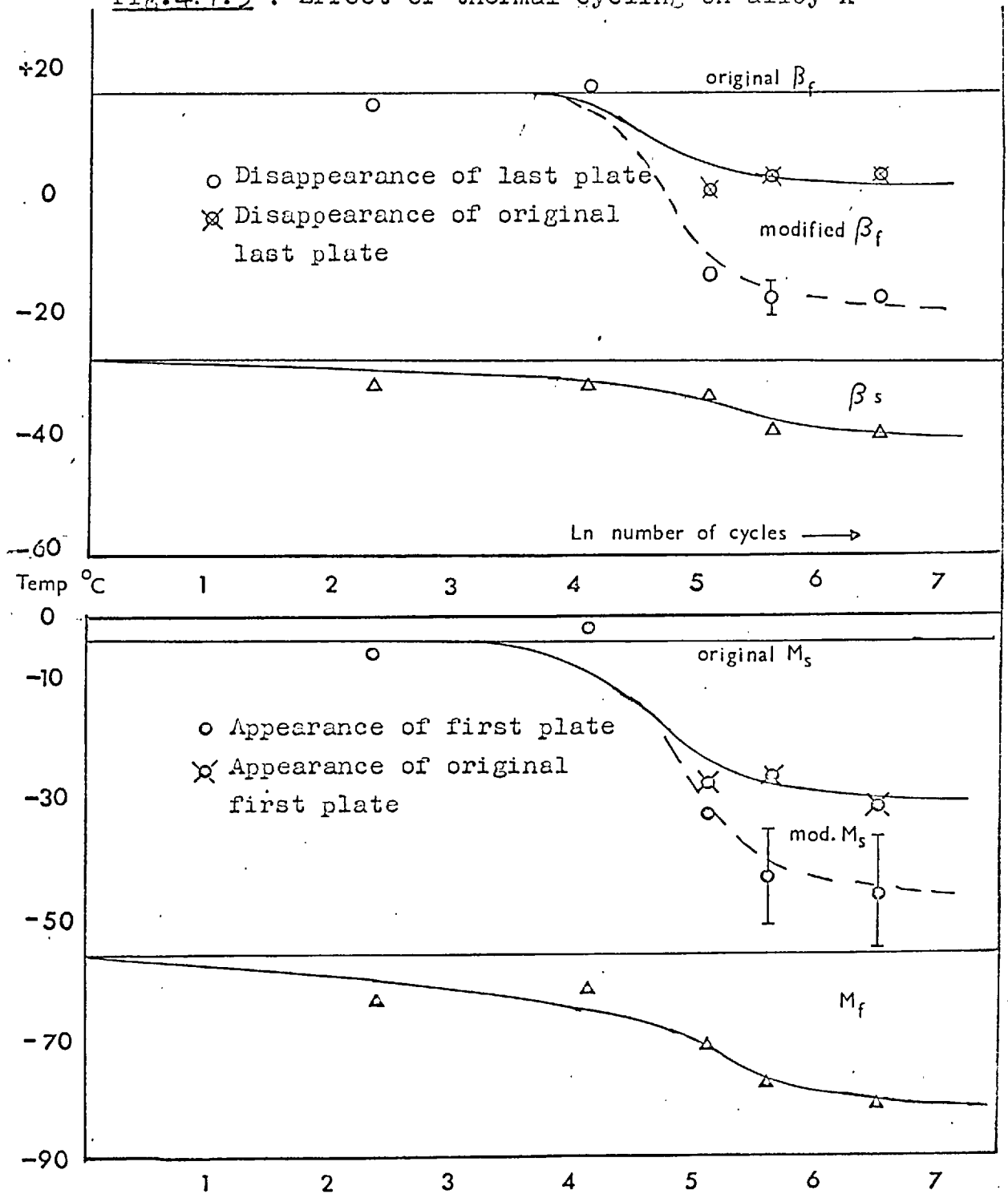
Thermal cycling sequence: Effect on transformation temperatures.

(f) A decrease in all T.T's with an increased number of transformations (see Fig. 4.7.5).

(g) Holding the specimen in the β condition produces a slight increase in transformation temperatures, however, towards their initial values.

The cumulative affect of repeated thermal cycling through the transformation temperatures on these temperatures is shown in Fig. 4.7.5. The temperature values are corrected to account for the increase in transformation temperature observed to occur on holding (item g above). The general form of this plot was observed in all specimens investigated, although the actual values of the reductions in T.T's showed some variation. As Fig. 4.7.5 shows, the M_s/β_f temperatures are more sensitive to thermal cycling than the M_s/β_s. The bursts observed when M_s is suppressed indicate that the delayed transformation has an ability to "catch up" as transformation progresses. The transformation range is slightly reduced therefore, by increasing the number of transformation cycles and the hysteresis is slightly increased.

Fig.4.7.5 : Effect of thermal cycling on alloy K



4.7.3 Electron Metallography

Observation of "in situ" transformation was carried out with the heating/cooling stage fitted to the EM6G microscope. As discussed in section 4.3 the martensite interface was observed to move smoothly and slowly under conditions of almost constant temperature as shown in Figs. 4.3.4 and 4.3.10. Growth rates during a complete transformation showed considerable variation however, indicating the "burst" phenomenon. This meant that it was not possible to select a region of β-phase at will, to observe the slow passage of the martensitic interface through it. In general it was necessary to find a thin region containing an interface and then change the temperature to promote growth or shrinkage of the martensite plate.

In the thinnest regions of the foil, the presence of the electron beam was frequently observed to produce shrinkage or, more commonly, growth of the martensite. The promotion of the reverse transformation may be expected since the heat generated by the impinging electrons cannot be removed so rapidly in the thin regions, particularly in the jet-polished discs since they are at the centre of the specimen, approximately 1 mm. from the holder. It is quite possible that there is a local temperature rise of several tens of degrees centigrade, depending on the intensity of the beam (see section 4.8 on precipitation in the microscope). The commonly observed growth of martensite when the beam is focussed on a thin part of the foil containing

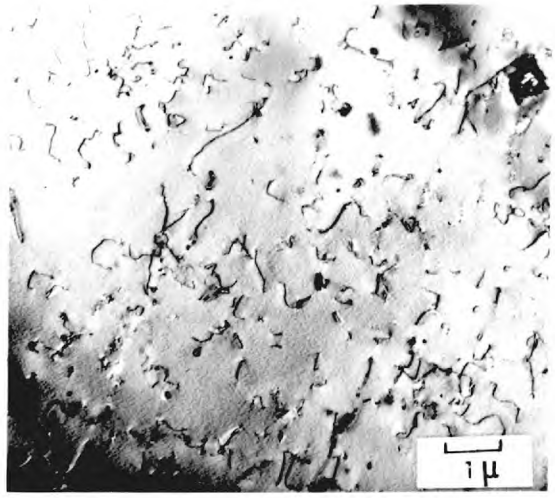
an interface is thought to be due to the development of elastic stresses since the foil can be seen to bend under these conditions Growth or shrinkage of plates did not occur in the thicker regions of the foil.

A complication in the observation of the passage of an interface through the field of view arises from the transformation displacements which change the foil orientation and reflecting conditions, making the recording of a growth sequence difficult (Fig. 4.7.6 a and b). These displacements are sufficient to cause a movement in the specimen as a whole, so that it was possible to detect the nucleation or growth of martensite plates in regions of the specimen beyond the field of view, by its vibration. Since light metallography showed that the martensite plates which formed at M_s were large and grew at high speeds, it is thought that the first martensite to form during cooling could be quite accurately detected by this method. Direct observation of the first plates to form is, of course, not possible due to the limited field of view available at any one time, and the proportion of the foil thin enough for transmission.

Sets of parallel platelets were frequently observed to form around the rim of the foil perforation when the electron beam was focussed there. Fig. 4.7.7 a shows an example of three interpenetrating sets, which have been analysed as thin filaments with $\{110\}_{\beta_1}$ habit, two of which are inclined at approximately 42° to the foil

Fig.4.7.6

"In situ" transformation by thermal cycling (Alloy G)



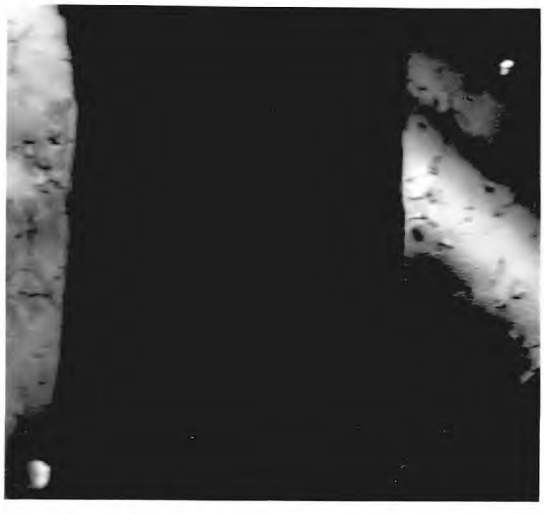
a) β before transformation



b) β after 1st. cycle



c) β after 2nd. cycle

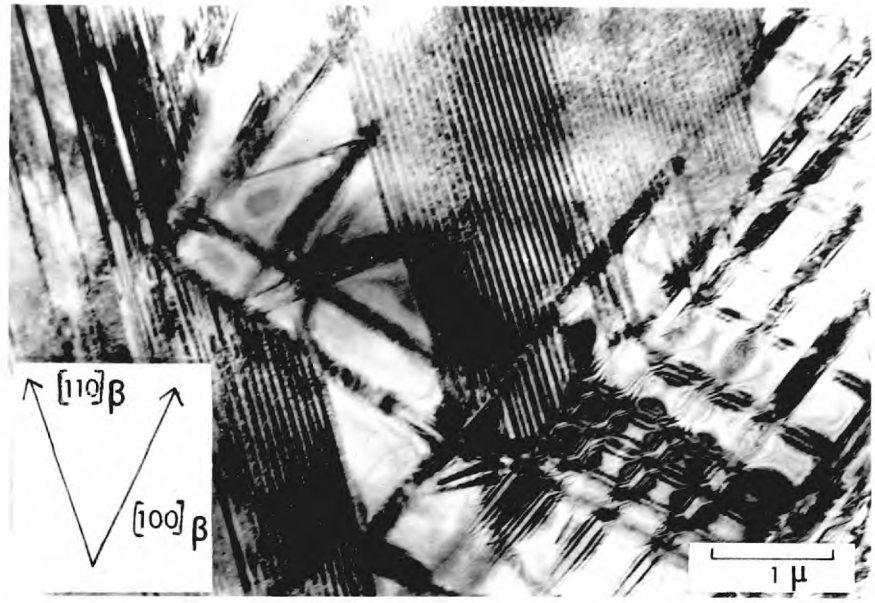


d) β + γ' during 3rd. cycle



e) β after 3rd. cycle

Fig.4.7.7 : γ' "twin filaments" near foil edge.
(Alloy G)



a) Three sets of interpenetrating filaments with $\{110\}\beta_1$ habit.



b) Region adjacent to a).
Nucleation observed at point ↘.

surface, the third perpendicular. The $\{110\}_{\beta_1}$ are parallel to the $\{121\}_{\gamma'}$, the twin plane observed in large plates of the martensite and the "twin filaments" perpendicular to the foil surface can be seen to have a similar appearance to a large twinned plate, although they generally advance individually into the β-phase, as can be inferred from the more irregularly "twinned" regions of Fig. 4.7.7 a. These martensitic features were never observed to catalyse the bulk transformation of the foil. Whilst it is not possible to state that they never do, because the whole course of a transformation in the thin foil cannot be observed; it became apparent from the many observations made that it is unlikely. These features also showed a high stability; they remained, after some shrinkage, at temperatures well above the β_f for bulk specimens (see also section 4.5.2).

The dominant feature of the transformations observed "in situ" was their extreme autocatalytic nature. With one single exception no martensite was ever observed to form completely surrounded by β-phase. The observed nucleation site is shown in Fig. 4.7.7b where a narrow "twin filament" has developed from it. The site is close to the specimen edge, so the formation of other filaments of different orientation have grown from this. The actual site appears to be a dislocation though this is not clear from the micrograph. (Further investigation of the region was prevented by completion of

the transformation). All other martensite formation which was observed in thin foils occurred at an already existing interface (or the foil edge, in the case of the filaments previously mentioned) i.e. nucleation was not observed by electron microscopy.

"In situ" cycling of a thinned region through the transformation range was not observed to repeat the formation of the same martensite plates. This is a consequence of the inability to observe the earliest plates to form - as discussed in connection with the light metallography. Fig. 4.7.6 shows the effect of three subsequent temperature cycles in which a completely different arrangement of plates has formed each time in the same region. In this sequence it can be observed how much more informative are the micrographs of re-transformed β-phase, containing surface traces from the γ', in identifying the extent and orientation of the martensite plates.

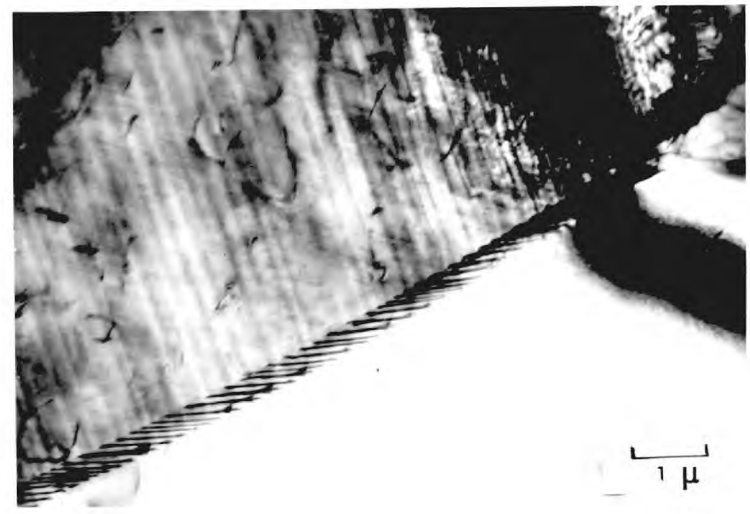
A suprising feature observed in the re-transformed β regions was the absence of alteration to the dislocation structure after such a large shape deformation as the formation of a martensite plate. Comparison of figures 4.7.6 a, b, c and e show this. Even more suprising was the observation of the unchanged matrix dislocations giving contrast within the martensitic structure, after the passage of the transformation dislocations through the region. The original matrix dislocations can be seen in Fig. 4.7.8 after the passage of

Fig.4.7.8 : β dislocations in γ'

(Alloy L)

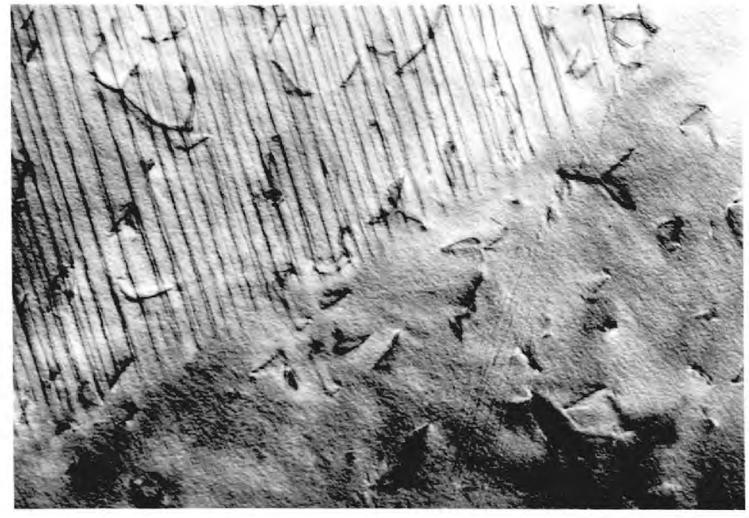
a) β_1 + γ'

showing interface of transformation dislocations

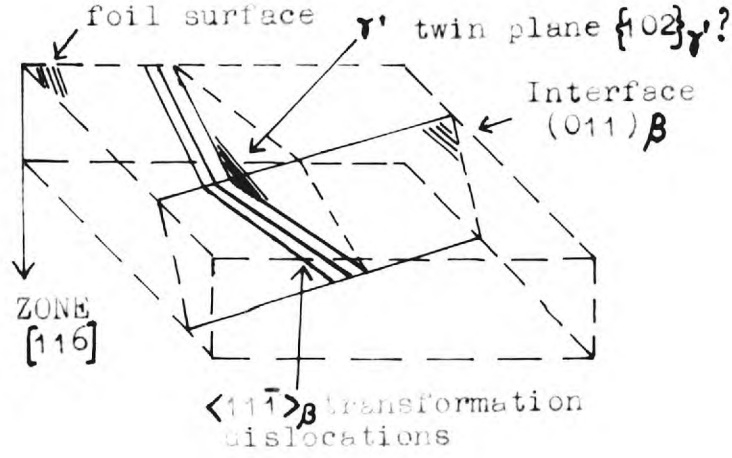


b) Field as a).

All β_1 showing γ' surface traces



c) Analysis of a).



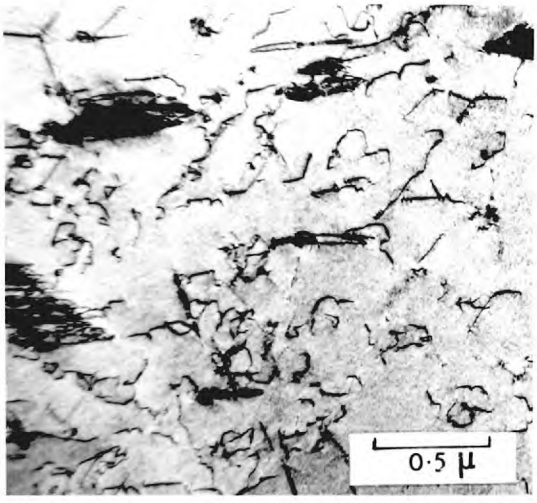
passage of a $\{110\}_{\beta_1}$ interface of <111> dislocations in the forward and reverse directions.

Observation of continuously cycled specimens in the electron microscope showed quite clearly, however, that plastic deformation of the β_1-phase does occur during transformation. A number of features were observed in increasing density, as the number of cycles previously performed on the specimen were increased (Fig. 4.7.9). The principal features commonly observed were:-

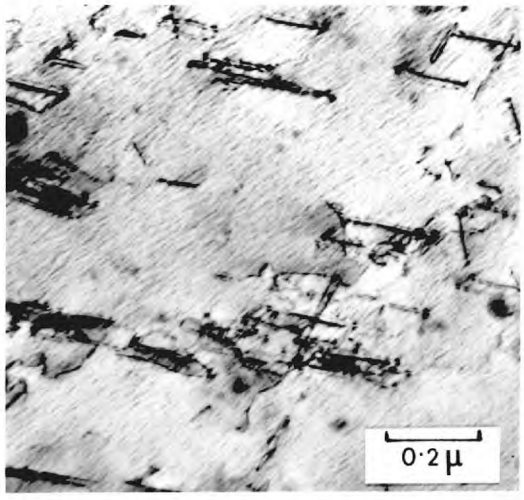
(a) Long traces in well defined directions which varied from specimen to specimen, and in the case of very long traces, (e.g. Fig. 4.7.9 c) and e) were not rational. In several cases, however, a transformation cycle "in situ" of the specimen produced surface traces parallel to the existing traces, and indicated the possibility of the latter being a fault, approximately perpendicular to the foil surface in a $\{110\}_{\beta}$ plane (Fig. 4.7.10).

(b) Large numbers of shorter, straight dislocations, parallel in direction (usually up to three predominant directions), both singly and in rows. Trace analysis was carried out on the row directions this indicated that the dislocations lay in a wide variety of possible slip planes for the b.c.c. structure, i.e. $\{110\}$, $\{112\}$ and $\{123\}$ type planes. In many cases these networks were similar in size and shape to the narrow filaments of martensite observed; Fig. 4.7.9f shows a striking example where the two sets of rows of different

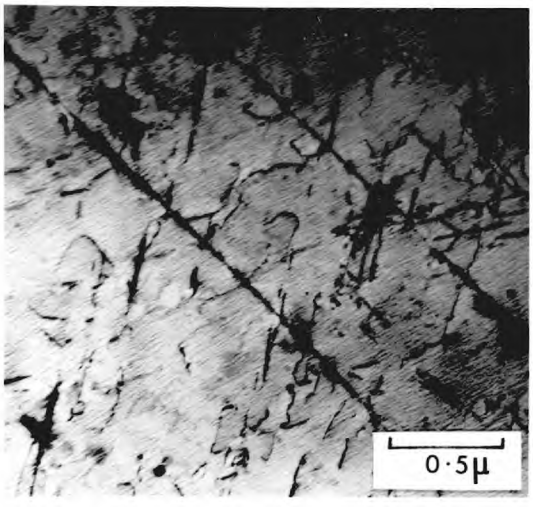
Fig.4.7.9: β dislocation structures in cycled specimens
(Alloy F : 1 hr 950°C - brine Q)



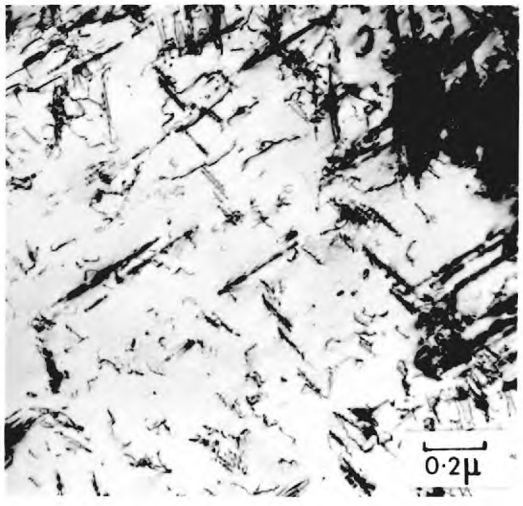
a) 5 cycles



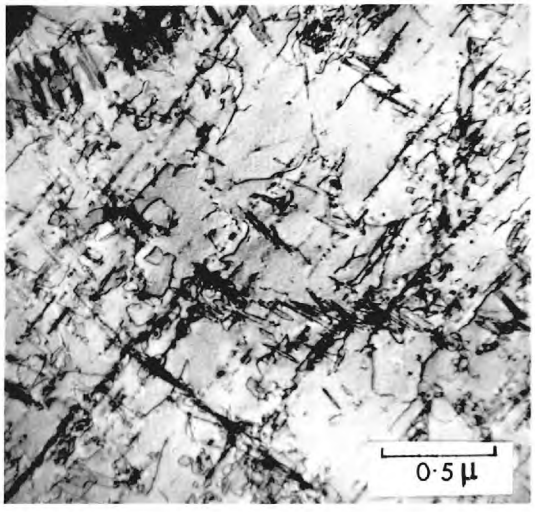
b) 30 cycles



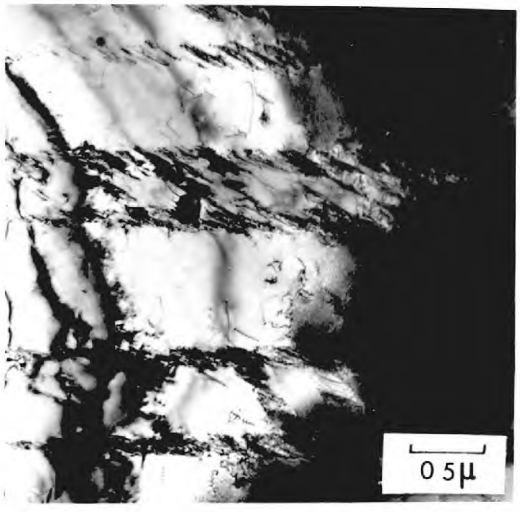
c) 30 cycles



d) 100 cycles



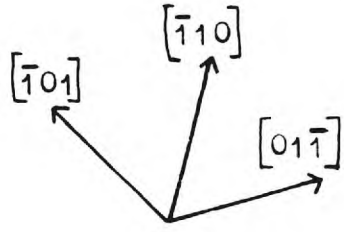
e) 500 cycles

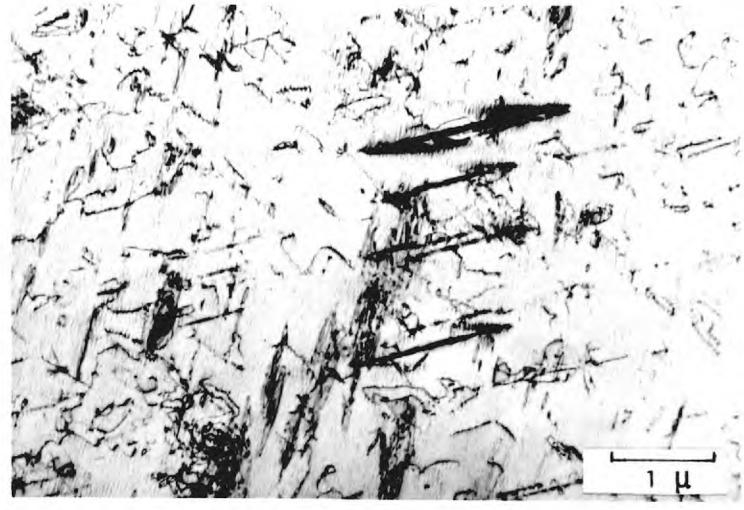


f)"ghost" martensite - 10 cycles

Fig.4.7.10 : Transformation at β defects
(Alloy F after 100 cycles)

a) Dislocations and large defects in β





b) Field as a) after transformation cycle. Surface traces.



c) Field as a) & b) after 2nd. cycle. Surface traces parallel to adjacent large defect in β.



orientation lie in $\{112\}_\beta$ planes.

(c) Fault contrast between some of the dislocations in rows of a $\{110\}_\beta$ or $\{112\}_\beta$ type plane (Fig. 4.7.11).

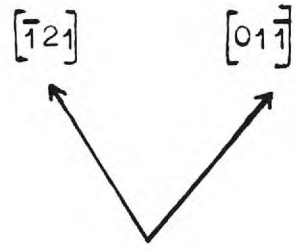
"In situ" transformation cycling of these specimens did not show that any of these features operated as nucleation sites for the transformation. It was clearly not possible to check on all of the networks during a transformation but the surface traces left in the retransformed β-phase enabled the course of the martensitic interfaces to be charted afterwards. Thus in Fig. 4.7.11 the traces can be seen passing uninterruptedly through the fault, with no indication that it had grown during the temperature cycle. A correlation between the surface traces and matrix imperfections was occasionally observed for the long traces of high contrast, as shown in Fig. 4.7.10, although in this case it is only after the second thermal cycle that there is an indication that a fault in a $\{110\}_\beta$ plane, perpendicular to the foil surface, may have nucleated a set of $\{112\}_\gamma$ twin filaments.

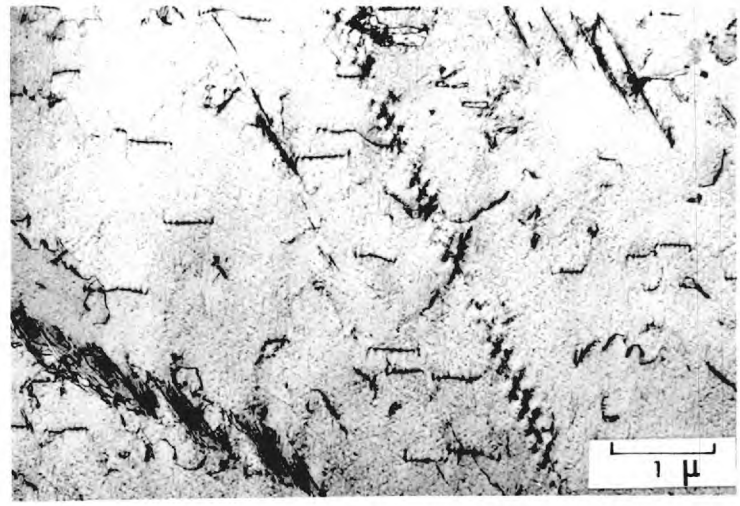
There has been little evidence therefore, from these observations that the transformation generates imperfections which could act as nucleation sites for subsequent transformations. This is in agreement with the direct observations of the course and temperature of successive transformation cycles. The autocatalytic nature of the reaction remains dominant; the sites of initial plates showed

Fig.4.7.11 : Faults in β from thermal cycling (Alloy F after 100 cycles)

a) b.f. $[3\bar{1}1]$ zone

$g = 01\bar{1}$



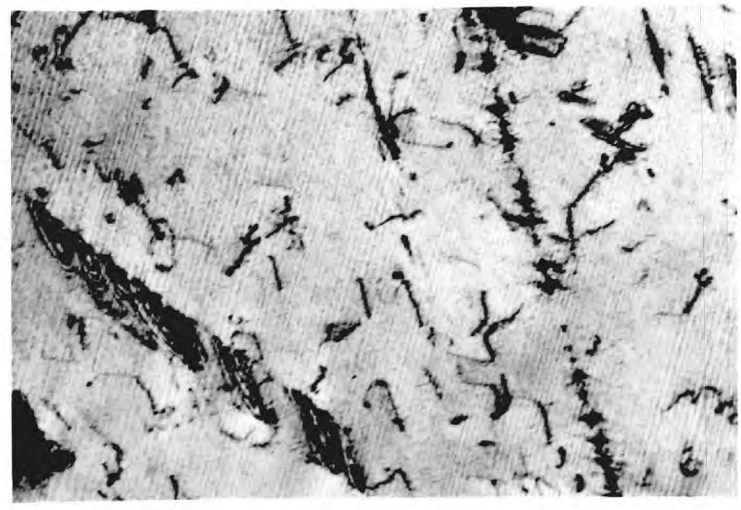


b) b.f. as a)

$[\bar{1}11]$ zone (30° rotation from $[3\bar{1}1]$ about $01\bar{1}$ axis)

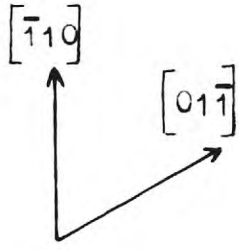
$g = \bar{1}10$

After transformation cycle.



c) b.f. as b)

After 2nd. cycle





little variation, and the transformation temperatures fell as the number of cycles was increased.

Thus the results of section 4.7.2 indicate that the complex dislocation arrays observed may suppress martensite nucleation rather than aid it. The passage of the interface appears to be less affected since the matrix dislocations were observed to remain unchanged during individual cycles, and so the M_f temperature is lowered less than the M_s. This causes a slight reduction in the temperature range of the transformation, whilst the hysteresis increases.

4.8 γ_2 Precipitation and the Martensite Transformation

4.8.1 γ_2 formed at high temperatures

Fast quenching is necessary to suppress the γ_2 precipitation in all the alloys studied; as the aluminium content increases the reaction becomes almost insuppressible (see table 4.2), and the characteristic rosette morphology of γ_2 is developed as described in section 4.2. In specimens which had spent long in the equilibrium $\beta_1 + \gamma_2$ phase-field dendritic γ_2 was observed. These large γ_2 crystals were always observed to promote the nucleation

of martensite. There was direct metallographic evidence of this during observed transformations by both light microscopy (Fig. 4.8.1) and electron microscopy, for both the large rosettes (Fig. 4.8.2 a) and dendritic structures (Fig. 4.8.2 b and c). In addition the transformation temperatures showed an increase in all specimens quenched sufficiently slowly to allow γ_2 precipitation or held in the $\beta_1 + \gamma_2$ phase-field (section 4.2).

The morphology of the martensites formed in a $\beta_1 + \gamma_2$ matrix also differed considerably from that normally encountered. The plate size was limited to the distance between γ_2 crystals, about one hundredth of the commonly observed plate size of several millimetres for single phase β_1 transformation, although the characteristic lens-shaped plate with midrib was still observed to be the predominant form of the martensite crystal (Fig. 4.8.2 d). In the electron microscope the "twin filaments" of martensite were observed to form in definite crystallographic orientations, identified as $\{112\}_\beta$ or $\{110\}_\beta$.

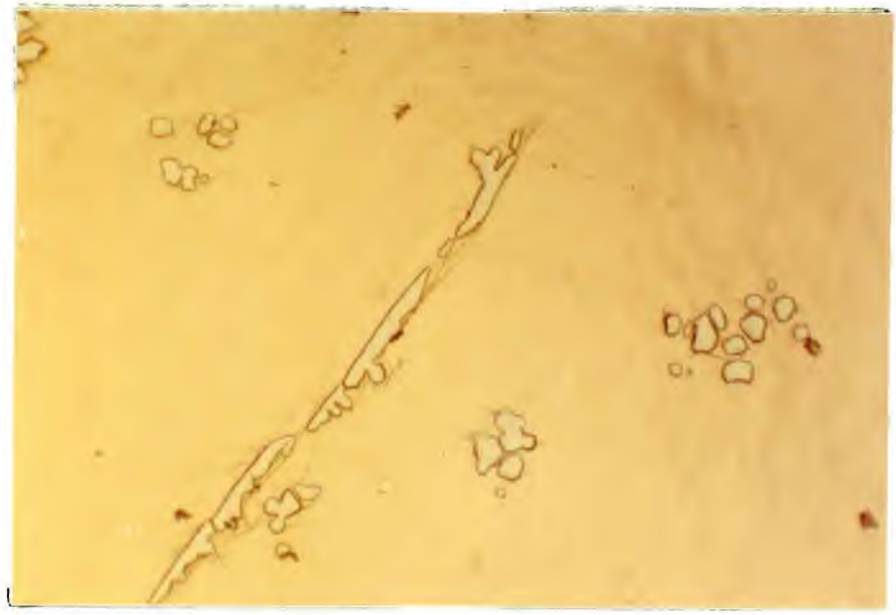
4.8.2 γ_2 formed by low temperature ageing

The transformation temperatures of the aged alloys described in section 4.2 were measured metallographically and the results for alloy H are shown in Fig. 4.8.3. These show an increase in

Fig.4.8.1 : Alloy F, 1 hr at 800, Q in iced brine X220.

Martensite formation at γ_2 formed at high temperature.

a) Room temperature



b) Cooled

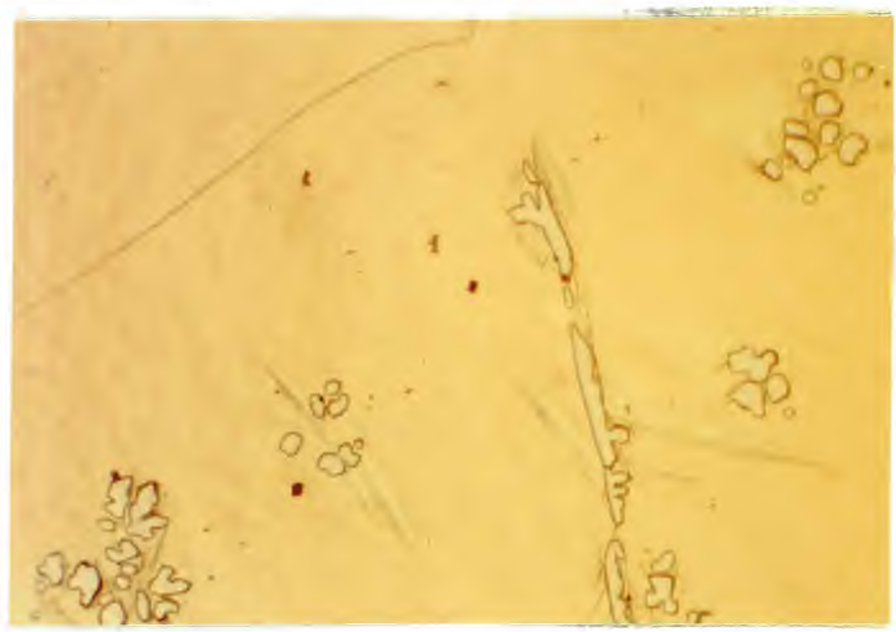
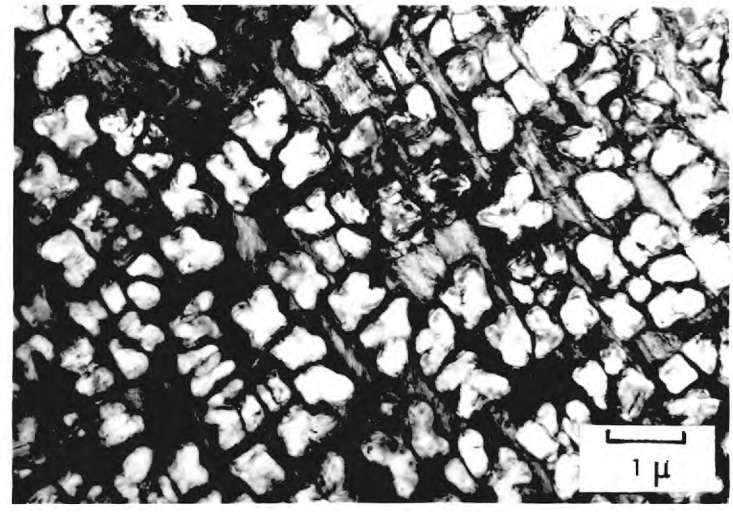


Fig.4.8.2 : Martensite formation at massive (unsuppressed) γ_2 precipitates.

a) Alloy F. (M_f=-34°C) Large γ_2 rosettes in martensitic matrix, at 20°C.



b) Alloy K. (M_s=-23°C) γ_2 dendrite formed during cooling after hot rolling. Martensitic border at 20°C.



c) Field as b) cooled to -15°C.

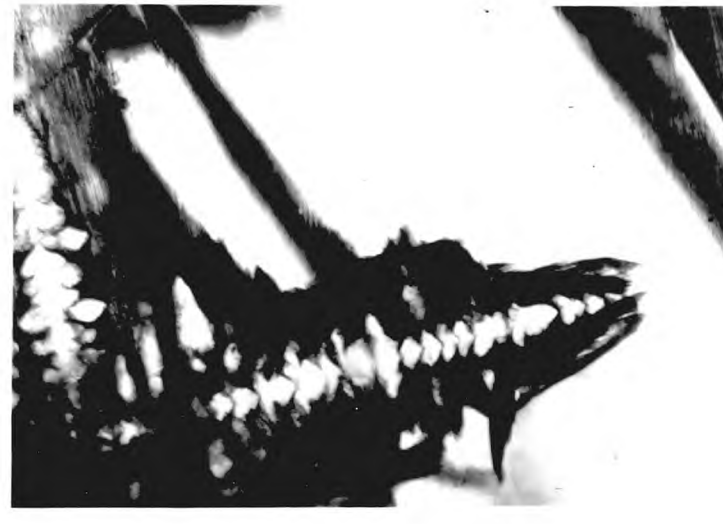


Fig.4.8.3 The effect of ageing on transformation temperatures.

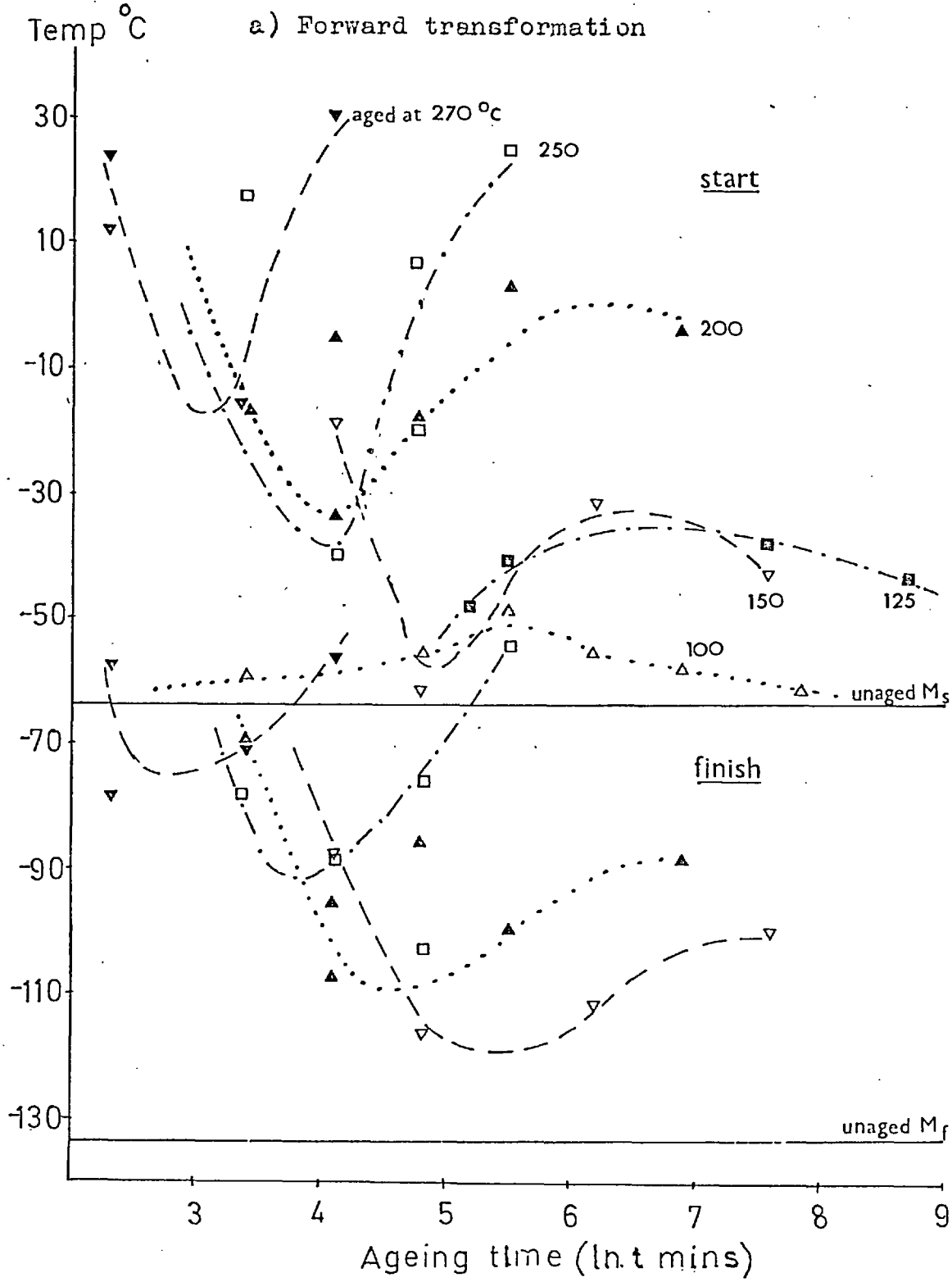
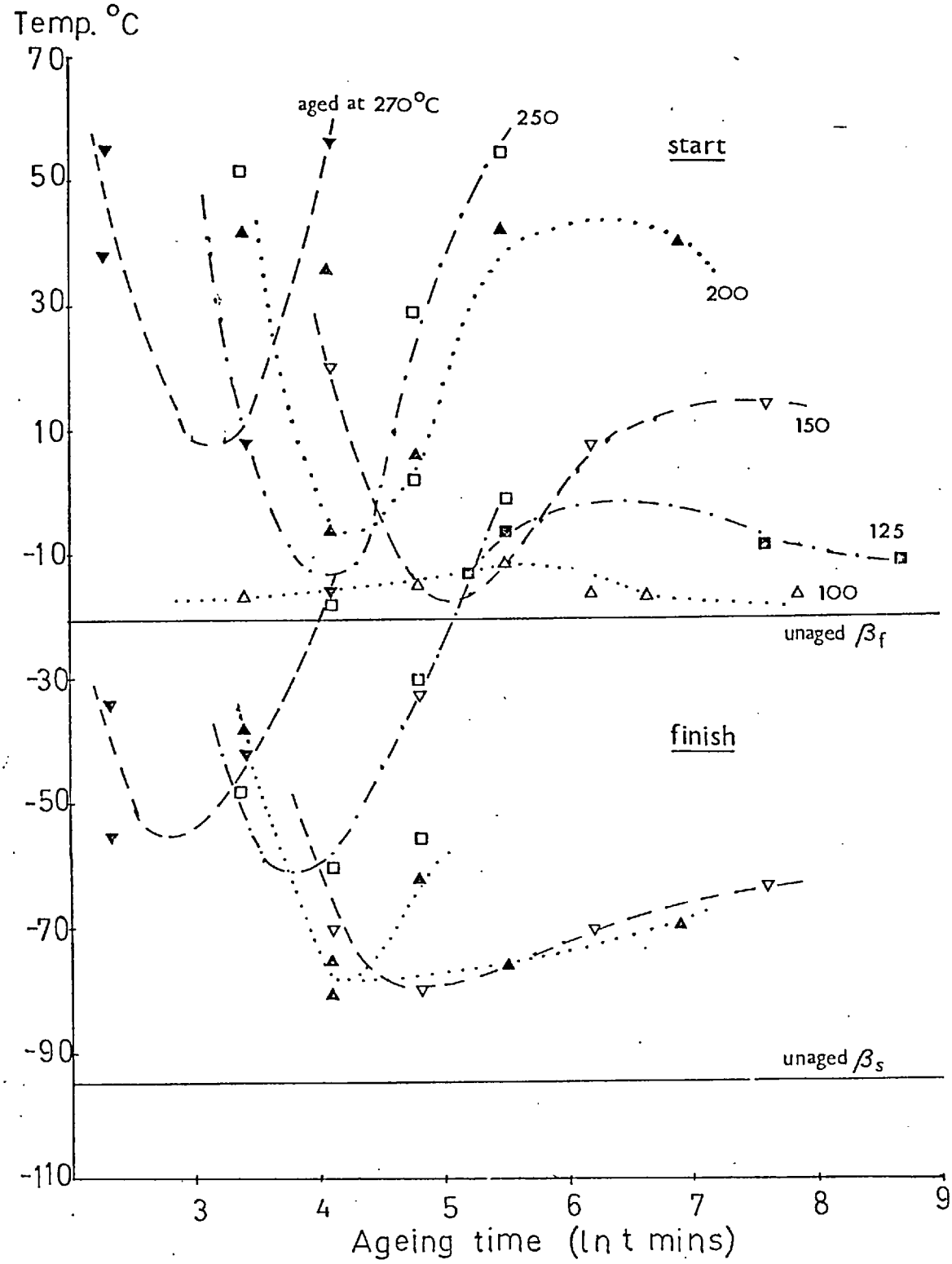


Fig.4.8.3b) Reverse transformation



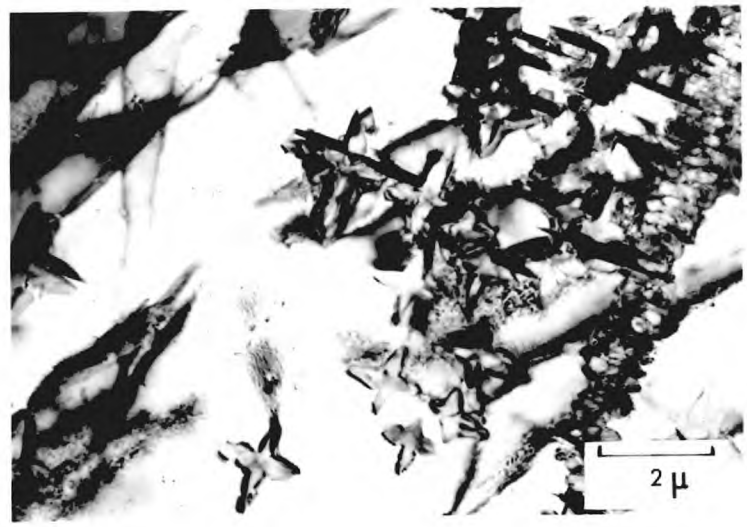
all transformation temperatures which becomes more significant as the time and the temperature of the ageing treatment were increased. This is consistent with the results of the previous section, and was supported by direct observation of γ_2 initiated nucleation in (heavily) aged specimens. Fig. 4.8.4 shows such a sequence for a specimen in which precipitation was induced by electron beam heating. The precipitates shown are somewhat larger than those produced by the low temperature ageing treatments, and they formed in a matter of minutes, which indicates that the temperature rise produced by the electron beam is considerable. The martensite morphology is similar to that observed adjacent to the γ_2 formed at high temperatures, -"twin filaments" in well defined directions, which later grow into large, finely twinned martensite plates.

The results of the temperature measurements after short-time ageing treatments (less than 1 hour) showed considerable variation between different specimens which had had a similar treatment, and no consistent relation to the time of ageing could be discerned. Most specimens showed a rise in the temperatures but in several the transformation appeared to have been inhibited. Despite careful repetition of the experiments on several different specimens under identical conditions at the same time, the only consistent feature of the results on these specimens was that the variation persisted for short-time ageing at all the temperatures investigated, between 125 ^{o}C and 275 ^{o}C. At 300 ^{o}C the precipitation reaction was observed to proceed

to the eutectoid

Fig.4.8.4 : Nucleation and growth of martensite at γ_2 "rosette" precipitates. (Alloy G. 1 hour at 950°C - brine Q, aged by beam heating)

a) Initial fine γ' twins at 20°C.



b) Field as a). Growth of γ' between precipitates - 20°C.



c) Field as a) and b). Transformation to γ' almost completed - 60°C.

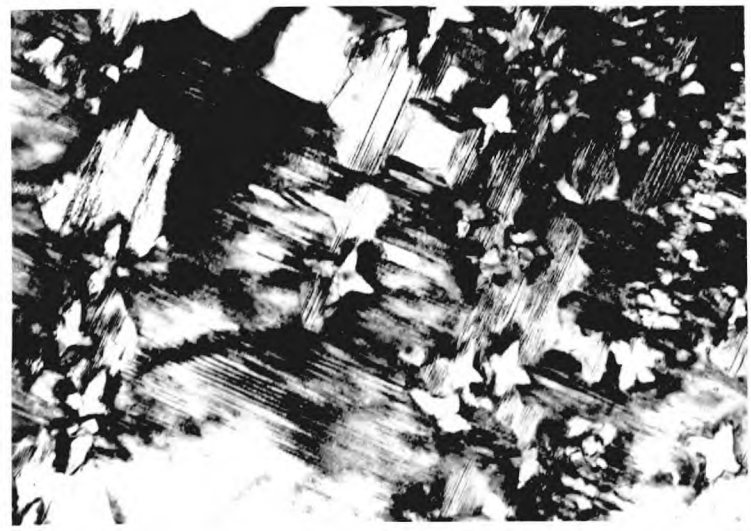
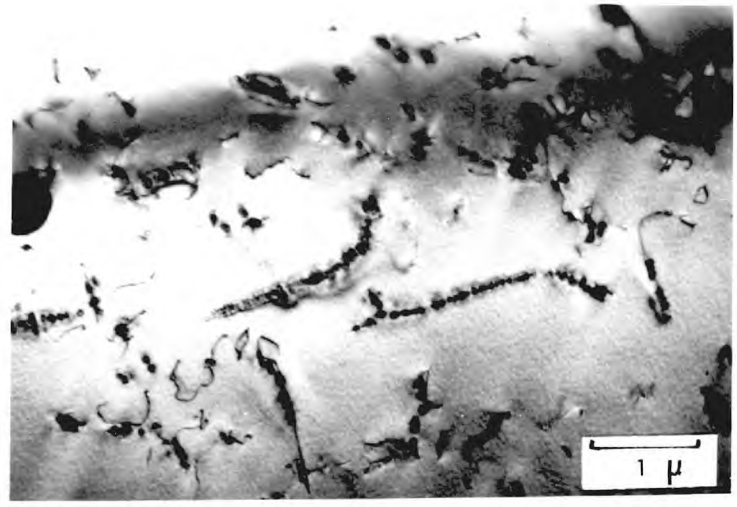
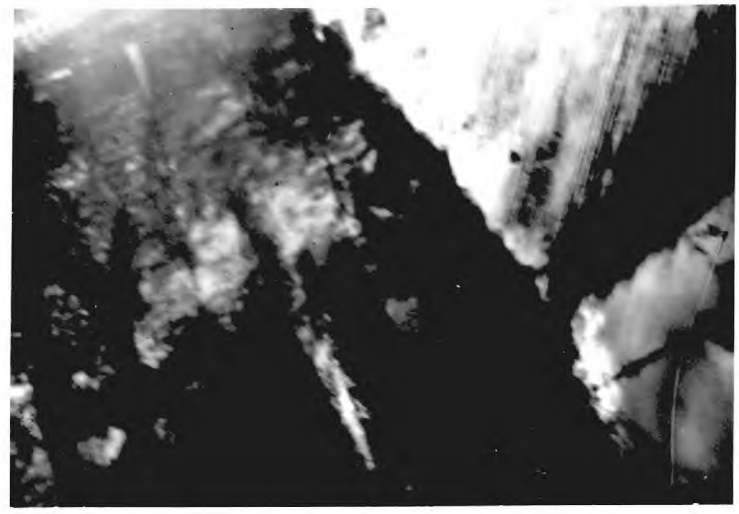


Fig.4.8.5 : Martensite plate growth through regions of "row" γ_2 precipitation. (Alloy H, 1 hr at 950°C - brine Q - aged 8 hr at 150°C).

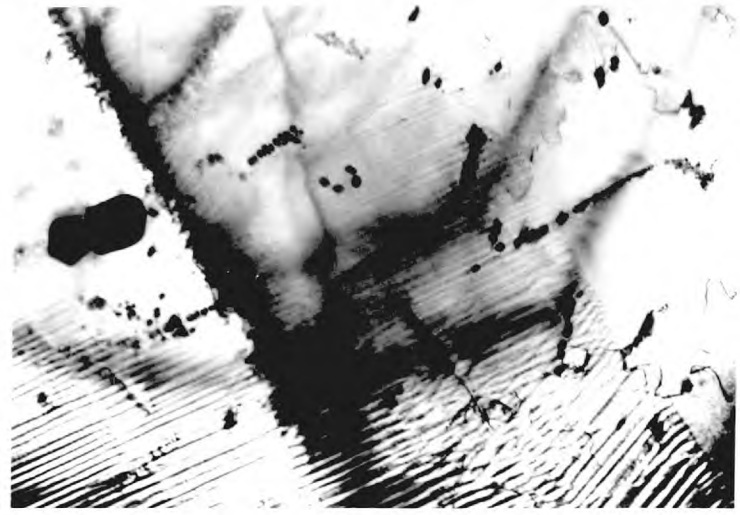
a) $\beta_1 + \gamma_2$
20°C



b) Field as a).
$\gamma' + \gamma_2$
- 117°C



c) Field as a) and b).
$\beta_1 + \gamma_2$
surface relief from traces of removed γ' twins.

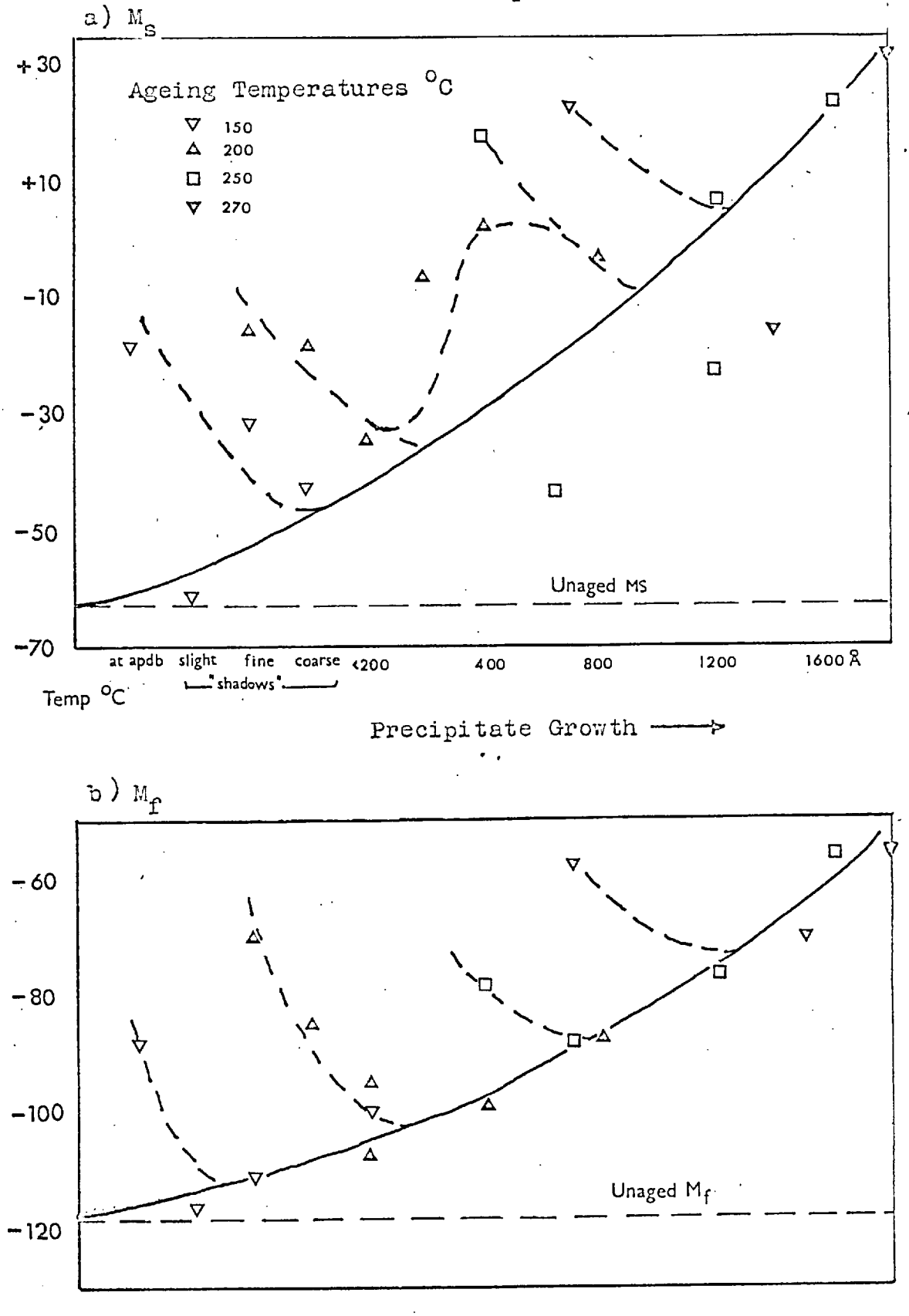


γ_2 + α structure after a few minutes. At 100 °C a slight increase in transformation temperatures was recorded after 4 hours heat treatment.

In an attempt to rationalise these results they have been plotted as a function of the degree of precipitation observed in the electron microscope in Fig. 4.8.6. The results for changes in M_s still appear erratic, but the M_f results lie on a set of curves which converge as the precipitate size increases at each ageing temperature. If, in view of the autocatalytic nature of the reaction, the M_f temperature is taken to be a measure of the equilibrium extent of martensite growth (i.e. largely independent of nulceation problems), then variations in M_f may be considered to reflect changes in the free energy of the matrix more accurately than M_s. The smoothly rising convergence of the M_f versus degree of precipitation curves may then represent the effect of aluminium depletion of the matrix on the transformation; whilst the individual falling curves represent the effect of some additional time dependent process, independent of temperature.

Difficulty was experienced in preparing foils with extensive thin areas for the "in situ" transformation studies, from specimens containing much γ_2 phase. The window technique which was used for single phase β specimens was liable to cause preferential

Fig.4.8.6 : Effect of precipitate development on transformation temperatures.



attack at the interphase boundaries, whereas the jetting method which overcame this did not produce such large thin areas. The "in situ" thermal cycling of the aged alloys was limited by these factors to a small number of specimens. It was quite clear however, that the smaller precipitates did not act as nucleation sites for the transformation. In contrast to the behaviour previously described the martensite interface was observed to pass smoothly through the precipitates and the presence had no discernable effect on the martensite morphology. (Fig. 4.8.5).

The limiting size of γ_2 precipitate which promoted nucleation of martensite appeared from the observations made, to be about 1000 Å. The smallest precipitates appeared to be associated with a single "twin filament" orientation so that there is little effect on the morphology of the resulting martensite plate, which may later appear to have enveloped the precipitates (Fig. 4.8.7). This size of precipitate corresponds to a point on the M_f versus precipitation graph beyond which there is a smooth rise in the transformation temperatures which is independent of the ageing temperatures (Fig. 4.8.6.). No indication of the cause of the erratic behaviour of the transformation temperatures for short-time ageing was obtained from the "in situ" transformations.

Fig.4.8.2d : Martensite morphology in a slow quenched specimen (Alloy F : 1 hr at 950°C - Q in CCl_4 at 20°C)

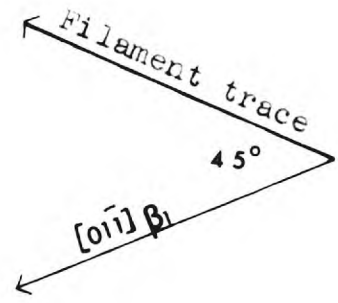


$\beta + \gamma_2 + \gamma'$ X300

Fig.4.8.7 : Nucleation of martensite at 1000Å diameter particles of γ_2 (Alloy F : 1 hr at 950°C - Q - 1 hr at 260°C)



a) b.f. $\beta + \gamma_2 + \gamma'$
filaments // $\{112\}_\beta$



b) Trace analysis
[Inclination of $(112)_\beta$ is 63° to (111)foil surface]

CHAPTER FIVE : DISCUSSION

"The great tragedy of science -
the slaying of a beautiful hypothesis
by an ugly fact."

T.H. Huxley.

CHAPTER 5 : DISCUSSION

5.1 The Effects of Ordering and γ_2 Precipitation on the Transformation

Direct observation of transformations in specimens containing γ_2 precipitates of a size greater than 1000 Å, has demonstrated their ability to nucleate the martensitic γ' phase, and this has been supported by measurement of transformation temperatures of these specimens. The γ_2, β and β_1 structures are very closely related (Fig. 2.2). The present work has confirmed that similar lattice vectors in the structures are parallel and that:

$$a(\gamma_2) = 3a(\beta) = \frac{3}{2}a(\beta_1)$$

It is to be expected therefore that the presence of γ_2 in the β_1 matrix does not create a high energy interface, since the positions of the atoms need not be displaced across such an interface. This is supported by the absence of stress fields around the precipitates observed in the microscope. Thus it would appear that the factor favouring the nucleation of martensite at the γ_2/β_1 interface is primarily chemical, rather than that of a reduction in strain or surface energy. Since the transformation has been shown to be very sensitive to aluminium content it is

clear that the formation of regions of aluminium-depleted β adjacent to the aluminium-rich γ_2 will favour the formation of martensite. The greater the extent of segregation, the greater will be the chemical driving force leading to the observed continuous rise in transformation temperatures with increased ageing times. This compositional interpretation is supported by the observation of a rise in transformation temperatures in a specimen aged at 100 °C where no γ_2 precipitates could be observed.

The results of the transformation temperatures measured in specimens aged for short times indicated however, that other factors must influence the transformation mechanism.

The earliest stages of precipitation have been recorded at the domain boundaries of the ordered β_1 structure in these alloys, in agreement with observations of Swann[74] on similar alloy. The $a/4$ <111> (B2) boundaries appear to be preferred to the $a/2$ <100> (DO_3) type and it was suggested that this was due to their higher energy. The observation of the small number of B2 type boundaries was presented in support of this. If, however, as the present work has indicated, the B2 order develops at a higher temperature than DO_3, then the B2 domains would be expected to be larger, because of the higher diffusion rates at temperatures just below the B2 ordering temperature. The B2 type boundaries

are associated with wrong first nearest neighbour atom pairs, whilst the DO_3 produce changes only in second nearest neighbour interactions, so that the equations for the energies of the two types of boundary depend on different parameters. Values calculated for the two types of Fe_3Al indicate that the B2 boundary energy is somewhat higher (101).

It has been pointed out[74], that the atomic arrangements at the DO_3 type boundary resemble those in the γ_2 structure more closely than do those at a B2 boundary which indicates that these cannot be very important, and are not responsible for the preference of precipitation on B2 boundaries.

Further differences in the two types of boundary in respect of precipitation were noticed at later stages of the reaction. The B2 boundaries appeared to be increasingly favoured to the DO_3. Since the DO_3 domains were much smaller, precipitation on them was always difficult to identify clearly, and showed up best in a bright field micrograph with a strong S_2 type reflection giving B2 contrast, in addition to the precipitate contrast within the B2 domains. Little evidence of precipitation on the DO_3 boundaries was obtained at later stages in the precipitation reaction. The B2 boundaries, by contrast, were observed to develop anisotropy in specimens aged for between one half and two hours at 200 ^{o}C; this was particularly apparent in a specimen

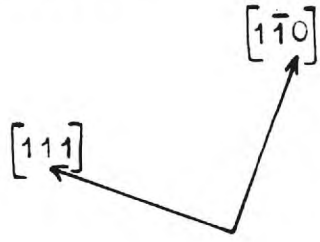
aged for one hour (Fig. 5.1 a). The alignment appears to be in {110} and {111} planes and was not observed for the DO_3 boundaries (Fig. 5.1 b). In many of these specimens the fine γ_2 precipitates were observed to be arranged in rows parallel to a straight or angled dislocation (Fig. 4.2.5 a). These dislocations have been observed associated with the aligned B2 boundaries (Fig. 5.2) although most of the aligned boundaries do not show contrast with a fundamental reflection operating (Fig. 5.1 c).

These dislocations, and those generated during the thermal cycling of specimens are often observed to be in pairs (see for example Figs. 4.7.9 b, 5.2 and 5.3). On ordering from β to the DO_3 β_1-phase the perfect dislocation $a/2\langle 111\rangle$ must become $a'\langle 111\rangle$ where a and a' are the lattice parameters of β and β_1 respectively, i.e. $a' = 2a$. This means that the presence of the perfect dislocation of the disordered β creates and antiphase boundary in β_1. Only when four of these travel together does the DO_3 structure remain unchanged. However the $a/2\langle 111\rangle$ is equivalent to the $a/2\langle 100\rangle$ or DO_3 type boundary and it has been pointed out that if the energy of the DO_3 boundary is significantly lower than that of the $a/4\langle 111\rangle$ B2 type then the superlattice dislocations may be expected to travel in pairs creating DO_3 boundaries, rather than B2 (101). Paired dislocation observed in the present alloys have not been clearly associated with DO_3 boundaries but

Fig.5.1 : Anisotropic B2 boundaries

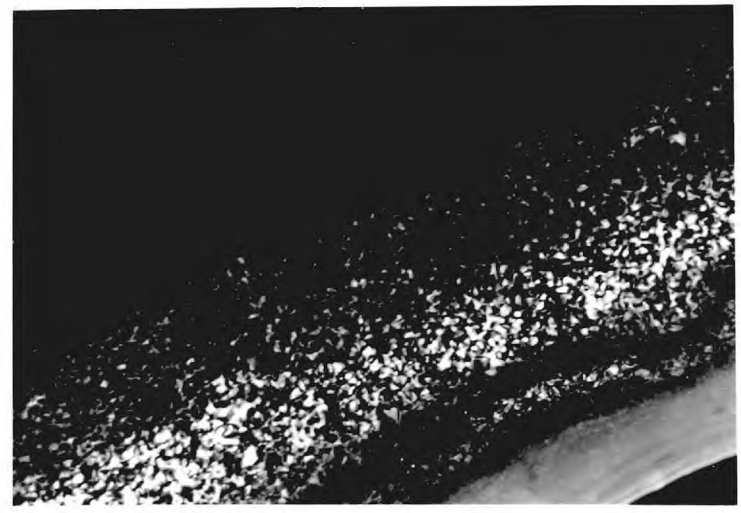
(Alloy H : 1 hr at 950°C - Q - 1 hr at 200°C)

a) h.r.d.f. g = 200 aligned B2 domain boundaries





b) h.r.d.f. g = 111 isotropic DO_3 domain boundaries



c) b.f. γ_2 and superlattice dislocations



Fig.5.2 : Aligned B2 boundaries and superlattice dislocations (Alloy H : 1 hr at 950°C - Q - 1 hr at 200°C)

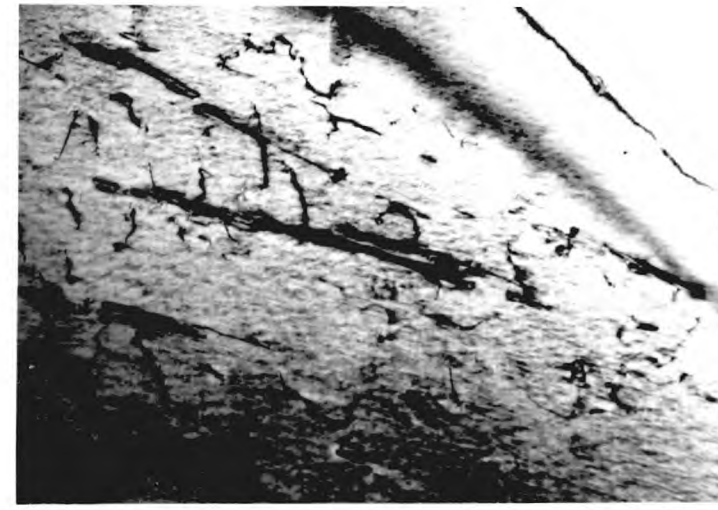
a) h.r.d.f. g = 222
B2 boundaries



b) h.r.d.f. as a)
g = 111
DO_3 and B2
boundaries



c) b.f. as a) & b)
γ_2 and superlattice
dislocations



it seems possible that this observation indicates a higher B2 boundary energy.

Thus it is suggested that precipitation of γ_2 is preferred on B2 boundaries because of their higher energy but that the resultant change in composition leads to anisotropy of boundary energy, aligning the boundaries in close-packed planes. The presence of a fine dispersion of γ_2 at the boundary appears to lead to the generation of dislocations of a similar shape to the precipitate clusters, that is the aligned B2 boundary. In contrast to this however, at a later stage in the ageing process, no observations of either the straight precipitate free dislocations or aligned boundaries were made, and the larger precipitates were still observed to be associated with the boundaries, as well as with randomly oriented dislocations (Fig. 4.2. 5c). These larger precipitates being observed to aid the nucleation of martensite.

The anomalous martensite transformation temperatures were obtained from the specimens which displayed the "shadowed" dislocation phenomenon described above. It has not been possible however, in the present study to elucidate any direct connection, since the process which led to this microstructure is not fully understood.

5.2 The effects of stress on the transformation

Quantitative investigations on the mechanical properties of these alloys were not possible since in order to achieve the quenching rates adequate to suppress γ_2 precipitation the alloys had to be hot rolled to 0.5 mm strip. Several qualitative observations of interest have been made, however.

The martensite induced by plastic deformation was observed not to catalyse transformation in the bulk of the specimen. The small needle-shaped martensite plates in the vicinity of the indentation (Fig. 4.6.1) are in contrast to the large broader plates which usually form, particularly at the start of the transformation. The structure of these plates was not investigated in the present work but at the time of writing, Otsuka and Shimizu report the observation of β'_1 martensite, induced by punching in an alloy of Cu-14.2 w/o Al - 4.3 w/o Ni [102]. This is surprising since, as discussed in section 2.4 there is considerable evidence that the martensite transformation is effected by a twinning shear at low temperatures, that is γ' martensite is formed, whereas the β'_1 martensite has itself been observed to deform by twinning rather than further faulting[80]. The presence of β'_1 in a specimen which transforms to γ' during cooling may be the reason for the lack of further growth of the stress

induced martensite, although in the present work and that of Swann and Warlimont[80] plates of mixed α'_1 and γ' martensite have been observed, indicating that the change can occur fairly readily.

There is a similarity between the situation of the indented regions of such a specimen and the edge of a thin foil under the electron beam. In both cases a combination of high surface to volume ratio and mechanical stress produces unusually small martensite plates which do not grow. In the latter case one reason for this appeared to be the impingement of the small "twin filaments" growing on different plates.

In contrast to this, specimens elastically deformed transformed to produce the characteristic broad plates of γ' martensite which grew readily on subsequent cooling. The transformation itself was observed to be elastic at low stress levels and the hysteresis was observed to increase as the stress level and volume of induced martensite increased, in agreement with the measurements of Rachinger[63]. A significant hysteresis in the transformation cycle means that removal of the stress will leave a significant volume fraction of the specimen martensitic at a constant temperature. This volume will have suffered a change in shape due to the capacity of the martensite to form in preferred orientations with respect to the direction of the applied stress. The volume change

of a relatively small amount of crystal may give a gross shape change to the specimen. For example a contraction or expansion in one small region on one side of the strip would kink the strip. The martensite, if it is still in elastic equilibrium with the matrix can then be removed by a small rise in temperature, thus removing the shape change. This is the sequence of events occurring in a "shape-memory" effect which has been observed in all the alloys studied. Shape reversal was completed at approximately the normal ϑ_f temperature for each alloy although an increase in the temperature was noted as the number of shape reversals increased. This is thought to be due to plastic deformation of the ϑ-phase.

This account suggests that the requirements of an alloy, for it to show this effect, are that the transformation should be thermoelastic and anelastic, two characteristics which are commonly found together since both imply that the transformation strains do not exceed the elastic limit of the parent and product phases.

The alloys in which the shape-memory effect has been observed appear to have more in common than the above feature, however. They all have ordered b.c.c. or f.c.c. parent phases which transform to an ordered hexagonal (i.e. orthorhombic) martensite. No memory effect was observed in partially ordered or disordered

Fe_3Pt although it was present when ordered [70]. There has as yet been no attempt to account for the apparent significance of the ordered structure.

Otsuka and Shimizu first observed the shape-memory effect in Cu-Al-Ni by deforming the martensitic γ' phase, rather than stress inducing it from β-phase. This has been done in the present study and similar behaviour was observed in all the alloys investigated. The observation of the shape-memory effect under these conditions implies that the γ' martensite can be elastically deformed to produce the new shape by the preferential movement of appropriately orientated interfaces within the γ' matrix, and that the new martensite orientations can then transform back to the original β orientation. This mechanism has not been investigated in the present work.

The γ' phase is softer than the β-phase and it was found that the memory effect could be repeated a greater number of times by deforming γ' without increase in hysteresis. This appears to indicate that the interfaces can move preferentially with respect to stress more easily in a martensitic matrix than a β matrix; a somewhat surprising conclusion.

5.3 Kinetic features of the transformation

The results from various sections of this study have confirmed that the course of the transformation is governed by the basic thermodynamic equation (1.3) which states that the transformation will occur when the excess of free energy of the martensite phase over the parent phase (the chemical driving force) is sufficient to provide for the strain and surface energies involved in creating a new crystal volume and interface. The chemical driving force has been shown to be strongly dependent on aluminium content, and less strongly on nickel content. The effect of the presence of large γ_2 precipitates on the transformation has been explained in terms of a changed chemical driving force. Grain boundaries were not observed to be sites for nucleation which indicates a lack of grain boundary segregation. In one specimen, persistent formation of the first martensite plates in a particular region at temperatures well above the rest of the specimen was shown by microprobe analysis to be due to local depletion of aluminium.

The martensite has been observed to form initially always in the region of the specimen where its strain and surface energy are lowest. That is in regions where the surface to volume ratio is largest. Transformation can be initiated in a particular area by creating a large surface to volume ratio, for example by electropolishing to perforation. Electron metallography has shown that

in the extreme case further growth may in fact be inhibited by the random growth of "twin filaments" on a variety of different $\{110\}_\gamma$ $\{121\}_\gamma$ and $\{301\}_\gamma$ planes (Fig. 4.5.3, 4.7.7 a). Similar effects have been observed by Hull (103) in thin foils of γ brass; the transformation was similar to the normal martensite transformation but with no specific habit plane, the transformation mechanisms operating were related to the surrounding constraints in the foil since these changed as the foil thickened.

The transformation has been observed to be completely athermal, growth occurring only during changing temperature. The speed of a particular interface was found to be dependent directly on the rate of temperature change, but a wide variety of growth rates was observed during a transformation. This is believed to be due to the co-operative nature of the transformation shears which increase the local stress level around a newly formed plate to promote transformation in that region. The transformation has been shown to be very sensitive to stress so this would account for the "bursting" frequently observed. This is a major source of the autocatalytic nature of the transformation although the dislocation arrangements at the interface are also important in providing the elements of the nucleation mechanism (see section 5.4).

The variety of growth rates is consistent with a thermoelastic view of the transformation since the restraining force on the growth

of a martensite crystal is understood to be the increase in strain energy due to the adoption of a less favourable shape when the original growth pattern is arrested. The observation of the largest plates forming at M_s supports this interpretation. These plates were observed to grow to the grain boundary and then to nucleate a differently oriented plate in the next grain. Thus a plate may start rapidly and gradually slow as it changes shape, although the temperature is falling at a constant rate.

The small hysteresis and temperature range of the transformation (30 °C to 50 °C), the exact replication of the course of the early stages of the transformation and the ability of the structure to undergo large numbers of transformation cycles with little change in the transformation temperatures and microstructures, are features clearly indicative of a heterogenously nucleated, autocatalytic transformation, involving displacements almost completely absorbed elastically by the two phases.

5.4 Transformation Mechanisms

The review of previous work on martensite transformations presented in the first two chapters of this thesis led to the conclusion that martensite nucleation was a dislocation reaction, possibly involving the formation of a planar fault with similar atomic arrangements to those of the martensitic phase.

Electron metallography of the product and parent phases during and after transformation was therefore expected to reveal the presence of such mechanisms. No clear picture has however emerged from the present study.

Nucleation was not observed during "in situ" thermal cycling and martensite interfaces were observed to pass through the matrix dislocations without altering them. It was apparent from the continuously cycled bulk specimens, that plastic deformation of the material does occur since the dislocation density increases with the number of cycles (Fig. 4.7.9). This deformation appears to occur irregularly within the specimen, for example the feature shown in Fig. 4.7.9 f occurred in a specimen which showed a low dislocation density elsewhere, as would be expected in view of the relatively low number of thermal cycles to which it had been subjected. This suggests that certain martensite plates exceed the elastic limit of the matrix as they grow. It is thought that this may occur during a "burst" formation of plates, the high growth rate causing a local disturbance of the thermoelastic equilibrium between the phases.

Rows of dislocations on a number of b.c.c. slip planes have been observed, including $\{110\}_\beta$ and $\{112\}_\beta$, both types of planes having particular significance in the $\beta_1 \rightarrow \gamma_1$ transformation. The twinning plane for b.c.c. is $\{112\}_\beta$ and the homogeneous

(lattice) shear of the transformation is believed to occur on these planes (appendix 1). The basal plane of the γ' structure is parallel to one set of $\{110\}_{\beta}$; internal faulting has been observed in these planes, and the reconstruction of the γ' cell requires a shear of alternate planes by $a/6\ \langle 110\rangle_{\beta}$ (appendix 1). In addition it is possible to produce a stacking fault in β_1 with a similar atomic distribution to that of two layers of γ' structure by a dislocation dissociation in $\{110\}_{\beta_1}$ (appendix 2). The other $\{110\}_{\beta_1}$ planes are parallel to the $\{121\}_{\gamma'}$ which are the planes on which the internal martensite twins occur. Thus the surface striations left in the retransformed β_1 can be indexed as traces of $\{110\}_{\beta_1}$ planes (Fig. 4.3.10).

As discussed in section 4.7.3 however it was only rarely that any direct connection was seen between these dislocation arrays left behind by the dislocation, and the γ' structure. It was therefore concluded that the plastic deformation produced during transformation is not significant in promoting nucleation of subsequent transformations.

The internal twinned structure of the γ' martensite has been observed to show remarkable complexity. Several different systems can operate within a single plate, and extremely thin twin filaments appear to be able to intersect one another.

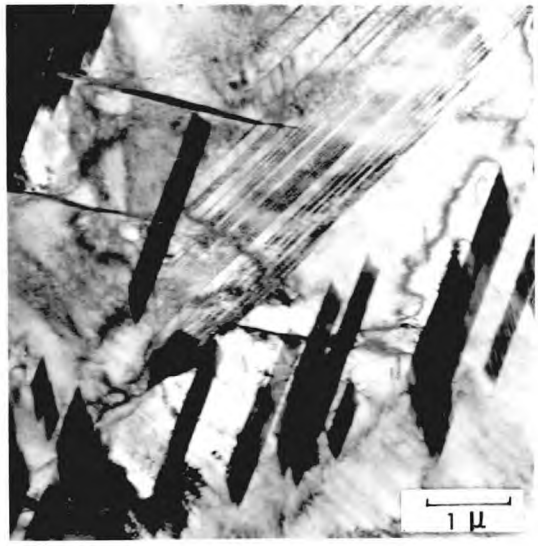
Figs. 5.3 a and b show these features with twins lying in four $\{121\}_{\gamma} // \{110\}_{\gamma_1}$ planes, two of which are perpendicular to the foil surface, so that there thickness can clearly be seen. The other two are inclined to the surface, displaying faulting parallel to the filament end, that is in $(001)_{\gamma'} // (101)_{\gamma_1}$.

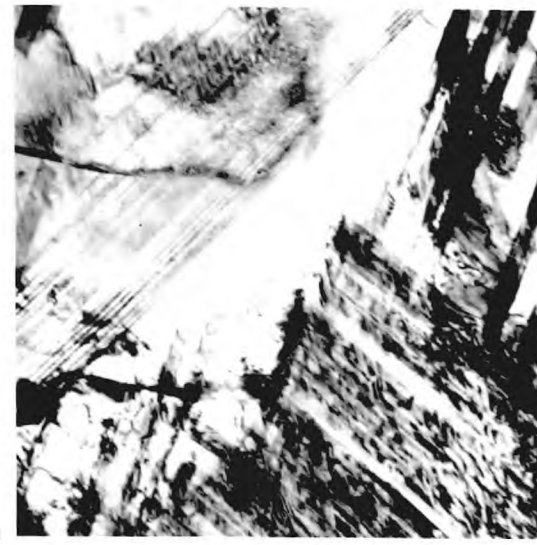
Similar twin filaments have been observed to grow within an already twinned γ' matrix in response to cooling or the stress effect of the electron beam's presence. Heating then removed these prior to the removal of the "matrix" twins. The ability of the γ' to re-twin suggests the source of the large shape changes which can be accommodated elastically in the γ' structure and then removed by heating, as in the "shape-memory" phenomenon (section 5.2).

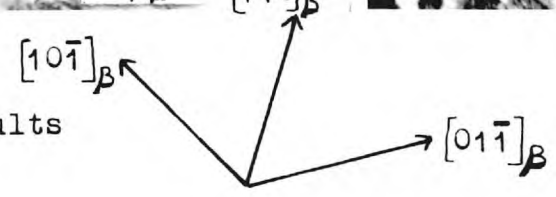
Many of these features are so thin that they may be mistaken for stacking faults, since the complex diffraction patterns produced made it difficult to distinguish twin symmetry. The orientation of the feature, the observation of fault contrast within it, and the comparison with other features in the same region, have all been used to confirm the presence of very thin twins. The 1 MEV EM7 microscope recently acquired by the group is expected to aid identification of these features by making possible the examination of thicker regions of the foil. Figs. 5.3 c and d show micrographs taken using this instrument. Initial observations indicate

Fig.5.3 : Substructure of γ'

(Alloy F)







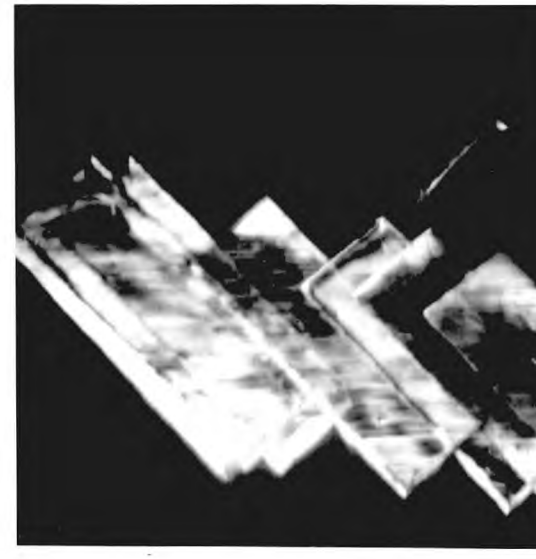
a) Twins and faults on $\{110\}_\beta$

b) Field as a) slightly tilted.



500KV

c) b.f. overlapping faulted platelets in γ'



500KV

d) h.r.d.f. as c).

that these complex twinned structures occur in the considerably thicker foils which it is possible to examine. It is apparent from this work and that on other transformations in thin foils (103) that the facility for examining foils of considerably varying thickness would be valuable to investigate more fully the influence of the reduction in constraints at regions of high surface to volume ratio, on the structure of the product phase.

During both the forward and reverse transformations isolated filaments with the same habit as the bulk γ' twins have been observed in the β_1 matrix (e.g. Fig. 4.3.5, 4.3.13 c). This is a $\{110\}_{\beta_1}$ plane, not parallel to the basal plane $(001)_{\gamma'}$ of the martensite. The mechanism of Duggin and Rachinger (appendix 2) requires faulting on the $\{110\}_{\beta_1}$ parallel to $(001)_{\gamma'}$, and then growth normal to this by rotation of a partial dislocation about a nodal dislocation. The observed filaments showed no signs of the fault contrast or thickening sequence expected from this mechanism. Fault contrast which was observed was on a different set of planes within the filament as can be seen in Fig. 5.3 a. No evidence of the dislocation dissociation in $\{110\}_{\beta_1}$ required by this mechanism was observed in the present work. Stacking faults are not generally expected in b.c.c. structures due to the high stacking fault energy and it must be concluded therefore that even the approach to the stacking sequence of the martensitic phase is not able to

reduce this energy sufficiently to favour the dislocation reaction given by equation 1.6.

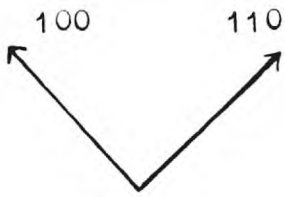
Similar features were occasionally observed on planes determined by trace analysis to be $\{112\}_{\gamma_1}$. Fig. 5.4 a shows an example imaged with a [400] fundamental reflection. Imaging with a [111] superlattice reflection caused almost complete invisibility of the feature as shown in Fig. 5.4 b. This appears to suggest that the feature is a fault produced by an a/3 [111] displacement in $(121)_{\gamma_1}$. This could be produced by dissociation of a perfect dislocation of the disordered structure a/2 [111] → a/6 [111] + a/3 [111] which has been suggested as a possible mechanism for twinning in b.c.c. The reaction reduces the energy of the dislocation but is expected to create a fault of high energy, so that its presence is surprising, as the atomic arrangements in the fault do not approach those of the γ' structure, (although a [111] homogeneous lattice shear in $(121)_{\gamma_1}$ is required in the shape change of the transformation).

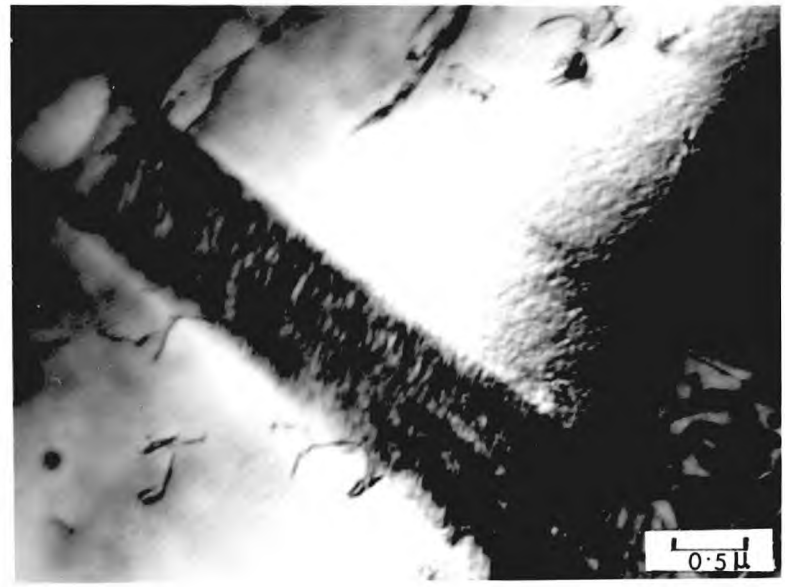
These filaments were observed to grow only from the thinnest regions of the foil, or more commonly from pre-existing martensite interfaces which supports the view that the matrix dislocations are not readily available for creating significant numbers of martensite nuclei, unless there is a severe reduction in the bulk constraints.

Study of the martensite/γ_1-phase interfaces has shown that the formation of new twin filaments occurs by the passage of interface dislocation, rather than by a true nucleation process involving matrix dislocations.

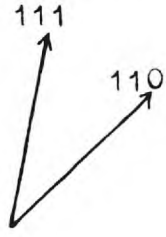
Fig.5.4 : Invisibility of a martensite filament (Alloy F)

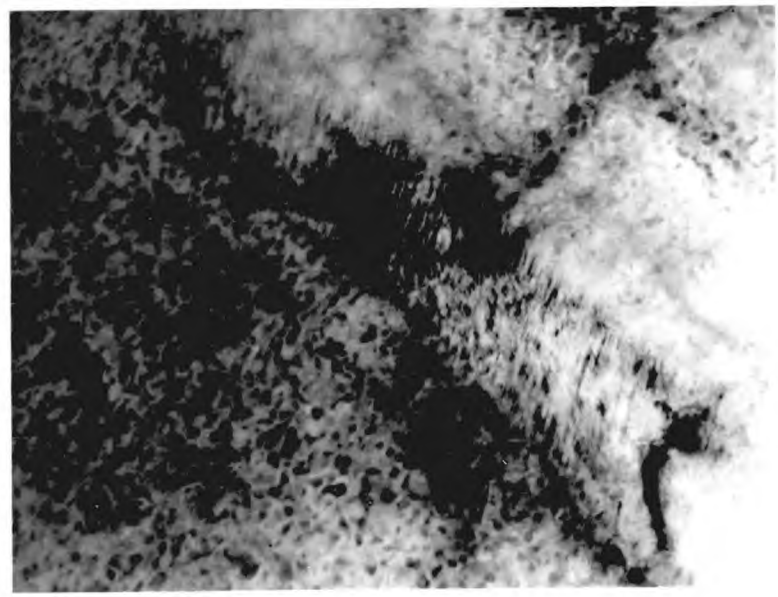
a) b.f. g = 400 (B2 domains from 200 reflection on bend contour)





b) b.f. as a) g = 111 (B2 & DO_3 domain contrast)





CHAPTER SIX : CONCLUSIONS AND FURTHER WORK

"Science moves, but slowly slowly

creeping on from point to point."

Tennyson

CHAPTER 6 : CONCLUSIONS AND FURTHER WORK

6.1 Conclusions

(1) The volume fraction of martensite is dependent only on the temperature and the growth rates of the martensite plates are dependent only on the rate of temperature change, as the transformation is completely athermal. It is therefore possible to follow the growth and shrinkage of a plate in the electron microscope during slow cooling or heating.

(2) The transformation temperatures of the alloys were found to be strongly dependent on their aluminium content (gradient -175 ^{o}C $\pm$ 15 ^{o}C per unit w/o Al) and less strongly on their nickel content (gradient -60 ^{o}C $\pm$ 10 ^{o}C per unit w/o Ni). The hysteresis and range of the transformation temperatures were found to be approximately constant in all the alloys studied.

(3) The structure of γ' martensite has been found to be orthorhombic with lattice parameters approximately 5.4 Å, 5.2 Å and 4.2 Å and orientation relationship $(110)[111]_{\gamma'} // (121)[210]_{\gamma'}$. Twinning was observed in $\{121\}_{\gamma}$ and faulting in $(001)_{\gamma'}$. These results confirm the findings of previous investigations. No specific habit plane was observed for the martensite in the thin foil specimens, interfaces being composed of fine twin filaments, often in

several different orientations in one plate and projecting into the γ-phase to produce a diffuse interface.

(4) Nucleation of plates in bulk γ-phase is an extremely rare event. The transformation usually begins in regions of high surface to volume ratio and proceeds by autocatalytic "nucleation" at the γ' / γ_1 interfaces.

(5) Repeated thermal cycling causes repeated transformation within approximately the same temperature range, the first plates forming in exactly the same sites and sequence. Some plastic deformation of the material occurs irregularly, and inhibition of nucleation sites was observed after large numbers of cycles. The dislocation arrays built up by continuous cycling have not in general been observed to provide nucleation sites for subsequent transformations, although they often lie in planes on which growth of isolated martensite filaments was observed.

(6) The isolated "twin filaments" forming both at the foil edge and in the bulk were commonly observed to have $\{121\}_{\gamma'} // \{110\}_{\gamma_1}$ habit plane, the multiplicity of different planes of this type increasing as the foil thickness decreased.

(7) No evidence of extensive faulting by dislocation dissociation in the γ-phase was observed. The earliest stages of the transformation to be observed were the thin "twin filaments" which were clearly three dimensional.

(8) The ordering reaction to DO_3 is insuppressible even at cooling rates in excess of 1000 °C/sec. This reaction was determined by thermal analysis to occur in the temperature range 500 - 550 °C for all alloys studied, with little dependence on aluminium or nickel content. For alloys containing more than 13.8 w/o Al the ordering process was observed, by metallography and thermal analysis, to form B2 order prior to the development of DO_3 order.

(9) The precipitation reaction forming γ_2 has a very low activation energy but is suppressible by cooling rates less than 1000 °C/sec. in all alloys containing less than 15.0 w/o Al. The structure was confirmed as cubic with lattice parameters 3x the disordered β-phase and an orientation relationship of similar lattice vectors parallel. Precipitation is associated with the superlattice domain boundaries at all stages of growth which could be observed metallographically. Preferred precipitation on a/4 <111> (B2) type boundaries was observed and appeared to cause anisotropy to develop in these boundaries at a critical stage of ageing. There is some evidence that these effects are due to the higher energy of the B2 boundary compared to the a/2 <110> (DO_3) type.

(10) γ_2 precipitates of a size greater than about 1000 Å in diameter are able to nucleate martensite. This is thought to be due primarily to changes in the chemical driving force due to aluminium segregation.

(11) A high density of straight dislocations adjacent to, and of similar shape to arrays of fine γ_2 precipitates was observed after limited ageing treatments. This structure was associated with the alignment of B2 boundaries and anomalous transformation temperature results, but the mechanism has not been elucidated.

(12) Transformation can be induced by stress at levels both exceeding and within the elastic limit. Martensite produced by the former does not catalyse the transformation of the rest of the specimen on subsequent cooling. That produced by the latter is elastic, with some stress hysteresis.

(13) The "shape-memory" effect occurs in both the nickel and non-nickel-containing alloys at temperatures within the normal transformation range. Shape reversal is possible after deformation of material initially γ_1 or γ'. Deformation is effected more easily in the γ' structure and the observation of the variety of internal twinning modes suggests a possible mechanism for this behaviour.

6.2 Suggestions for Further Study

The results of the present work have indicated the significance of a number of parameters on the nature and course of the transformation, but these have failed to indicate the nucleation mechanism. A study of the β-phase dislocation structure before and after transformation has provided insufficient information in view of the importance of γ' twin filament growth at the γ'/β boundaries. A more detailed analysis of the growth features at stopped interfaces is required than has at present been attempted. Diffraction analysis of the γ' phase is complicated by the fine internal structure which causes diffuseness of the reflections. This places a severe limitation on the orientations which can be readily analysed and these may be difficult to realize for an interface of interest which appears during the course of a transformation. In view of the variety of features observed in the present study, the collection of comprehensive data on the structural changes at the interface is expected to be a time-consuming procedure.

A fuller investigation of the influence of the surface and strain restraining forces on the structure of the martensitic phase should further the understanding of the transformation mechanisms. The operation of a number of different crystallographic systems for filament growth in the thinnest regions of specimens has been observed

to produce unusual martensite morphologies with no specific habit plane. The conditions under which nucleation in these preferred regions can lead to transformation of the bulk of the specimen have yet to be determined; the process was observed in bulk specimens by light metallography but not in the limited field of view offered by electron metallography. Transformation of specimens in the 1 MEV microscope fitted with a heating/cooling stage would provide the opportunity to observe a much wider range of specimen thickness and so bridge the gap between these light and electron microscopy results. High voltage metallography would also facilitate the understanding of the complex internal structure of the γ' phase and indicate the extent to which this is a function of surface to volume ratio.

An "in situ" study of the stress induced transformation and shape-memory effect, by high voltage microscopy is expected to produce valuable results, particularly concerning the thermally reversible shape deformation of γ' phase. A comparative study of a number of alloys displaying the shape-memory effect may indicate the reason for the close similarity of their structures including the significance of the ordered structure. In the present alloys, however, the transformation shears appear to be independent of the order domain structure.

The B2 and DO_3 ordering temperatures should be the subject of further study by metallography of step-quenched specimens and

by thermal analysis. Neither method is applicable to the alloys of higher aluminium content unfortunately due to γ_2 precipitation. The compositions between $(CuNi)_3Al$ and (CuNi) - 14 w/o Al in which this is suppressible, are of particular interest, however. $(CuNi)_3Al$ is the stoichometric composition for both B2 and DO_3 order, and in the present work a B2 ordering reaction was not detected in alloys containing 13.8 w/o Al or less.

A careful investigation of the early stages of the γ_2 precipitation reaction is necessary to confirm the influence of this reaction on the anisotropy of the a/4 <111> (B2) domain boundaries observed in some specimens. The anomalous martensite transformation temperatures recorded after such ageing treatments also require further investigation, possibly by an alternative technique such as thermal analysis or electrical resistivity measurements. These measurements of bulk changes in the specimen can then be followed up by electron microscopy to determine the relationships between the domain boundaries, γ_2 precipitates and γ' structure.

APPENDICES

(1) Construction of γ' structure from β_1 structure

This account follows that of Kurdyumov et al.[89].

(a) Reconstruction of c.p.h. lattice from b.c.c. lattice.

(i) A new unit cell is chosen with directions $[11\bar{1}]_{\beta_1}$ $[\bar{1}11]_\beta$ and $[101]_\beta$ for co-ordinate axes (Fig. A.1 a). This unit cell is body centred with $a_1 = a/\sqrt{3/2}$ and $c_1 = a\sqrt{2}$. The angle between the axes in the basal plane is $109^\circ 30'$ (Fig. A.1 b).

(ii) $[\bar{1}11]_\gamma$ and $[11\bar{1}]_\gamma$ shears must act on this cell on (121) and $(12\bar{1})_\gamma$ to increase the basal plane angle to 120° (Fig. A.1 c).

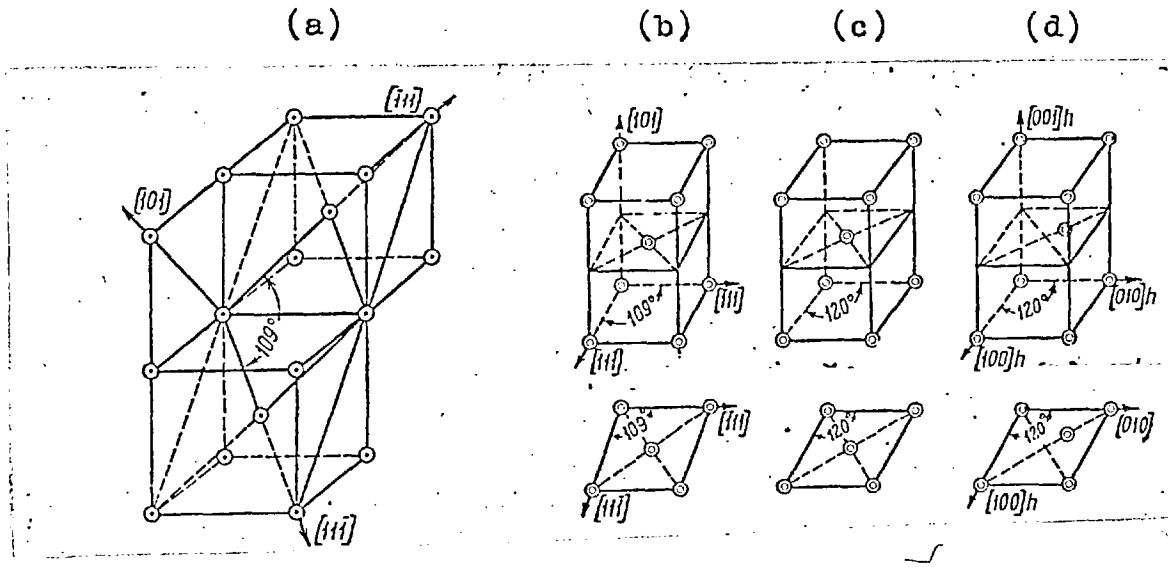
(iii) Alternate $[001]_\gamma$, ($[101]_\beta$) planes must shear with respect to each other in $[\bar{1}10]_\gamma$, direction by a/6 $[\bar{1}10]_\gamma$, to move the body centred atoms (Fig. A.1 a).

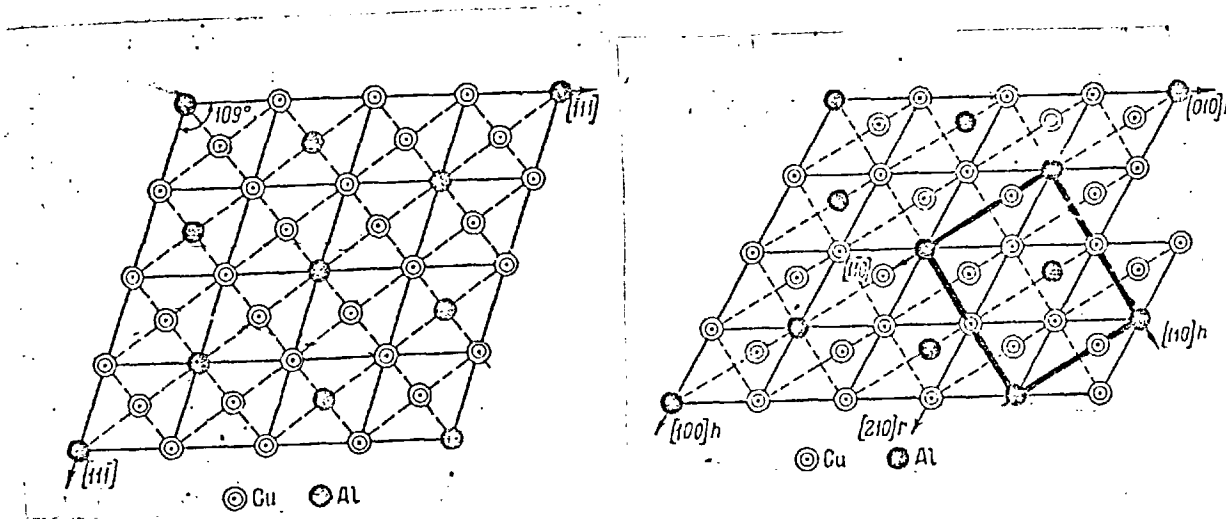
(iv) There must be a dilatation of 0.06 Å in the $(001)_\gamma$, interplaner spacing.

(b) Reconstruction of orthorhombic cell from DO_3 cell.

The period of identity along the <111> β co-ordinate axes is four times that of the disordered structure (Fig. A.1 c) so that a simpler unit cell can be chosen with orthorhombic

Fig. A.1: Construction of γ' unit cell from β_1 structure (from ref. 89)





symmetry (compare the region enclosed by the heavy line in Fig. A.1 f with 2.4 e). In this case the shear in step (a) (iii) above is of $(001)_{\gamma}$ planes by $a_1/6\,[\bar{1}00]_{\gamma'}$.

(2) A Nucleation mechanism for γ' martensite

This account is based on the work of Duggin and Rachinger[46,104].

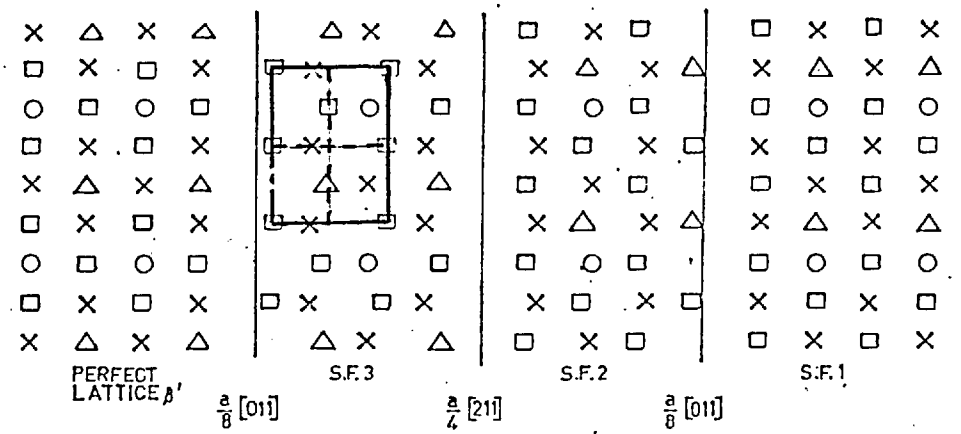
Since the identity period is increased by four times in $\langle 111\rangle_{\gamma_1}$ due to the DO_3 ordering, the $a/2\,[111]_{\gamma}$ dislocation will create stacking faults in γ_1 structure, producing Al - Al nearest neighbours. It is suggested that the energy of this dislocation can be reduced by the dislocation reaction:

$$\frac{a}{2}\,[111] \rightarrow \frac{a}{8}\,[011] + \frac{a}{4}\,[211] + \frac{a}{8}\,[011] \qquad (1.6)$$

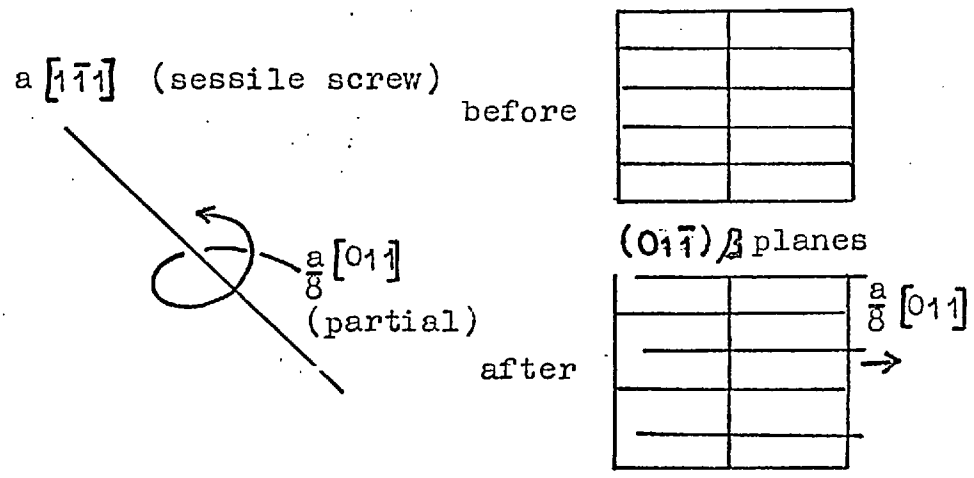
This introduces further stacking faults as shown in Fig. A.2 a which represents 2 successive $(110)_{\gamma}$ layers in the plane of the page. Since the Al - Al interatomic distances are increased in the SF3 region it is predicted that this fault will have a relatively low energy and so be extensive. Comparison of the enclosed area of Fig. A.2 a with Fig. 2.4 e and A.1 f shows that the atomic configurations of SF3 and γ' martensite are very similar. The displacement is $a/8\,[011]_{\gamma}$ whereas that required by the reconstruction described in appendix 1 is $a/6\,[011]_{\gamma}$.

Fig.A.2 : A nucleation mechanism for γ' martensite (from refs.46 and 104)

a) Stacking arrangement produced by the dissociation of an $^{a}/_{2}[111]_{\beta_1}$ on a $(110)_{\beta}$



b) Pole mechanism to effect the correct stacking sequence in adjacent $\{110\}_{\beta}$



Growth perpendicular to the (110) γ plane by a pole mechanism requires the presence of a sessile nodal dislocation to produce the $a/8\,[0\bar{1}1]_{\gamma}$ displacement of alternate $(110)_{\gamma}$ planes. This must be of the type $a\,[1\bar{1}1]\,\gamma_1$ (screw), with a component $a\,[0\bar{1}1]\,\gamma_1$ so that the partial $a/8\,[0\bar{1}1]\,\gamma_1$ climbs the spiral ramp to produce the displacements shown on Fig. A.2 b.

REFERENCES

1. F. Osmond; Bulletin de la Societe d'Encouragement, 10, 476 (1895) [reviewed in J.I.S.I., (i), 47, 456 (1895)]
2. I. Isiatshov,E.Kaminsky and G. Kurdyumov; Trans AIME, 128, 361, (1938)
3. A.R. Trciano and A.B. Greninger; Metal Progress, 50, 308 (1946)
4. G. Kurdyumov and O.P. Maksimova; Dokl. Akad. Nauk. S.S.S.R. 61, 83 (1948) and ibid 73, 95 (1950)
5. R. Cech and J. Holloman; Trans AIME 197, 685 (1953)
6. G. Kurdyumov; J.I.S.I. 95, 26 (1960)
7. F. Osmond; Metallographist, 1, 271 [quoted by L. Dumas; J.I.S.I. 68, 255 (1905)]
8. B.A. Bilby and J.W. Christian; Inst. of Mets. Monograph and Reports Series no. 18, p 121 (1955)
9. F.C. Frank; "Relation Between Structure and Mechnical Properties of Metals" p 248 (HMSO 1963)
10. J. W. Christian; "Physical Properties of Martensite and Bainite" I.S.I. special report no.93 p. 1 (1965)
11. D.W. Borland; J. Austr. Inst. Mets. 11, 284 (1960)
12. L. Kaufman and M. Cohen; Progress in Metal physics 7, 165 (1958)
13. A.B. Greninger and V. Mooradian; Trans, AIME 128, 337, (1938)
14. F. Osmond and G. Cortaud; J.I.S.I. 71, 444 (1906)

REFERENCES/Continued

15. E.C. Bain; Trans AIME 70, 25 (1924)

16. A.B. Greninger and A.R. Troiano; Trans AIME, 185, 590 (1949)

17. C.M. Wayman; "Introduction to the Crystallography of Martensitic Transformations" p. 84 (Macmillan 1964)

18. P.M. Kelly, J. Nutting; J.I.S.I. 197, 199, (1961)

19. M.S. Wechsler, D.S. Lieberman and T.A. Read; Trans AIME 197, 1503 (1953)

20. V.S. Bowles and J.K. Mackenzie; Acta. Met. 2, 129 and 138 (1954)

21. D.S. Lieberman, M.S. Wechsler and T.A. Read; J. Appl. Phys. 26, 473 (1955)

22. J.S. Bowles and J.K. Mackenzie; Acta Met. 2, 224 (1954) and 5, 137 (1957)

23. R.L. Patterson and C.M. Wayman; ibid 14, 347 (1966)

24. C.M. Wayman; "The Physical Properties of Martensite and Bainite" I.S.I. Special report, 93, p 163 (1965)

25. A.G. Crocker and B.A. Bilby; Acta Met. 9, 678 (1961)

26. A.G. Crocker; ibid 13, 815 (1965)

27. D.S. Lieberman and R. Bullough; Phys. Stat. Solidi 12, 657 (1965)

28. D.S. Lieberman; Acta Met. 14, 1723 (1966)

29. N. Ross and A.G. Crocker; ibid, 18, 405 (1970)

30. F.C. Frank; ibid, 1, 15, (1953)

31. B.A. Bilby and F.C. Frank; ibid, 8, 839, (1960)

32. R. Bullough and B.A. Bilby; Proc. Roy. Soc. B 68, 1276, (1953)

33. J.C. Fisher, N.H. Holloman and D. Tumbull; Trans. AIME 185, 688 and 691,(1949)

34. J.C. Fisher; ibid, 197, 918, (1953)

35. J.C. Fisher; Acta Met 1, 32 (1953)

36. R. Cech and D. Tumbull; Trans. AIME 206, 124, (1956)

37. J. Holloman and D. Turnbull; Progress in Metal Physics 4, 374, (1953)

38. M. Cohen, E.S. Machlin and V.G. Paranjpe; "Thermodynamics in Physical Metallurgy" p 242 (A.S.M. 1949)

39. H. Knapp and U. Dehlinger; Acta. Met. 4, 289, (1956)

40. C.L. Magee and H.W. Paxton; Ph.D Thesis, Camegie Inst. of Tech. (1966)

41. V. Raghavan and A.R. Entwisle; "The Physical Properties of Martensite and Bainite" I.S.I. special report 93 p 30 (1965)

42. M. Cohen; Trans. AIME, 212, 171, (1958)

43. J.W. Christian; Proc. Roy. Soc. A 206, 51 (1951)

44. A.H. Cottrell and B.A. Bilby; Phil. Mag. 42, 573 (1951)

45. J.A. Venables; ibid 6, 379, (1961); J. Phys. Chem. Solids, 25, 693, (1964)

46. M.J. Duggin and W.A. Rachinger; Acta. Met. 12, 529, (1964)

REFERENCES/continued

47. E. de Lamontte and C. Altstetter; Trans. AIME 245, 651,(1969)

48. S. Dash and N. Brown; Acta Met. 14, 595,(1966)

49. A.J. Rogers and W.A. Burgers; Ibid 12, 529, (1964)

50. K. Shimizu, Mooka and C.M. Wayman; ibid 18, 1005, (1970)

51. K.E. Easterling and H. Miekk-Oja; ibid, 15, 1133, (1967)

52. K.E. Easterling and P.R. Swann; Inst. Mets. Monograph 33, 152, (1968)

53. H. Warlimont; "The Physical Properties of Martensite and Banite" I.S.I. special report 93, (1965)

54. J.B. Cohen, R. Hinton, M. Lay and S. Sass; Acta Met. 10, 894,(1962)

55. G. Kurdyumov and L.G. Khandros, Dokl. Akad Nauk, SSSR 66,211(1949)

56. R.W. Cahn; Nuovo Cimento (suppt) 10, 350, (1953)

57. R.I. Garber; Dokl. Akad. Nauk SSSR, 21, 229, (1938);57, 555 (1947) J. Phys USSR, 2, 313, (1940); 11, 55, (1949)

58. E. Scheil; Z. Anorg. Chem. 207, 21, (1932)

59. J. Patel and M. Cohen; Acta Met., 1, 531, (1953)

60. J. Reynolds and M. Bever; Trans. AIME, 194, 1065 (1952)

61. L. Chang and T. Read; ibid 189, 47, (1951)

62. I. Arbuzora, A. Kirdyumov and L. Khandros; Phys. Met. Metallog 11, 116, (1961)

63. W.A. Rachinger; Br. J. Appl. Phys. 9, 250, (1958)

REFERENCES/Continued

64. R.J. Wasilewski; Scripta Met. 5, 131, (1971)

65. R.A. de Lange and J.H. Zijderveld; J. Appl. Phys 39, 2195, (1968)

66. W.J. Buehler and R.C. Wiley; A.S.M. Trans. Quart. 55, 269,(1962)

67. K. Otsuka and K. Shimiza; Scripta Met. 4, 569, (1970)

68. A. Nagaswa and K. Kawachi; J. Phys. Soc. Jap. 30, 296, (1971)

69. K. Enami and S. Nenno; Met. Trans.

70. C.M. Wayman; Scripta Met. 5, 489, (1971)

71. M. Hansen; Constitution of binary alloys. p. 89 (McGraw Hill, (1956)

72. A.J. Bradley, H.J. Goldschmidt and H. Lipson; J. Inst. Met. 63, 149, (1938)

73. G. Wasserman; Metallwirtschaft, 13, 133, (1934)

74. P.R. Swann; Phil, Mag. 129, 461, (1966)

75. Ismo Elo; Annals of Turku Univ. Seriest A p 129 (1969)

75a. A.V. Kurdyumov; Zhurmal Tech Fiz. 18, 999, (1948)

76. W.O. Alexander; J.I.M. 63, 163, (1938)

77. V. Gawranek, E. Kaminsky and G. Kurdyumov; Metallwirtschaft 15, 370, (1936)

78. G. Kurdyumov and T. Stelletskaja; ibid 13, 304

79. A.B. Greninger; Trans. AIME, 133, 204 (1939)

80. P.R. Swann and H. Warlimont; Acta Met. 11, 511, (1963)

81. V. Gridnew and G. Kurdyumov; Metallwistschaft, 15, 437, (1936)

REFERENCES/Continued.

82. A. Kurdyumov and V. Miretsky; J. Tech Phys, 8, 1777 (1933)

83. C.W. Chen; J. of Metals. 9, 1202, (1957)

84. D. Ryder; Inst. of Mets. Monograph and Reports series no. 18 p 320 (1956)

85. R. Haynes; J.I.M. 82, 493, (1953) 83, 105, and 357 (1954)

86. D. Hull and R. Garwood; ibid, 86, 485, (1958)

87. J. Jellison and E. Klier; Trnas. AIME, 233, 1694, (1965)

88. E. Klier, E.S.M. Grymko; ibid, 185, 611, (1949)

89. G. Kurdyumov, V. Miretsky, T. Stelletskaja; J. Phys.(USSR) 3, 298 (1940)

90. M. Wilkens and H. Warlimont; Acta Met 11, 1099, (1963) Z. Metallik, 55, 382, (1964); 56, 850 (1965)

91. Z. Nishiyama and S. Kajiwara; Jap. J. Appl. Phys. 2, 475, (1963)

92. H. Sato, R.S. Toth and G. Honjo; Acta. Met. 15, 1381, (1967)

93. H. Sato, R.S. Toth and G. Honjo; Phys. and Chem. of Solids, 28, 143, (1967)

94. K. Otsuka and K. Shimizu; Jap. J. Appl. Phys. 8, 1196, (1969)

95. W. Hume-Rothery; "Atomic Theory for Students of Metallurgy" p 260 (Inst. of Mets.)

96. H. Ali, R. Adams and P.R. Swann; to be published in J. Sci. Instr.

97. A.R.G. Brown, K.J. Jepson and J. Heavens; J. Inst. Meta. 93, 542, (1965)

REFERENCES/Continued

98. K.J. Jepson, A.R.G. Brown and A.G. Gray; "The Science, Technology and Applications of Titanium" p 677 (Pergamon 1970)

100. M.J. Marcinkowski and N. Brown; J. Appl. Phys. 33, 537, (1962)

101. M.J. Marcinkowski; "Electron Microscopy and strengths of crystals" p 333, (Interscience 1963)

102. K. Otsuka and K. Shimizu; Phil. Mag. 23, 188, p 481 (1971)

103. D. Hull; ibid, 7, 550, 1962.

104. M.J. Duggin; Acta. Met. 14, 123, (1966)

ERRATA

PAGE NO.	LINE NO.	
10	equation 1.5	for F_x read V
22	15	add bar (011) $0\bar{1}1$)
	equation 1.6	add bar $^{9}/_{2}$ $\bar{1}11$, and $^{9}/_{4}$ $\bar{2}11$
39	10/11	delete "This they ..... appendix 1"
68	1	add ".. at which _ has maximum"..
84	8	add s^{-1} "$1^{o}C$ s^{-1}"
	12, 14	for mm read
93	18, 20	add brackets $1\bar{1}0$ and 110
157	11	for 5.3 read 5.1
170	3	for "there" read "their"
175	14	for "5.4$\mathring{A}$" read "4.5$\mathring{A}$"
182	9/10	add bars $(12\bar{1})$ and $(\bar{1}21)$
184	equation 1.6	add bars $^{9}/_{2}$ $\bar{1}11$ and $^{9}/_{4}$ $\bar{2}11$
186	4/5	add bars a $1\bar{1}1$ and a $1\bar{1}1$
194		add "99. M.Bouchard: Ph.D Thesis, Imperial College, London,(1970)."
192	Ref.69	add "1487, 2, (1971)."
136	Fig.4.7.7.c)	for $\{102\}_{\gamma'}$ read $\{213\}_{\beta_1}$